TheoPhysEval: Assessing AI agents at autonomous theoretical physics problem solving

A. Ramesh Chandra,[1,*,‡] Aaghaz Mahajan,[2,*] Ainesh Sanyal,[3,*] Mianqi Wang,[4,*,‡] Shubhadeep Chakraborty,[1,‡] Sudip Chakraborty,[5,6,‡] Shailesh Chandrasekharan,[7,‡] Rama Govindarajan,[1,‡] Akshit Goyal,[1,‡] Jonathan J. Heckman,[8,‡] Yasir Iqbal,[9,‡] Divya Jaganathan,[10,‡] Saumav Kapoor,[1,‡] Andreas Karch,[3,‡] Pushkar Khandare,[11,‡] Sandeep Krishna,[2,‡] Anupam Kundu,[1,‡] Alok Laddha,[12,‡] Tongyan Lin,[13,‡] Swarnendu Maity,[11,‡] Nilmani Mathur,[2,‡] Shani Nadir Meynet,[8,‡] Alessandro Mininno,[14,‡] Abhijeet Mishra,[5,6,‡] Vidur Niranjan,[15,‡] Abhishodh Prakash,[5,6,‡] Pratik Rath,[2,‡] Durbar Roy,[1,‡] Debargha Sarkar,[11,‡] Srikanth Sastry,[11,‡] Gary Shiu,[14,‡] Aninda Sinha,[16,17,‡] Thomas Van Riet,[18,‡] Praneeth Netrapalli,[19,†] and Suvrat Raju[1,†,‡]

[1] *International Centre for Theoretical Sciences;* [2] *Tata Institute of Fundamental Research;* [3] *University of Texas at Austin;* [4] *Kavli IPMU (WPI), The University of Tokyo;* [5] *Harish-Chandra Research Institute;* [6] *Homi Bhabha National Institute;* [7] *Duke University;* [8] *University of Pennsylvania;* [9] *Indian Institute of Technology Madras;* [10] *Harvard University;* [11] *Jawaharlal Nehru Centre for Advanced Scientific Research;* [12] *Chennai Mathematical Institute;* [13] *University of California, San Diego;* [14] *University of Wisconsin–Madison;* [15] *Monash University;* [16] *Indian Institute of Science;* [17] *University of Calgary;* [18] *KU Leuven;* [19] *Google DeepMind*

arXiv:2610.16733v2 [hep-th] 12 Nov 2026

We present a suite of 50 unpublished research-level theoretical physics problems with verifiable answers. Without AI assistance, a typical problem in our collection could be solved by a world expert in about a day or less but would take considerably longer for experts in adjacent specialties. We test the ability of off-the-shelf AI agents to tackle these problems autonomously, without human hints. When given access to tools available in a realistic setting, including the ability to search the literature and write scripts for numerical and symbolic work, the best-performing agent, GPT-6-Astra harnessed in Codex, obtains the final answers with a near-perfect accuracy of 98% at an average cost under USD 3 per problem. On average, agents show only small changes in accuracy when denied web search and access to background research papers, suggesting significant memorization of the literature. These results suggest that state-of-the-art agents can accurately perform concrete calculations required across theoretical physics research. We comment on the broader implications of these findings and discuss possible explanations for the current lack of agent-led breakthroughs in theoretical physics despite their outstanding problem-solving abilities.

[*] Moderator · [†] Coordinator · [‡] Problem Contributor

Author contributions. Problems were supplied by expert problem contributors. The moderators fine-tuned the problems, wrote the code for the benchmark and performed the evaluation. The coordinators initiated the evaluation, recruited expert contributors and provided guidance. The manuscript was drafted by the coordinators and moderators, who are accountable for its text. Correspondence may be sent to `suvrat@icts.res.in`

I. Introduction

In the past few months, AI agents — by which we refer to a combination of a Large Language Model (LLM) and a harness that gives it access to tools — have developed the ability to perform a variety of scientific tasks with little or no human supervision. This impact is most visible in mathematics, where important open problems [1–4], including the Navier–Stokes Millennium Prize problem [5] and the "dying percolation conjecture" [6], have been solved by AI agents. In some cases, the agents were prompted by humans with no formal mathematical expertise themselves [7].

So far, autonomous agents have had a less significant impact on theoretical physics and have not achieved a notable breakthrough. But they have rapidly become important in research. Experts have used agents in their research [8–10], and agents have autonomously solved mathematically well-defined problems [11]. Moreover, many researchers use agents to discuss ideas, perform calculations, search the literature [12] and draft manuscripts. The objective of this paper is to scientifically evaluate one aspect of this progress at the current time — the ability of AI agents to solve well-posed and verifiable problems autonomously.

To this end, we present a suite of problems drawn from current research and sourced from world experts in a range of areas in theoretical physics. This collection does not include any important open research problems, since we advised potential contributors to prioritize direct publication of such results. The problems in our collection can be best thought of as "turn-the-crank" research problems, where known techniques are used to generalize an extant result. The result of each problem is, strictly speaking, novel, and sometimes even publishable, but not pathbreaking.

All our problems have verifiable solutions, either in the form of a symbolic expression or a numerical answer that cannot be guessed. To the best of our knowledge,

at the time of our evaluation, none of the answers to our problems were available publicly. However, we expect that solutions to some problems will appear in the literature in the near future, and one such solution (see §10a) was published after completion of the experiments described in this paper. Moreover, the problems do not meet a stricter criterion of being "untouched by AI." In some cases, human experts used AI tools for assistance in solving the problems, and so we cannot rule out data leakage.

Our problems are presented in Appendix A of this paper, and we strongly urge readers to glance over them.

It is nontrivial to construct problems that are relevant to research, are not significant in their own right, and have a solution that is verifiable, cannot be guessed, and is not publicly available. We asked experts to come up with the hardest possible problems in their respective areas. However, we did not reject problems merely because they were soluble by AI agents. Therefore, our evaluation suite aims to be representative of problems in theoretical physics, rather than an adversarial benchmark.

We evaluated agents on two tracks, which we term the "isolated track" and the "realistic track." These are distinguished by whether or not the agent is allowed to access the internet.

In our experiments we found that, in the realistic track, GPT-6-Astra with Codex (Astra) achieved a near-perfect accuracy of 98%, and both Astra and Opus 5.5 with Claude Code CLI (Opus) achieved an accuracy of 92% in the isolated track. The average change in accuracy for most agents between the two tracks was quite small. Since many of our problems rely on formulas from the literature, this indicates that leading LLMs have effectively memorized large parts of the theoretical physics literature.

Our results indicate that some frontier models may have already surpassed the best human researchers in their ability to perform concrete calculations, even in specialized topics. This is a significant milestone, with implications for education [13] and research in theoretical physics.

The ability to solve concrete problems has traditionally been highly valued in theoretical physics. Problem solving is central to physics education [14, 15]. Students are evaluated through high school competitions such as the International Physics Olympiad [16], examinations used in graduate admissions [17], and graduate qualifying exams [18].

However, problem-solving abilities are only one of the skills that theoretical physicists require. The main aim of the field is to construct theories of the physical world. Second, it is necessary to ask the "right" high-level questions of the theory. Third, it is necessary to convert these questions into concrete calculations. Therefore, it is only at a late stage in the scientific process that one is faced with a concrete calculation with a verifiable answer.

As a corollary, the excellence of AI agents at problem solving does not immediately imply their all-round excellence at autonomous physics research. Human experts are required in the loop. Autonomous excellence at research might emerge in the near future but will require more than problem-solving ability.

We hope that the assessment presented in this paper will aid discussions in the theoretical physics community on the evolution of pedagogical and research practices. Similar discussions are underway in the mathematical community [19, 20]. It is desirable for the theoretical physics community to have these discussions in advance, before AI has a significantly disruptive impact.

Several agents included in this study do not yet saturate our evaluation. For example, among open-weight models, DeepSeek-V4.1-Flash (DeepSeek) harnessed in Codex scored 54% and 50% on the realistic and isolated tracks, respectively. We hope that our collection of problems will be useful for model developers. It might serve as a method of measuring the abilities of agents to assist theoretical physicists in their research.

A. Previous work

There has been considerable previous work on benchmarking the abilities of LLMs on school [21, 22], competition [23, 24], and undergraduate physics [25]. Benchmarks such as TPBench [26], SciCode [27], FrontierScience [28], PRL-Bench [29], QMBench [30] and notably CritPt [31] include research-level problems in addition to simpler problems. Our paper adds to this literature but is distinguished by its exclusive focus on modern research-level problems. Our evaluation methods are also different since most other evaluations do not usually allow agents to access the full range of tools that they would have access to in the real world.

Terminal-Bench-Science [32] is broader in its coverage than this assessment, which is focused on theoretical physics and provides deeper coverage within that field. Moreover, since we seek to evaluate agents on realistic problems that physicists would encounter, we do not discard problems simply because they can be solved by agents.

Our evaluation is roughly comparable to the "First Proof" challenge in mathematics [33–36] in the sense that it involves unpublished research-level problems. However, while First Proof involves human assessment of proofs, our evaluation is automated and only based on the final answers.

This paper is organized as follows. In Section II we explain the class of problems included in our collection. In Section III we describe the procedure used to evaluate agents on this collection. In Section IV, we provide a summary of the quantitative and qualitative conclusions of our evaluation. We conclude with some discussion in Section V. The appendices provide details. In particular, Appendix A contains a full list of our problems.

Example problem

Consider a black-string background with two branes at equal angles, $\pi/10$, from the vertical in AdS_4. By comparing minimal surfaces that extend from the defect to the brane to minimal surfaces that extend from a defect on one side of the horizon to the other, find the Page time for this configuration in units where the temperature is $1/(2\pi)$.

Expected answer flow

Step 1: Locate arXiv:2012.04671 [37] that discusses a similar problem in AdS_5.

Step 2: Adapt the equations derived there to $d = 3$.

Step 3: Write a numerical script to solve the resultant differential equations, while being careful about singularities at the end points.

Step 4: Analyze the solutions and obtain the answer.

(a) Black-string Page time.

Example problem

Consider one-dimensional class D fermionic systems, with no microscopic symmetries other than fermion parity. Restrict to the trivial phase and to free-fermion models. Using the suspension construction, construct a two-parameter Hamiltonian corresponding to a fermion parity pump. What is the central charge of the critical theory at the diabolical point? Under free-fermion perturbations, what does the diabolical point destabilize to?

Expected answer flow

Step 1: Use the suspension construction of arXiv:2605.20339 [38].

Step 2: Start with an odd-parity $0d$ ground state whose phase is self-inverse under stacking.

Step 3: Arrange copies along a chain and deform each to even parity using two nearest-neighbor dimerizations.

Step 4: Identify an instability of the diabolical point and determine its effect.

(b) Fermion parity pump.

Example problem

A fluid is flowing in the x direction over a flat plate of length L. The fluid approaches the flat plate at free stream velocity U_0. The Reynolds number based on L and U_0 is $Re = 160000$. Calculate the spanwise normalized length scale (L_s/L) of the *dominant initial* streamwise spatial perturbation velocity structures that develop on a horizontal plane at a vertical height of $y/L = 0.01$ from the plate. Assume spanwise to be periodic with length-scale L.

Expected answer flow

Step 1: Set up the 3d computational domain for the flat-plate configuration.

Step 2: Solve the unsteady incompressible Navier–Stokes equations numerically.

Step 3: Extract the velocity data at the required horizontal plane.

Step 4: Analyze the extracted field and compute the length scales required.

(c) Flat-plate boundary layer.

Box 1. Three example problems and their expected solution trajectories.

II. Problems

The problems in our collection were obtained by soliciting world experts from different areas of theoretical physics.

We asked experts to contribute problems that met the following three criteria.

1. Problems related to current physics research;
2. A known solution that was simple to verify but difficult to guess;
3. A solution that could not be looked up in the published literature or elsewhere.

We also requested that contributors not publish their solutions in the near future, to avoid contamination of the evaluation.

These criteria are quite restrictive. In particular, they exclude problems from ongoing research that the experts intended to publish in the near future.

One pathway for contributors to satisfy these criteria was to give us a problem from their research notes that they had worked out but not taken the trouble to publish.

A more common alternative was for contributors to adapt a problem solved in one of their recent papers. By changing some parameters in a physics calculation, it is often possible to obtain a new problem with an answer that cannot be guessed from the old answer. Problem contributors could solve such a problem by modifying their existing code or calculations. But another expert human, or an AI agent, would need to locate and understand the original solution; reconstruct the calculation in detail; and then adapt it to the modified problem.

Such an exercise is often assigned to graduate students who are starting research, since it helps them survey the literature and master the relevant techniques. This method is also sometimes used by researchers to write "incremental papers."

Therefore, none of the problems in our dataset constitute breakthrough open problems. Solving them does not require great originality or the ability to construct new physical theories. However, it does require familiarity with current research, and the ability to understand and accurately adapt cutting-edge calculational techniques.

A. Example problems

Box 1a shows an example of such a problem and the expected solution trajectory. The problem statement there is closely related to a problem solved in a paper that appeared on the hep-th arXiv [37]. The statement of the problem is deliberately terse and it requires a deep understanding of recent developments in holography to decipher the statement.

A human attempting this problem would presumably start by locating this paper. This would help them understand the terms and the scope of the problem. The setup of [37] involved a five-dimensional spacetime, and the next step would be to generalize the equations there to a four-dimensional spacetime as asked in the problem. This is a straightforward step but requires some care.

The resulting equations cannot be solved analytically. They give rise to a singular boundary-value problem. One must solve the equations in a series expansion near the singular points and then use a "shooting" routine [39] to obtain the full solution.

When presented as above, the individual steps in the solution might seem straightforward. However, the solution requires several components including a familiarity with the relevant literature and also a familiarity with numerical techniques. It took an author of the previous paper (SR) about a day to adapt the original calculations and perform the new calculation accurately. We estimate that before the advent of modern agents, only a small number of experts would have had both the physics background and familiarity with the relevant numerical techniques to solve the problem; moreover, it would have taken these experts several days to reconstruct the old calculation and perform the new one.

A human expert working with a frontier AI agent can now solve this problem both accurately and rapidly with ease. This might require the human to provide hints to the agent, or perhaps provide the agent with the high-level algorithm above. Our assessment seeks to determine whether agents can solve this problem entirely autonomously by performing all the steps in the answer flow with no hints beyond the given prompt.

Box 1b presents a second example, involving a class D fermion parity pump, together with a sketch of the solution. Box 1c presents a third example, involving flat-plate boundary-layer perturbations, together with a numerical solution sketch.

These problems are a small subset of our larger collection. But specialists in the area of one of these problems are unlikely to be familiar with the terminology of the other two problems. And, given the specialized nature of research, most physicists would find all three problems challenging to tackle autonomously. Therefore, the fact that agents are able to attempt these problems at all is already noteworthy.

B. Distribution of problems

We obtained a total of 50 problems spanning a range of areas of theoretical physics. Table I summarizes their distribution by theme. These themes cover a large number of topics. We do not believe that any physicist would have the expertise to attempt more than a fraction of these problems. Given the level of specialization in modern physics, it might often be difficult for a single expert to attempt all problems in a given thematic class.

Our problems do not provide an exhaustive survey of all areas of theoretical physics. The distribution of problems is partly influenced by network effects, since the coordinators and moderators invited experts they knew. However, there is also an intrinsic scientific influence on the distribution. While some fields, such as quantum field theory, naturally lend themselves to a number of hard calculations with verifiable answers, it is harder to construct such problems in other fields.

Theme	**Problems**
Classical physics	5
Stochastic processes and biological physics	5
Nonequilibrium statistical mechanics	3
Lattice theories	3
Quantum phases of matter	5
Electronic structure theory	4
Quantum field theory	7
Particle physics	2
Scattering amplitudes	5
Holography and entanglement	5
Gravitation and cosmology	6
Total	**50**

TABLE I. Thematic distribution of problems

The full list of problems is provided in Appendix A. We urge readers to read these problems. The problems can also be downloaded from Hugging Face [40].

III. Evaluation

As explained above, every problem in our dataset has a verifiable answer. In some cases, such as the problem given in Box 1a, our problems naturally had numerical answers that could be checked against the answer provided by the agent.

But it is also common to present the answers of analytical calculations in physics using symbolic expressions. In some cases, it is nontrivial to verify whether a given answer matches the reference answer because the same mathematical expression can be written in many equivalent ways. Moreover, notation is not always standard, and different agents might choose different symbols to refer to the same physical quantity.

Original question

Compute the rate for axion conversion to photons via scattering off the electrons in a dielectric medium. Assume that there is no external electric field and the medium is a conventional solid state material (non-magnetic, zero temperature), that the axion only interacts via an $aF_{\mu\nu}\widetilde{F}^{\mu\nu}$ coupling. Consider both relativistic and non-relativistic axions.

Addition

Consider the case when the dielectric function of the medium satisfies

$$\mathrm{Im}\left[\frac{-1}{\varepsilon_L(\omega,q)}\right] \;=\; \frac{\pi}{2}\,\omega_p\,\delta(\omega-\omega_p), \tag{1}$$

Working in natural units ($\hbar = c = 1$), take the axion-photon coupling $g_{a\gamma\gamma} = 10^{-10}\,\mathrm{GeV}^{-1}$, frequency $\omega_p = 16.6\,\mathrm{eV}$, refractive index $n = 1.5$, and axion velocity $v_a = 10^{-3}$. Evaluate the rate Γ_{NR} for (1) $m_a = 25\,\mathrm{eV}$ and (2) $m_a = 15\,\mathrm{eV}$. Express the final numerical answer in scientific form in eV units in the order [(1),(2)]

Box 2. An original question and an addition requesting a numerical answer.

One option is to solve this problem by relying on an LLM as a judge. The LLM can convert the expression provided by the agent to standardized notation and then use a symbolic manipulation program to determine its equality with a reference solution. However, this introduces an extraneous source of error.

Therefore, we chose to convert all expressions to numerical values by giving the agents numerical values, both for relevant and also irrelevant physical quantities. See Box 2 for an example of this kind. These numerical modifications lead to floating-point numbers or sequences of whole numbers that cannot be guessed easily.

Agent solutions were graded on these numerical answers. However, after completion of the final runs, an automated analysis of answers revealed two prompts (§9a and §11d) where conventions were not fully specified. Our grading key allows for the convention choices we observed in our runs. Attention is also required for §1b, which, as discussed in Appendix B, is resistant to numerical conversion. While we have tried our best to report objective scores, readers who seek to reproduce the evaluation should pay attention to these, and other possible undetected ambiguities, as potential sources of error.

We evaluated the models using the Harbor framework [41] used in Terminal-Bench [42]. Harbor allows us to set fine-grained controls for the tools that the models can use. The full configuration used in our evaluation is available on Hugging Face. Each agent was tested under two separate tracks.

1. In the realistic track, the agent was allowed access to both web search and local tools.

2. In the isolated track, the agent was allowed to use local tools. But web search was disabled except for calls to the model provider itself.

These evaluations serve distinct purposes. The isolated track is relevant for model builders who want to test the agent's innate knowledge of physics, and its ability to regenerate research-level code and calculations from scratch. However, for a physicist using an agent as a research assistant, there is no reason to disable web search or reinvent the wheel: publicly available scientific code or literature relevant for the problem should be used. Therefore, the realistic track offers a better sense of the utility of the agents for professional physicists.

For the isolated track, agents ran in local Docker sandboxes managed by Harbor, with internet access disabled. We examined agent trajectories using an automated analysis and this analysis did not reveal any instances of the agents escaping the sandbox.

For standardization, the final evaluation was carried out on e2-standard virtual machines on Google Cloud. Each task was assigned 2 vCPUs, 4 GB of memory and 10 GB of storage. No restriction was placed on the total cost or tokens used by the agent. However, tasks that did not complete in 8 hours were cut off as having produced no output. The multi-task problems of Appendix A 6 were allocated a total of 20 hours.

To economize time and costs, we only ran the full evaluation suite once for each agent through the API. This might lead to statistical errors in the measurement of the total accuracy since, with nonzero temperature, models can yield differing outputs on differing runs. We encourage readers to keep this uncertainty in mind when interpreting our accuracy scores. We also encourage readers who wish to obtain a more accurate evaluation to run the benchmark directly using our Hugging Face resources.

IV. Results

A. Quantitative analysis

We evaluated five agents: GPT-6-Astra [43] with Codex [44] (Astra); Opus 5.5 [45] with Claude Code CLI [46] (Opus); Gemini 3.8 Flash [47] with Antigravity [48] (Gemini); DeepSeek-V4.1-Flash [49] with Codex (DeepSeek); and GLM 5.3 [50, 51] with Claude Code CLI (GLM). Reasoning effort was set to max for all mod-

els except Gemini 3.8 Flash, where "high" is the highest available reasoning effort. All agents were evaluated on the realistic and the isolated tracks.

In this section we report summary scores for the pass rates, costs and token usage by each agent. Appendix C breaks these figures down by problem and gives additional details.

Figure 3 shows pass rates on the realistic track. Astra has the highest pass rate solving 49/50 problems. It is closely followed by Opus, which solved 46/50 problems. Gemini solved 34/50 problems, and the open-weight models DeepSeek and GLM solved 27/50 and 21/50 problems, respectively.

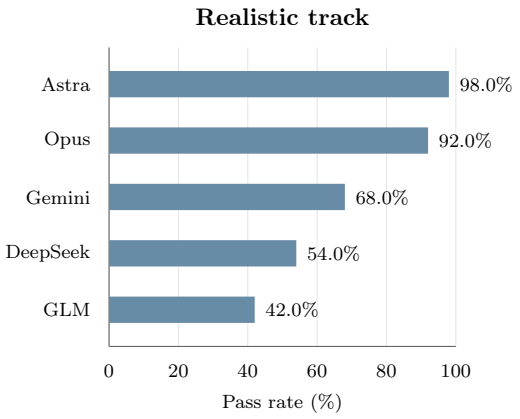

FIG. 3. Pass rates on the realistic track.

Figure 4 shows pass rates on the isolated track. Astra and Opus had the highest scores, solving 46/50 problems each. They were followed by Gemini at 31/50, GLM at 26/50 and DeepSeek at 25/50.

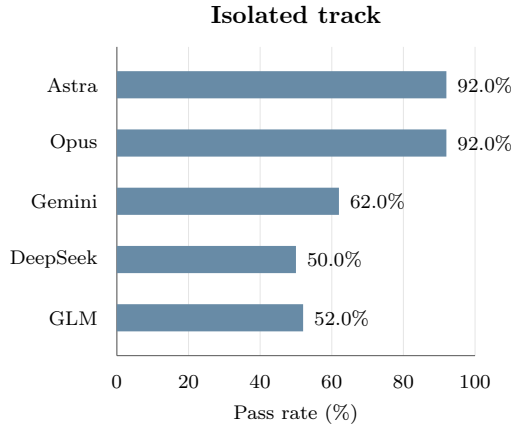

FIG. 4. Pass rates on the isolated track.

The pass rates in our evaluation are higher than those reported by some other benchmarks. However, upon visual inspection, it appears to us that our problems are, on average, more advanced than those in other extant collections of theoretical physics problems, including CritPt. Recent literature suggests that some theoretical physics benchmarks might suffer from inaccurate evaluations [52, 53]. It is of interest to understand this discrepancy better.

Table II summarizes the tokens consumed by each agent. Since the agent writes scripts, reads their outputs and accesses the web on the realistic track, the number of input tokens is much larger than the number of prompt tokens. We have separated cached and uncached input tokens, since they are priced separately by all providers, although this division has limited scientific significance and depends on the instantaneous runtime conditions at the API endpoint.

Table III summarizes the evaluation costs for the two tracks. The costs for all models except GLM are calculated by multiplying the token usage with the API rates. Opus incurred substantially higher costs than other models. Although GLM's API costs were notionally high, we used a coding plan, with an actual cost of USD 180 for both tracks combined.

B. Qualitative analysis

We now present a qualitative analysis of the errors made by the models.

On the realistic track, Astra fails on only one problem in our evaluation suite. This problem (§1b) is an inverse problem, which requires the model to find an autonomous differential equation that would lead to a given curve. Unlike forward problems, an inverse problem generated synthetically in this manner involves information asymmetry between the agent and the creator of the question.

Moreover, as Appendix B explains, the solution involves some play on the terms in the prompt. Nevertheless, we chose to include this question in our suite since it is reminiscent of a situation that a researcher might face, in which they are presented with slightly imprecise data and must unearth the underlying physics that produced the data, even bending some rules along the way.

It is noteworthy that we initially assessed that Astra had made errors in several additional problems. However, upon closer examination and consultation with the experts, we found that there were subtle errors in the original solutions. In all these cases, after the experts corrected their solutions, Astra's solution was found to be correct.

The inverse problem was not solved by any model. Therefore, the sets of problems solved correctly by other models, and by Astra on the isolated track, are each a *strict subset* of those solved correctly by Astra on the realistic track.

On the isolated track, Astra failed on three additional problems, including two that it incorrectly rejected as being impossible to solve.

Although Opus made more errors than Astra on the realistic track, its errors were subtle. In the realistic track, for §1c, Opus used initial data from the reference [54].

	Realistic				Isolated			
Agent	Uncached input	Cached input	Output	Total	Uncached input	Cached input	Output	Total
Astra	2.93	33.55	0.92	37.41	1.87	21.66	1.00	24.53
Opus	11.78	192.25	7.15	211.18	18.13	203.09	7.21	228.43
Gemini	41.99	558.96	5.76	606.71	35.24	552.93	6.02	594.20
DeepSeek	12.84	989.73	23.02	1025.60	10.75	799.72	23.50	833.97
GLM	16.55	945.72	9.69	971.96	22.29	1079.79	13.52	1115.61

TABLE II. Token usage for each agent and evaluation track, in millions of tokens. Rounded components may not sum exactly to the reported totals.

Agent	**Realistic**	**Isolated**
Astra	116.28	95.20
Opus	240.43	275.46
Gemini	95.01	90.48
DeepSeek	37.42	36.23
GLM	180[†]	

TABLE III. Evaluation costs (USD) inferred from token usage. [†]GLM's coding plan covered both tracks; API costs would have been USD 311.71 for the realistic track and USD 371.46 for the isolated track.

The paper is relevant for the problem, but the prompt itself specified different initial data. It did not make this error in the isolated track. In another case (§9a), it stated an incorrect conclusion about the rate of convergence of an infinite series in both the realistic and the isolated tracks. Finally, for the problem §7a, it produced no valid output on the realistic track by hitting the maximum token output limit repeatedly; it solved this problem successfully on the isolated track. On the isolated track, Opus made a small error in setting up the modular differential equation (§7d) that it did not make on the realistic track.

All other models made a larger number of errors, some of which would have been obvious to an expert human. For instance, while attempting the Page time problem of Box 1a (§10d) on the realistic track, both Gemini and GLM utilized formulas from [37], which are valid for five dimensions but must be modified for the four-dimensional case in the problem. On the isolated track, Gemini, GLM and DeepSeek evaluated geodesic lengths rather than the minimal areas that are required.

In another case (§11f), GLM incorrectly asserted that the problem was equivalent to another one on both the realistic and isolated tracks. The problem requires solving ordinary differential equations and finding the smallest allowed frequencies. DeepSeek chose an incorrect basis of solutions on the isolated track and Gemini made a similar error on the realistic track. DeepSeek solved the problem correctly on the realistic track, whereas Gemini did not produce an output on the isolated track.

The higher overall accuracy of GLM on the isolated track compared to the realistic track is largely due to a set of linked electronic structure problems given in Appendix A 6. Since some key references were provided to the models to set up the framework for the problem, the agent on the isolated track was at less of a disadvantage. The agent on the realistic track made a sign error early in its analysis, which propagated across the problems.

Our results show that the accuracy of the agents changes very little between the realistic and the isolated tracks. The change in accuracy is well within the statistical uncertainty in our evaluation, which comprises a single run. This is remarkable because a number of our problems require detailed formulas from the literature that, in most cases, were not provided to the model as background. For example, it would be impossible for a human to attempt §11f without looking up the text of the background paper mentioned there [55] to understand what the notation means.

The fact that models can solve such problems on the isolated track suggests that they have memorized large parts of the physics research literature and can reproduce key formulas without looking them up.

V. Discussion

In this paper, we have presented a large collection of unpublished problems drawn from different areas of theoretical physics. The central conclusion of our evaluation is that frontier agents can now solve verifiable problems in theoretical physics with great accuracy. Not only does their breadth exceed that of any individual, but their calculational abilities now match those of world experts even in specialized domains.

It might be possible to reduce the accuracy of agents by constructing problems adversarially. For instance, no agent was able to solve the inverse problem (§1b) and it should be possible to construct more examples of such problems. We have chosen not to do so, since our suite is meant to be representative of difficult problems that are actually encountered in research.

On the other hand, in a realistic environment, human researchers engage agents in a multi-turn process where they examine the agent's output and ask for refinements. We believe that with such feedback, the accuracy of even the weakest agents in our evaluation can be increased

substantially.

In this evaluation, we used common consumer harnesses. It is possible to design specialized harnesses for scientific work [56–61], and such tools have had success in mathematics [62, 63]. It is of interest to understand whether such harnesses can improve the accuracy of agents in our evaluation. Moreover, while it is natural to pair Astra, Opus and Gemini with Codex, Claude Code and Antigravity, respectively, we chose to pair DeepSeek with Codex and GLM with Claude Code. It is possible that different combinations of models and harnesses might perform better. We encourage interested readers to try such combinations.

Our results show that modern agents have matured into powerful tools that professional physicists can use to expand the scale and scope of their work. This is likely to accelerate scientific discovery in the near future and might lead to breakthroughs in longstanding problems.

However, this progress also creates structural challenges. Until recently, some problems in our collection might have been appropriate as initial research projects to train early-career researchers for advanced research and as an opportunity to obtain an original result. It is no longer appropriate to assign such problems to starting researchers, unless it is clearly understood that the objective is purely to work through the problem rather than to obtain the final result.

Theoretical physics research has historically required fewer resources than experimental research, and this has had an equalizing effect on the field. While the problems in our collection can be solved without much expenditure, we expect that more advanced problems will require greater resources. This raises concerns about access and equity in physics research.

Finally, we return to the point that solving verifiable problems is only one aspect of physics research. A concrete calculation emerges only after a suitable problem is identified in a theory. The problem originally identified may turn out to be too hard to solve. A good researcher can then find a related but simpler and equally interesting problem to solve. In our experience, current agents are not adept at dynamically switching direction in this manner.

There is a shared understanding among physicists, although far from a consensus, of what constitutes an interesting problem. At the moment, agents do not appear to have the same "taste" in problems. We have observed that, when asked to come up with new problems, agents focus excessively on details that a human might find uninteresting.

Therefore, human experts are necessary to guide current agents and to set directions. At present, agents cannot simply be given a major physics problem and expected to solve it autonomously.

The observations above are based on our experiences and conversations. We are unable to quantify them and acknowledge that other researchers might have had different experiences. They certainly do not constitute claims about the future development of AI.

At least one tendency in theoretical physics has been to exhort researchers to "shut up and calculate" [64]. As intangibles such as taste and vision gain significance, physicists might need to "stop and think."

VI. Acknowledgments

We would like to thank P. Ajith, Riddhipratim Basu, Brian Campbell-Deem, Alejandra Castro, Sarthak Chandra, Patrick Hayden, Yu-tin Huang, Raghu Mahajan, Xiaoliang Qi, Madan Rao, Sthitadhi Roy, Ujjwal Sen, Tejaswi Venumadhav and Ashvin Vishwanath for helpful discussions and collaboration in the early stages of this project. AI agents, including Astra, Gemini and Opus, were used to write code to perform the evaluation, analyze the results and assist with the preparation of this manuscript.

[1] B. Georgiev, J. Gómez-Serrano, T. Tao, and A. Z. Wagner, Mathematical exploration and discovery at scale (2025), arXiv:2511.02864 [cs.NE].

[2] N. Sothanaphan, Resolution of Erdős problem #728: a writeup of Aristotle's Lean proof (2026), arXiv:2601.07421 [math.NT].

[3] N. Alon, T. F. Bloom, W. T. Gowers, D. Litt, W. Sawin, A. Shankar, *et al.*, Remarks on the disproof of the unit distance conjecture (2026), arXiv:2605.20695 [math.CO].

[4] OpenAI, Sharing AI progress in mathematics (2026), published October 6, 2026. `https://openai.com/index/sharing-ai-progress-in-mathematics/`.

[5] OpenAI, Finite time blowup for Navier–Stokes, OpenAI preprint (2026), released September 8, 2026; announcement and formal proof: `https://openai.com/index/navier-stokes-solution/`. `https://cdn.openai.com/pdf/32d9f210-8b73-45e0-91bc-82a30aef8a9a/navier-stokes.pdf`.

[6] J. Leder, $\theta(p_c) = 0$ for Bernoulli bond percolation on $\mathbb{Z}^d$ in all dimensions $d \geq 2$: A guide to the Lean formalization, GitHub (2026). `https://github.com/anthropics/formal-math/blob/795efb86f191735c5481675763537cfb4ff37e55/percolation/summary.pdf`.

[7] D. N. Giraudin, A counterexample to a conjecture of Thakur on Carlitz-Wieferich primes (2026), arXiv:2607.15305 [math.NT].

[8] G. Parisi and F. Zamponi, A proof of an identity for the critical exponents of jamming, J. Stat. Mech. **2026**, 073301 (2026), arXiv:2606.03300 [cond-mat.stat-mech].

[9] Q. Chen and Y. Yin, Exact all-level positivity of the bosonic Veneziano amplitude (2026), arXiv:2608.25183 [hep-th].

[10] N. Craig, A gauge-invariant measure for lattice chiral fermions (2026), arXiv:2610.09093 [hep-lat].

[11] M. von Hippel, Yes, Claude can do Nine Loops, Anthropic Science (2026), published 25 September 2026; with an addendum by Lance Dixon. https://www.anthropic.com/research/yes-claude-can-do-nine-loops.

[12] H. Guo, M. Tikhanovskaya, P. Raccuglia, A. Vlaskin, C. Co, D. J. Liebling, *et al.*, Expert evaluation of LLM world models: A high-T_c superconductivity case study, Proceedings of the National Academy of Sciences **123**, e2533676123 (2026), arXiv:2511.03782 [cond-mat.supr-con].

[13] W. Yeadon and T. Hardy, The impact of AI in physics education: a comprehensive review from GCSE to university levels, Physics Education **59**, 025010 (2024), arXiv:2309.05163 [physics.ed-ph].

[14] L. Hsu, E. Brewe, T. M. Foster, and K. A. Harper, Resource letter RPS-1: Research in problem solving, Am. J. Phys. **72**, 1147 (2004).

[15] J. L. Docktor and J. P. Mestre, Synthesis of discipline-based education research in physics, Phys. Rev. ST Phys. Educ. Res. **10**, 020119 (2014).

[16] R. Hayano, Nurturing the future stars of physics—the International Physics Olympiad (IPhO), Acta Phys. Pol. B Proc. Suppl. **17**, 7 (2024).

[17] C. W. Miller, B. M. Zwickl, J. R. Posselt, R. T. Silvestrini, and T. Hodapp, Typical physics Ph.D. admissions criteria limit access to underrepresented groups but fail to predict doctoral completion, Sci. Adv. **5**, eaat7550 (2019).

[18] N. Newbury, M. Newman, J. Ruhl, S. Staggs, and S. Thorsett, *Princeton Problems in Physics with Solutions* (Princeton University Press, Princeton, New Jersey, 1991).

[19] J. Alper, M. Barany, A. Chavarri Villarello, S. Dahmen, W. Dean, K. Ganapathy, *et al.*, Leiden Declaration on Artificial Intelligence and Mathematics, Zenodo (2026). https://leidendeclaration.ai/.

[20] A. Avila, M. Bhargava, C. Birkar, P. Deligne, Y. Deng, S. Donaldson, *et al.*, A severe misalignment of AI in mathematics, Math and AI (2026). https://mathandai.org/.

[21] J. Ding, Y. Cen, and X. Wei, Using large language model to solve and explain physics word problems approaching human level (2023), arXiv:2309.08182 [cs.CL].

[22] S. Qiu, S. Guo, Z.-Y. Song, Y. Sun, Z. Cai, J. Wei, *et al.*, PHYBench: Holistic evaluation of physical perception and reasoning in large language models (2025), arXiv:2504.16074 [cs.CL].

[23] C. He, R. Luo, Y. Bai, S. Hu, Z. Thai, J. Shen, *et al.*, OlympiadBench: A challenging benchmark for promoting AGI with olympiad-level bilingual multimodal scientific problems, in *Proceedings of the 62nd Annual Meeting of the Association for Computational Linguistics (Volume 1: Long Papers)* (Association for Computational Linguistics, 2024) pp. 3828–3850.

[24] F. Yu, H. Wan, Q. Cheng, Y. Zhang, J. Chen, F. Han, *et al.*, HiPhO: How far are (M)LLMs from humans in the latest high school physics olympiad benchmark? (2025), arXiv:2509.07894 [cs.AI].

[25] X. Xu, Q. Xu, T. Xiao, T. Chen, Y. Yan, J. Zhang, *et al.*, UGPhysics: A comprehensive benchmark for undergraduate physics reasoning with large language models, in *Proceedings of the 42nd International Conference on Machine Learning*, Proceedings of Machine Learning Research, Vol. 267 (PMLR, 2025) pp. 69849–69877.

[26] D. J. H. Chung, Z. Gao, Y. Kvasiuk, T. Li, M. Münchmeyer, M. Rudolph, *et al.*, Theoretical physics benchmark (TPBench)—a dataset and study of AI reasoning capabilities in theoretical physics, Machine Learning: Science and Technology **6**, 030505 (2025), arXiv:2502.15815 [cs.LG].

[27] M. Tian, L. Gao, S. D. Zhang, X. Chen, C. Fan, X. Guo, *et al.*, SciCode: A research coding benchmark curated by scientists, in *Advances in Neural Information Processing Systems*, Vol. 37 (2024).

[28] M. Wang, R. Lin, K. Hu, J. Jiao, N. Chowdhury, E. Chang, *et al.*, FrontierScience: Evaluating AI's ability to perform expert-level scientific tasks (2026), arXiv:2601.21165 [cs.AI].

[29] T. Miao, W. Jin, M. Zhang, J. Tan, Y. Hu, T. Guo, *et al.*, PRL-Bench: A comprehensive benchmark evaluating LLMs' capabilities in frontier physics research (2026), arXiv:2604.15411 [cs.LG].

[30] Y. Wang, Y. Jiang, D. Golovanova, K. Das, H. Bae, Y. Zhao, *et al.*, QMBench: A research level benchmark for quantum materials research (2025), arXiv:2512.19753 [cond-mat.mtrl-sci].

[31] M. Zhu, M. Tian, X. Yang, T. Zhou, L. Yuan, P. Zhu, *et al.*, Probing the critical point (CritPt) of AI reasoning: a frontier physics research benchmark (2025), arXiv:2509.26574 [cs.AI].

[32] Terminal-Bench-Science Team, Terminal-Bench-Science: Evaluating AI agents on research workflows across scientific domains, Computer software (2026). https://github.com/harbor-framework/terminal-bench-science.

[33] M. Abouzaid, A. J. Blumberg, M. Hairer, J. Kileel, T. G. Kolda, P. D. Nelson, *et al.*, First Proof (2026), arXiv:2602.05192 [cs.AI].

[34] M. Abouzaid, A. J. Blumberg, M. Hairer, J. Kileel, T. G. Kolda, P. D. Nelson, *et al.*, First Proof solutions and comments (2026). https://1stproof.org/documents/FirstProofSolutionsComments.pdf.

[35] M. Abouzaid, N. Srivastava, R. Ward, and L. Williams, First Proof Second Batch (2026), arXiv:2606.18119 [cs.AI].

[36] T. Feng, J. Jung, S.-h. Kim, C. Pagano, S. Gukov, C.-C. Tsai, *et al.*, Aletheia tackles FirstProof autonomously (2026), arXiv:2602.21201 [cs.AI].

[37] H. Geng, A. Karch, C. Perez-Pardavila, S. Raju, L. Randall, M. Riojas, *et al.*, Information Transfer with a Gravitating Bath, SciPost Phys. **10**, 103 (2021), arXiv:2012.04671 [hep-th].

[38] S. Singam, N. G. Jones, and A. Prakash, Textured phase diagrams of featureless insulators (2026), arXiv:2605.20339 [cond-mat.str-el].

[39] W. H. Press, S. A. Teukolsky, W. T. Vetterling, and B. P. Flannery, *Numerical Recipes in C: The Art of Scientific Computing*, 2nd ed. (Cambridge University Press, New York, 1992).

[40] TheoPhysEval: Assessing AI agents at autonomous theoretical physics problem solving, Hugging Face dataset repository (2026). https://huggingface.co/datasets/RameshChandra1/TheoPhysEval.

[41] Harbor Framework Team, Harbor: A framework for evaluating and optimizing agents and models in container environments, Computer software (2026). https://doi.org/10.5281/zenodo.20953922.

[42] M. A. Merrill, A. G. Shaw, N. Carlini, B. Li, H. Raj, I. Bercovich, *et al.*, Terminal-Bench: Benchmarking

agents on hard, realistic tasks in command line interfaces, in *International Conference on Learning Representations* (2026) arXiv:2601.11868.

[43] OpenAI, GPT-6 Astra System Card (2026), published September 3, 2026. https://deploymentsafety.openai.com/gpt-6-astra.

[44] OpenAI, Codex is now generally available (2025), published October 6, 2025. https://openai.com/index/codex-now-generally-available/.

[45] Anthropic, Introducing Claude Opus 5.5 (2026), published September 22, 2026. https://www.anthropic.com/claude-opus-5-5.

[46] Anthropic, Claude 3.7 Sonnet and Claude Code (2025), published February 24, 2025. https://www.anthropic.com/news/claude-3-7-sonnet.

[47] Google DeepMind, Gemini 3.8 Flash: Model Card (2026), published September 2, 2026. https://deepmind.google/models/model-cards/gemini-3-8-flash/.

[48] The Antigravity Team, Introducing Google Antigravity, a new era in AI-assisted software development (2025), published November 18, 2025. https://antigravity.google/blog/introducing-google-antigravity.

[49] DeepSeek-AI, DeepSeek-V4.1-Flash: Pushing the limits of KV cache compression (2026), arXiv:2609.19969 [cs.CL].

[50] GLM-5-Team *et al.*, GLM-5: from vibe coding to agentic engineering (2026), arXiv:2602.15763 [cs.LG].

[51] Z.ai, GLM-5.3, Model card (2026), accessed October 6, 2026. https://huggingface.co/zai-org/GLM-5.3.

[52] A. Ansari, H. Sun, A. Z. Liu, M. Jabbour, Y. Ding, S. Girvin, *et al.*, How good are frontier models at physics? expert re-grading reveals broken evaluations and near-saturation of leading benchmarks (2026), arXiv:2609.13009 [cs.AI].

[53] W. Yeadon, S. Juárez, P. Mackay, T. J. Dowling, E. Agra, O.-o. Inyang, *et al.*, The answer is not the argument (2026), arXiv:2609.00264 [cs.AI].

[54] S. Kapoor, D. Jaganathan, and R. Govindarajan, Trapping and extreme clustering of finitely dense inertial particles near a rotating vortex pair, Journal of Fluid Mechanics **996**, A44 (2024), arXiv:2405.04949 [physics.flu-dyn].

[55] I. Bena, S. Giusto, E. J. Martinec, R. Russo, M. Shigemori, D. Turton, *et al.*, Smooth horizonless geometries deep inside the black-hole regime, Phys. Rev. Lett. **117**, 201601 (2016), arXiv:1607.03908 [hep-th].

[56] E. Morgensztern, C. Fierro Cota, and A. Mininno, Solver Agent: an agentic AI framework for theoretical physics computations applied to F-theory uplifts of O3-planes and S-folds (2026), arXiv:2609.35958 [hep-th].

[57] M. D. Schwartz, BootLoops 1.0 (2026), accessed October 8, 2026. https://bootloops.ai/.

[58] Anthropic, Claude Science, an AI workbench for scientists, is now available (2026), published June 30, 2026. https://www.anthropic.com/news/claude-science-ai-workbench.

[59] J. Gottweis, W.-H. Weng, A. Daryin, T. Tu, A. Palepu, P. Sirkovic, *et al.*, Towards an AI co-scientist (2025), arXiv:2502.18864 [cs.AI].

[60] C. Lu, C. Lu, R. T. Lange, Y. Yamada, S. Hu, J. Foerster, *et al.*, Towards end-to-end automation of AI research, Nature **651**, 914 (2026), arXiv:2606.15497 [cs.AI].

[61] A. Hell and L. Thiele, LLMs with in-context learning for algorithmic theoretical physics (2026), arXiv:2605.08212 [cs.LG].

[62] J. Schmitt, T. Gehrunger, J. Dekoninck, G. Bérczi, U. Kreitner, L. Price, *et al.*, ProofCouncil: An LLM agent for solving open mathematical problems (2026), arXiv:2607.09474 [cs.AI].

[63] G. Tsoukalas, A. Kovsharov, S. Shirobokov, A. Surina, M. Firsching, G. Bérczi, *et al.*, Advancing mathematics research with AI-driven formal proof search (2026), arXiv:2605.22763 [cs.AI].

[64] N. D. Mermin, What's wrong with this pillow?, Physics Today **42**, 9 (1989).

[65] I. Arav, T. Bertrand, S. Chapman, G. Policastro, and S. Waeber, Energy Transmission Across Holographic Conformal Interfaces in General Dimensions (2026), arXiv:2609.38318 [hep-th].

Appendix A: Problem collection

This Appendix contains a complete list of the problems in our collection. The objective of this appendix is to provide a quick and readable summary of the questions. For ease of reading we have lightly edited some of the prompts for readability. Output instructions provided to the agent are also omitted where this can be done without affecting the import of the question. Auxiliary data files are not included and LaTeX commands in prompts have been rendered rather than displayed verbatim. The full prompts used in the evaluation are available on Hugging Face and those are the ones that should be used for reproducibility.

1. Classical physics

a. Dominant spanwise scale of boundary-layer perturbations

A fluid is flowing in the x direction over a flat plate of length L. The fluid approaches the flat plate at free stream velocity U_0. The Reynolds number based on L and U_0 is $Re = 160000$. Calculate the spanwise normalized length scale (L_s/L) of the *dominant initial* streamwise spatial perturbation velocity structures that develop on a horizontal plane at a vertical height of $y/L = 0.01$ from the plate. Assume spanwise to be periodic with length-scale L.

b. Reconstructing an autonomous differential equation from its trajectory

Find an autonomous differential equation where no derivative is of order greater than 1, whose solution matches the figure given in Fig. 5 in the shown range. Assume that the equation has no more than five terms, and all coefficients are round numbers between -1000 and 1000.

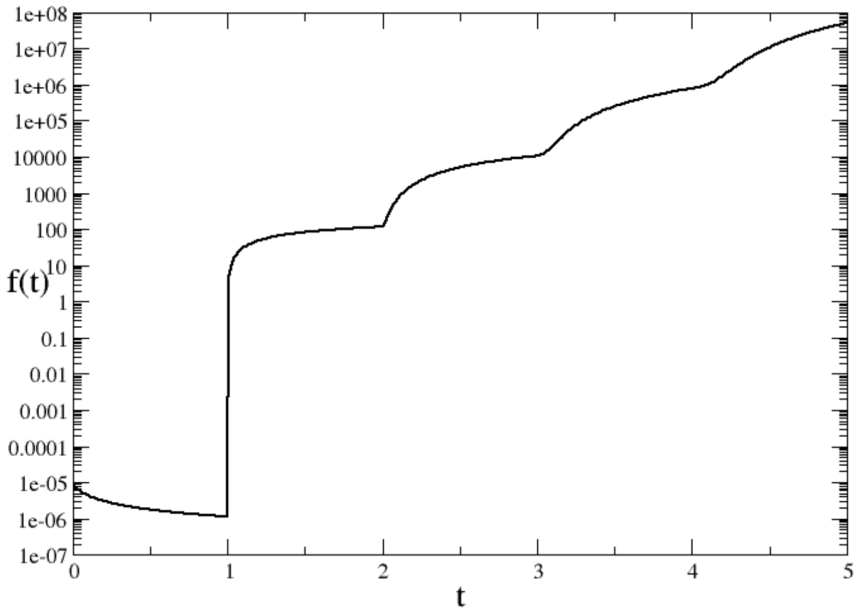

Figure 5: Source trajectory for reconstructing the autonomous equation.

c. Inertial-particle attraction basins in co-rotating vortex flows

Consider a flow field, $\boldsymbol{u}(\boldsymbol{x},t)$, as a function of space, $\boldsymbol{x}$, and time, t, due to a pair of co-rotating vortices, except that the flow field goes as $1/r^n$ away from the vortices (instead of the typical $1/r$), given by

$$\boldsymbol{u}(\boldsymbol{x},t)=\pi\hat{e}_z\times\left[(1-e^{-|\boldsymbol{x}-\boldsymbol{X}|^{n+1}/b^{n+1}})\frac{\boldsymbol{x}-\boldsymbol{X}}{|\boldsymbol{x}-\boldsymbol{X}|^{n+1}}+(1-e^{-|\boldsymbol{x}+\boldsymbol{X}|^{n+1}/b^{n+1}})\frac{\boldsymbol{x}+\boldsymbol{X}}{|\boldsymbol{x}+\boldsymbol{X}|^{n+1}}\right], \tag{A1}$$

where $\boldsymbol{X}=(\cos(2\pi t)/2,\sin(2\pi t)/2)$ (given in the Cartesian coordinates), and the center of the two vortices are at $\boldsymbol{X}$ and $-\boldsymbol{X}$; b measures the vortex radius. In this flow field we put one way coupled inertial particles, denser than the background fluid, in the unsteady Stokes regime, following the Maxey-Riley equation with Basset-Boussinesq history force included, without Fàxen corrections. This is similar to the work in https://doi.org/10.1017/jfm.2024.706. The particle is characterised by its Stokes number, St, (with vortex-corotation time period as the reference time scale) and density ratio parameter, $R=3/(2\rho_p/\rho_f+1)$, where ρ_p and ρ_f are the particle and fluid densities. This system has inertial particle attractors. Start the particles at rest in the co-rotating frame of reference, $\boldsymbol{v}(t)=0_{rot}$ for $t\leq 0$. For this initial condition, areas of the basins of attraction, for attractors *not* passing through the vortices, at the parameter values $(n,b,St,R)=(1.5,0.2,0.15,1/1.7)$ is B_1, at $(n,b,St,R)=(1.5,0.2,0.2,1/1.5)$ is B_2, and at $(n,b,St,R)=(1.5,0.2,0.211,1/1.2)$ is B_3. Calculate $(B_1+10^5B_2+10^6B_3)/d^2$ rounded up correctly to the first decimal place, where d is the distance between the centers of the vortices.

d. Radiation damping in modified electrodynamics

In ordinary Maxwell electrodynamics the retarded Green function has support on the light cone,

$$G(x,y)=\delta(\lambda)\,\theta(x^0-y^0),\qquad \lambda=(x-y)^2. \tag{A2}$$

Consider instead the covariant short-distance modification

$$G_d(x,y)=\delta(\lambda+d^2)\,\theta(x^0-y^0), \tag{A3}$$

where $d>0$ is a small length scale. The support of the propagator is moved from the light cone to a timelike hyperboloid. A charged particle therefore interacts with its own motion at a finite retarded time. The resulting radiation-reaction equation is a state-dependent neutral functional differential equation (FDE), rather than the third-order Lorentz–Dirac ODE.

Use the mostly-positive metric, with $x^0=t$,

$$A\cdot B=-c^2A^0B^0+\boldsymbol{A}\cdot\boldsymbol{B}. \tag{A4}$$

The potential generated by a four-current is

$$A^\mu(x)=\frac{1}{2\pi\epsilon_0 c}\int j^\mu(y)G_d(x,y)\,d^4y. \tag{A5}$$

Let a particle of charge magnitude q have worldline $\alpha^\mu(\tau)$, parametrized by proper time. Starting from Eq. (A3), derive the retarded self-field. Next, add an attractive Coulomb force from a fixed, oppositely charged source at the origin,

$$\boldsymbol{f}_{\rm C}(t)=-k_eq^2\frac{\boldsymbol{r}(t)}{|\boldsymbol{r}(t)|^3},\qquad k_e=\frac{1}{4\pi\epsilon_0}. \tag{A6}$$

Define

$$\boldsymbol{u}=\gamma\boldsymbol{v},\qquad \gamma=\sqrt{1+\frac{|\boldsymbol{u}|^2}{c^2}}, \tag{A7}$$

so that the velocity is

$$\boldsymbol{v}=\frac{\boldsymbol{u}}{\gamma}. \tag{A8}$$

For numerical work, use the nine-component state

$$Y = (\boldsymbol{r}, \boldsymbol{u}, \boldsymbol{a}_u), \qquad \boldsymbol{a}_u = \frac{d\boldsymbol{u}}{dt}, \tag{A9}$$

and the neutral differential-algebraic form

$$\dot{\boldsymbol{r}} = \frac{\boldsymbol{u}}{\gamma}, \qquad \dot{\boldsymbol{u}} = \boldsymbol{a}_u, \qquad 0 = -\boldsymbol{a}_u + \frac{\boldsymbol{f}_{\mathrm{C}} + \boldsymbol{f}_{\mathrm{self}}}{m}. \tag{A10}$$

Note that the appearance of the delayed $\boldsymbol{a}_u$ in the self-field makes Eq. (A10) a functional differential equation (FDE).

Use the following SI values:

$$c = 299\,792\,458\,\mathrm{m\,s^{-1}}, \qquad q = 1.602\,176\,634 \times 10^{-19}\,\mathrm{C}, \tag{A11}$$

$$m_e = 9.109\,383\,713\,9 \times 10^{-31}\,\mathrm{kg}, \qquad k_e = 8.987\,551\,786\,17 \times 10^{9}\,\mathrm{N\,m^2\,C^{-2}}, \tag{A12}$$

$$d = 3.381\,528\,384\,551\,39 \times 10^{-14}\,\mathrm{m}. \tag{A13}$$

Here c and q are exact SI defining values, while m_e and k_e use the 2022 CODATA values. Treat q as the positive magnitude of the electron charge; the minus sign making the external interaction attractive is already present in Eq. (A6).

The bare mass appearing in the equations of motion is not m_e. Use

$$m = m_e - \frac{k_e q^2}{2dc^2} = 8.729\,826\,059\,154\,17 \times 10^{-31}\,\mathrm{kg}. \tag{A14}$$

The subtracted electromagnetic contribution is restored locally by the self-interaction.

For numerical conditioning you may nondimensionalize the problem. The following scales reproduce the original dimensionless normalization exactly:

$$L_* = 3.381\,528\,384\,551\,39 \times 10^{-11}\,\mathrm{m}, \qquad T_* = 3.383\,869\,367\,939\,26 \times 10^{-17}\,\mathrm{s}, \tag{A15}$$

$$M_* = 4.554\,691\,856\,95 \times 10^{-31}\,\mathrm{kg}, \qquad Q_* = 1.602\,176\,634 \times 10^{-18}\,\mathrm{C}. \tag{A16}$$

They give $c = 300$, $m_e = 2$, $q = 0.1$, $k_e = 1500$, and $d = 10^{-3}$ in scaled units.

An FDE requires a complete past history, not merely a state at $t = 0$. Supply the following circular history for every $t \le 0$, or at minimum over every past interval requested by the solver.

Define

$$v_0 = 0.0072973527c = 2.187\,691\,302\,825\,94 \times 10^{6}\,\mathrm{m\,s^{-1}}, \tag{A17}$$

$$\gamma_0 = \frac{1}{\sqrt{1 - v_0^2/c^2}} = 1.0000266267416513, \tag{A18}$$

$$R_0 = \frac{k_e q^2}{m_e \gamma_0 v_0^2} = 5.291\,631\,009\,790\,22 \times 10^{-11}\,\mathrm{m}, \tag{A19}$$

$$\Omega = \frac{v_0}{R_0} = 4.134\,247\,642\,699\,23 \times 10^{16}\,\mathrm{rad\,s^{-1}}. \tag{A20}$$

Thus the ordinary cyclic frequency is

$$\nu_0 = \frac{\Omega}{2\pi} = 6.579\,859\,483\,015\,98 \times 10^{15}\,\mathrm{Hz}. \tag{A21}$$

Notice that the physical electron mass m_e, rather than the bare mass m, appears in the circular-history radius. This is equivalent to adding the local electromagnetic mass correction back to m.

The full nine-component history is

$$\boldsymbol{r}_h(t) = \begin{pmatrix} R_0 \cos(\Omega t) \\ R_0 \sin(\Omega t) \\ 0 \end{pmatrix}, \qquad \boldsymbol{u}_h(t) = \begin{pmatrix} -\gamma_0 v_0 \sin(\Omega t) \\ \gamma_0 v_0 \cos(\Omega t) \\ 0 \end{pmatrix}, \tag{A22}$$

and

$$\boldsymbol{a}_{u,h}(t) = \begin{pmatrix} -\gamma_0 \Omega v_0 \cos(\Omega t) \\ -\gamma_0 \Omega v_0 \sin(\Omega t) \\ 0 \end{pmatrix}. \tag{A23}$$

In particular,

$$\boldsymbol{r}(0) = (5.291\,631\,009\,790\,22 \times 10^{-11}\,\mathrm{m}, 0, 0), \tag{A24}$$

$$\boldsymbol{u}(0) = (0, 2.187\,749\,553\,917\,07 \times 10^{6}\,\mathrm{m\,s^{-1}}, 0), \tag{A25}$$

$$\boldsymbol{a}_u(0) = (-9.044\,698\,436\,097\,94 \times 10^{22}\,\mathrm{m\,s^{-2}}, 0, 0). \tag{A26}$$

The numerical solution must be continuous with this history at $t = 0$.

Final question and deliverables What are the first three values of

$$t > 3.383\,869\,367\,94 \times 10^{-19}\,\mathrm{s} \tag{A27}$$

at which

$$\frac{d^2|\boldsymbol{r}|}{dt^2} = 0? \tag{A28}$$

Report the three times in attoseconds to four decimal places in the format "ZEROES=[z1, z2, z3]". A zero at, or numerically indistinguishable from, $t = 0$ must not be counted. Do not neglect to use the keyword ZEROES and the precise output format given for your final deliverable.

e. *Two-body problem in modified electrodynamics*

Consider two moving charges with no external force. Use dimensionless units with $c = R = q = 1$ and charges $q_1 = +1$, $q_2 = -1$. We will modify the standard electromagnetic propagator to

$$G_d(x, y) = \delta\big((x - y)^2 + d^2\big)\,\theta(x^0 - y^0).$$

Take $d = 1/4$. We use the notation

$$\dot{\boldsymbol{r}}_i = \boldsymbol{u}_i/\gamma_i, \qquad \gamma_i = \sqrt{1 + |\boldsymbol{u}_i|^2/c^2}.$$

Also, define $\beta_0 = .05$ and $\Omega = \beta_0 c/R = 0.05$. With $\gamma_0 = (1 - \beta_0^2)^{-1/2}$, use Coulomb's constant

$$k_e = \frac{4\gamma_0\beta_0^2 c^2 R}{q^2}.$$

Take the particle masses to be

$$m = 1 - \frac{k_e q^2}{2dc^2}$$

For every $t \le 0$ we prescribe

$$\boldsymbol{r}_{1,h} = R(\cos\Omega t, \sin\Omega t, 0)$$

with $\boldsymbol{r}_{2,h} = -\boldsymbol{r}_{1,h}$.

Question Let $T_0 = 2\pi/\Omega = 40\pi$, which is the naive period of the orbit. Determine $\boldsymbol{r}_1(10T_0)$ and $\boldsymbol{r}_2(10T_0)$, with $10T_0 = 400\pi$. Report the two coordinate triples up to an absolute accuracy of 10^{-4} per coordinate.

2. Stochastic processes and biological physics

a. *Theta-logistic growth*

Consider a microbial species whose population abundance $X_t > 0$ follows θ-logistic growth with environmental noise, described by the Itô stochastic differential equation

$$dX_t = X_t\left[1 - \left(\frac{X_t}{K_\theta}\right)^{\theta}\right]dt + \sqrt{\sigma_\theta}\,X_t\,dW_t, \tag{A29}$$

where W_t is standard Brownian motion and time is measured in units of the intrinsic growth timescale. Compare ordinary logistic growth, $\theta = 1$, with $\theta = 2$. For each model, choose $K_\theta > 0$ and $0 < \sigma_\theta < 2$ so that the stationary probability distribution supported on $(0, \infty)$ has mean 1 and variance 1, in the chosen abundance units.

An instantaneous sample of volume V contains a Poisson-distributed number of cells with conditional mean VX_t, with abundance and volume measured in compatible reference units. Assume that the species is detected if the sample contains at least one cell. Let V_θ be the smallest sample volume for which the detection probability, averaged over stationary population fluctuations, is 95%. Derive the stationary distributions and determine V_2/V_1. Report the ratio to one decimal place.

b. Microbial cross-feeding

Consider S microbial species with abundances $N_i(t) \geq 0$, interacting with M resources with concentrations $R_\alpha(t) \geq 0$. Their dynamics are

$$\frac{dN_i}{dt} = N_i \left[\sum_{\alpha=1}^{M} g_{i\alpha} R_\alpha - m_i \right], \tag{A30}$$

$$\frac{dR_\alpha}{dt} = K_\alpha - \omega_\alpha R_\alpha - R_\alpha \sum_{i=1}^{S} c_{i\alpha} N_i + \sum_{i=1}^{S} p_{i\alpha} N_i. \tag{A31}$$

Here $c_{i\alpha}$, $g_{i\alpha}$ and $p_{i\alpha}$ describe depletion, growth and secretion, respectively. The parameter $m_i > 0$ is the maintenance cost, $K_\alpha \geq 0$ is the external supply, and $\omega_\alpha > 0$ is the resource loss rate.

For each (i, α), the three coefficients are jointly Gaussian, with means $(\mu_c, \mu_g, \mu_p)/M$ and standard deviations $(\sigma_c, \sigma_g, \sigma_p)/\sqrt{M}$. Different pairs are independent, and

$$\mathrm{corr}(c, g) = \rho, \qquad \mathrm{corr}(c, p) = r, \qquad \mathrm{corr}(g, p) = \rho r. \tag{A32}$$

Here $\mu_c, \mu_g, \mu_p \geq 0$ and $\sigma_c, \sigma_g, \sigma_p > 0$ are of order one; $0 < \rho \leq 1$ and $-1 \leq r \leq 1$. The m_i, K_α and ω_α are independent of these couplings.

Consider the limit of large S and M at fixed S/M. Let S^* be the number of surviving species at an uninvadable fixed point, and define the total removal rate of resource α by

$$F_\alpha = \omega_\alpha + \sum_{i=1}^{S} c_{i\alpha} N_i. \tag{A33}$$

Assume that $0 < S^*/M < 1$, $F_\alpha > 0$ and $R_\alpha > \max(0, r\sigma_p/\sigma_c)$ for every resource. Use the self-averaging cavity approximation on the branch with $-\partial N_i/\partial m_i > 0$ for surviving species and $\partial R_\alpha/\partial K_\alpha > 0$.

Replace each maintenance cost m_i by $m_i + \varepsilon\xi_i$, where the ξ_i are independent, have zero mean and unit variance, and are independent of all model parameters. Evaluate the response at $\varepsilon = 0$, holding the surviving set fixed, and define

$$Y = \frac{1}{S^*} \sum_{i:N_i>0} \left(\frac{dN_i}{d\varepsilon} \right)^2. \tag{A34}$$

Within this approximation, derive the threshold $\rho^\star$ above which Y remains finite. Express it using only r, σ_p/σ_c, S^*/M, and statistics of the resource distribution, expressed as averages of functions of R_α and F_α. Any auxiliary quantity must be determined by the same parameters and statistics.

Evaluate $\rho^\star$ to four significant figures for $r = -0.8$, $\sigma_c = 4$, $\sigma_p = 5$, $\sigma_g = 3$, $S/M = 1.5$ and $S^*/M = 0.4$, when three fifths of the resources have $(R_\alpha, F_\alpha) = (4, 10)$ and two fifths have $(R_\alpha, F_\alpha) = (0.25, 1.25)$.

c. Minimum of a rescaled positive random-walk bridge

Let X_n be a simple random walk of length N with $X(0) = X(N) = 0$ and $X_n > 0$ for $0 < n < N$. Consider the process $Y_n = X_n/(n(N-n))$. Let the minimum of the process Y_n be $R_N = \min_{1 \leq n < N-1}(Y_n)$. Find the probability that $R_N \leq rN^{-2}$ for r order 1, and large but finite N. Prove this result analytically. Report the numerical value of the coefficient in the leading-order asymptotic probability when $r = 2, 6, 9$.

d. *Minimax strategies in the three-hole game*

There are two players who play alternately, starting with player 1. Initially, there are 3 labelled holes, and each player sits in a different hole with one hole being empty. Each player knows which hole they are in but does not know where the other player is. Each player, on their turn, can order an air strike to any of the holes (including the one they are in). If they hit the opposing player, the game ends immediately and they win. If not, the game continues and it is now the opposing player's turn. (If they hit themselves, we allow them to remain unhurt and the game continues). Players can note down or remember the locations of all previous air strikes by both players, i.e. there are no restrictions on the players' memory. Players are allowed to use random numbers or any other methodology to determine where to strike on their turn, i.e. stochastic strategies are allowed.

Find the best play for each player, and the expected payoff for each when both are using this strategy to play (assume 1 point for a win, and 0 for a loss).

Or if it needs to be more precise: Compute the minimax strategy for Player 1 and Player 2, and the expected payoff for each when both are using the minimax strategy to play (assume 1 point for a win, and 0 for a loss).

e. *Minimax lysogeny strategies in bacteriophage competition*

Consider a system consisting of one type of bacteria, with population density B, and two types of bacteriophage, with densities P1 and P2, which can infect these bacteria. Cross infection is not allowed, i.e. if a bacterium is infected by type 1, then it cannot be infected by type 2 phage. Infection happens at a rate eta per bacterium per phage, same for both types of phage. Upon infection, at a rate delta, an infected bacterium either dies releasing beta new phage of the same type, or becomes a lysogen of that type (thus there are two types of lysogen bacteria with densities L1 and L2.) The probability of the infected bacterium become a lysogen is f1 or f2, depending on the type of phage. Phage of both types will attempt infection of lysogens with the same rate constant eta, but the lysogens simply absorb such phage without any effect to themselves. All bacteria exhibit logistic growth with a growth rate gamma and a carrying capacity K.

Set up Lotka Volterra like population dynamics equations describing the above system For the case where gamma=K=eta=1, beta=100 and delta is infinitely large, run the population dynamics starting with initial bacteria at 0.001, lysogens at 0, and both phage densities at 10^{-7}. At steady state, compute payoff=(L1-L2)/(L1+L2). Do this for as many pairs of (f1,f2) values as you need to compute the minimax strategy for both phage to a precision of 0.01. That is, I want you to compute the (f1*,f2*) pair such that if phage 1 used any other strategy f1 against phage 2 using f2* it would result in a lower payoff, and if phage 2 used any other strategy f2 against phage 1 using f1* then it would result in a higher payoff. Show the code used to compute the final answer.

3. Nonequilibrium statistical mechanics

a. *Analytical thermostat evolution in sheared SLLOD dynamics*

Consider the Gaussian thermostatted SLLOD equations of motion for particles that are subject to a simple shear flow with a fixed strain rate $\dot{\gamma}$ in the $\hat{x}$ direction.

$$\dot{r}_i = \frac{p_i}{m_i} + \hat{i}\,\dot{\gamma}\, r_{yi}, \tag{1}$$

$$\dot{p}_i = F_i - \hat{i}\,\dot{\gamma}\, p_{yi} - \alpha p_i, \tag{2}$$

where

$$\alpha = \frac{\sum_i \frac{1}{m_i}\left(F_i \cdot p_i - \dot{\gamma}\, p_{xi} p_{yi}\right)}{\sum_i \frac{p_i \cdot p_i}{m_i}}. \tag{3}$$

We derive the numerical integration scheme for the equations of motion above using the operator-splitting method. To do so, we split these equations into two groups, **A** and **B**, where

$$\mathbf{A}: \qquad \dot{r}_i = \frac{p_i}{m_i} + \hat{i}\,\dot{\gamma}\,r_{yi}, \qquad \dot{p} = 0, \tag{4}$$

$$\mathbf{B}: \qquad \dot{r}_i = 0, \qquad \dot{p}_i = F_i - \hat{i}\,\dot{\gamma}\,p_{yi} - \alpha p_i. \tag{5}$$

The numerical integration scheme for part **A** can be easily derived. In the equations for part **B** note that α explicitly depends on the momenta, precluding the use of the operator-splitting method. To remedy this, we split the part **B** equations of motion further into two groups, $\mathbf{B}_1$ and $\mathbf{B}_2$, where

$$\mathbf{B}_1: \qquad \dot{r}_i = 0; \qquad \dot{p}_i = -\hat{i}\,\dot{\gamma}\,p_{yi} - \alpha_1 p_i; \qquad \text{where} \qquad \alpha_1 = \frac{\sum_i \frac{1}{m_i}\left(-\dot{\gamma}\,p_{xi}p_{yi}\right)}{\sum_i \frac{p_i \cdot p_i}{m_i}}. \tag{7}$$

$$\mathbf{B}_2: \qquad \dot{r}_i = 0; \qquad \dot{p}_i = F_i - \alpha_2 p_i; \qquad \text{where} \qquad \alpha_2 = \frac{\sum_i \frac{1}{m_i}\left(F_i \cdot p_i\right)}{\sum_i \frac{p_i \cdot p_i}{m_i}}. \tag{8}$$

It is now possible to get analytical expressions of α_1 and α_2 as a function of time. Derive the expression for $\alpha_1(t)$. Assume that $\alpha_1(0) = C_0$ and $\dot{\alpha}_1(0) = C_1$. Report the value of $\alpha_1(2)$ assuming $C_0 = 0.75$ and $C_1 = 0.25$.

b. Random walk model of glass yielding

Consider a random walk model with $2N + 1$ states. The states labeled i denote the energy basins in a glass whose depths are given by $\epsilon_i = i/2N$ with $i \in [0, 2N]$. The system is subjected to repeated cycles of strain of a given amplitude γ. The system, residing in a given basin i, will become unstable in a given cycle if $\epsilon_i < \gamma^2$ and will make a transition to state $i \pm 1$ with transition probability

$$p_{i\to j} = \left(1 - \frac{i}{2N}\right)\delta_{i+1,j} + \frac{i}{2N}\delta_{i-1,j}. \tag{1}$$

The transition rates are given by rates $W_{i\to j} = p_{i\to j}/\tau_i$. The time required to make a transition out of state i then becomes

$$\tau_i = \begin{cases} 1, & \text{for } \epsilon_i < \gamma^2, \\ 1 + \dfrac{\left(\sqrt{\epsilon_i} - \gamma\right)^2}{2\alpha P_U(t)}, & \text{for } \epsilon_i > \gamma^2. \end{cases} \tag{2}$$

where $P_U(t)$ is the instantaneous probability of being in unstable states, defined to be the set of states for which $\epsilon_i < \gamma^2$.

Below what strain amplitude γ^* will the system always remain in a frozen state ($P_U = 0$) regardless of the initial condition of the system, assuming that the detailed balance condition holds within the set of stable states. Consider $N = 210$ and $\alpha = 10^{-9}$.

c. Steady-state energies under cyclic shear

Consider the following stochastic mesostate model for an athermal, quasistatically sheared amorphous solid. Each mesostate is characterized by a minimum energy $E_0 < 0$ and a stress-free strain γ_0. At an applied strain γ, the energy of the mesostate is

$$E(\gamma; E_0, \gamma_0) = E_0 + \frac{\mu}{2}(\gamma - \gamma_0)^2.$$

The mesostate is stable within the interval

$$\gamma_- < \gamma < \gamma_+, \qquad \gamma_\pm = \gamma_0 \pm \sqrt{-E_0}.$$

Whenever the applied strain reaches either stability boundary, the system immediately transitions to a new mesostate. The new value of E_0 is drawn independently from the Gaussian density of states

$$P_0(E_0) = \frac{1}{Z} \exp\left[-\frac{(E_0+0.5)^2}{2(0.05)^2}\right], \qquad -1 < E_0 < 0,$$

where Z is the normalization constant. The new stress-free strain γ_0 is set equal to the applied strain at which the transition occurs. Take $\mu = 2$.

Initialize the system in the mesostate

$$E_0 = -0.1, \qquad \gamma_0 = 0.$$

Subject it to 1000 quasistatic shear cycles, with each cycle following the strain path

$$0 \longrightarrow \gamma_{\max} \longrightarrow -\gamma_{\max} \longrightarrow 0, \qquad \gamma_{\max} = 0.9.$$

At the end of each cycle, when $\gamma = 0$, record both the minimum mesostate energy E_0 and the total energy

$$E(0; E_0, \gamma_0) = E_0 + \frac{\mu}{2}\gamma_0^2.$$

For each realization, average these quantities over cycles 801 through 1000. Then average the resulting values over 100 independent realizations.

What are the resulting ensemble-averaged late-time values of E and E_0?

4. Lattice theories

a. Chiral susceptibilities of interacting staggered fermions

Consider two flavors of Grassmann-valued fermion fields, $\psi_{a,i}$ and $\bar{\psi}_{a,i}$, where the flavor index is $a = 1, 2$ and the lattice site is denoted by $i = (x_i, y_i, z_i)$, with $x_i, y_i, z_i = 0, 1, \cdots, L-1$. The lattice is a three-dimensional cubic lattice with periodic geometry. Let $\hat{e}_\alpha$ ($\alpha = 1, 2, 3$) denote the unit vectors on the lattice in the x-, y-, and z-directions, respectively.

The Euclidean action is $S = S_{\text{free}} + S_{\text{int}}$, where the first term is the free massless staggered-fermion action given by

$$S_{\text{free}} = \sum_{i,j,a} \bar{\psi}_{a,i} M_{ij} \psi_{a,j}, \tag{1}$$

with the fermion matrix

$$M_{ij} = \frac{1}{2} \sum_{\alpha=1}^{3} \eta_{i,\alpha} \left(\delta_{i,j+\hat{e}_\alpha} - \delta_{i,j-\hat{e}_\alpha}\right). \tag{2}$$

The staggered phase factors are $\eta_{i,1} = 1$, $\eta_{i,2} = (-1)^{x_i}$, $\eta_{i,3} = (-1)^{x_i+y_i}$, which correspond to a π-flux through every elementary plaquette. Although the lattice is periodic, the fermion fields satisfy anti-periodic boundary conditions in all three spatial directions. Equivalently, the matrix M is taken to obey anti-periodic boundary conditions. The second term in the action S defined above is the interaction term given by

$$S_{\text{int}} = -U_B \sum_{a,i,\alpha} \left(\bar{\psi}_{a,i}\psi_{a,i}\right)\left(\bar{\psi}_{a,i+\hat{e}_\alpha}\psi_{a,i+\hat{e}_\alpha}\right) - U_I \sum_i \left(\bar{\psi}_{1,i}\psi_{1,i}\right)\left(\bar{\psi}_{2,i}\psi_{2,i}\right). \tag{3}$$

The first term above is a nearest-neighbor four-fermion interaction between fermions of the same flavor, while the second term is an on-site four-fermion interaction between different flavors.

For any observable O depending on the Grassmann fields, define its expectation value by

$$\langle O \rangle = \frac{1}{Z} \int \prod_i [d\bar{\psi}_{1,i} d\psi_{1,i}][d\bar{\psi}_{2,i} d\psi_{2,i}]\, e^{-S} O, \tag{4}$$

where the partition function is

$$Z = \int \prod_i [d\bar{\psi}_{1,i} d\psi_{1,i}][d\bar{\psi}_{2,i} d\psi_{2,i}]\, e^{-S}. \tag{5}$$

Using this definition, consider the two chiral condensate susceptibilities

$$\chi_1 = \frac{1}{2L^3} \sum_{i,j} \left\langle \bar{\psi}_{1,i} \psi_{1,i} \bar{\psi}_{1,j} \psi_{1,j} \right\rangle, \tag{6}$$

$$\chi_2 = \frac{1}{2L^3} \sum_{i,j} \left\langle \bar{\psi}_{1,i} \psi_{1,i} \bar{\psi}_{2,j} \psi_{2,j} \right\rangle. \tag{7}$$

Problem: Compute χ_1 and χ_2 for a lattice of size $L = 10$ with couplings $U_B = 1$, $U_I = 0.01$. Your numerical results should be accurate to approximately 1%.

b. Finite-temperature correlations in a three-state lattice model

Consider a quantum many-body system defined on a two-dimensional square lattice. The lattice sites are labeled by $i = (x_i, y_i)$, where $x_i, y_i = 0, 1, \ldots, L-1$. Periodic boundary conditions are imposed in both spatial directions.

At each lattice site i there is a three-dimensional local Hilbert space with orthonormal basis states $|s_i\rangle$ where $s_i = 0, 1, 2$. In a matrix notation we will define

$$|0\rangle = \begin{pmatrix} 1 \\ 0 \\ 0 \end{pmatrix}, \qquad |1\rangle = \begin{pmatrix} 0 \\ 1 \\ 0 \end{pmatrix}, \qquad |2\rangle = \begin{pmatrix} 0 \\ 0 \\ 1 \end{pmatrix}.$$

In this matrix notation we define the following local operators acting on the Hilbert space at site i:

$$P_i = \begin{pmatrix} 0 & 0 & 0 \\ 0 & 0 & 0 \\ 0 & 0 & \mu \end{pmatrix}, \qquad Q_i = \begin{pmatrix} 0 & q & 0 \\ q & 0 & 1 \\ 0 & 1 & 0 \end{pmatrix}, \qquad R_i = \begin{pmatrix} 0 & 1 & 0 \\ 1 & 0 & 1 \\ 0 & 1 & 0 \end{pmatrix}. \tag{8}$$

Each operator acts non-trivially only on site i and as the identity on all other lattice sites.

The lattice Hamiltonian is given by

$$H = -\sum_{\langle ij \rangle} Q_i Q_j - \sum_i P_i, \tag{9}$$

where $\langle ij \rangle$ denotes nearest-neighbor pairs on the square lattice.

Consider the finite-temperature Euclidean correlation function

$$C_{ij}(t) = \frac{1}{Z} \operatorname{Tr}\left[e^{-(\beta - t)H} R_i e^{-tH} R_j \right], \qquad 0 \le t \le \beta, \tag{10}$$

where the partition function is

$$Z = \operatorname{Tr}\left(e^{-\beta H} \right). \tag{11}$$

Using this correlation function, define the observables

$$\chi = \frac{1}{L^2} \sum_{i,j} \int_0^\beta dt\, C_{ij}(t), \tag{12}$$

$$F_t = \frac{1}{L^2} \sum_{i,j} \int_0^\beta dt\, C_{ij}(t) \cos\left(\frac{2\pi t}{\beta} \right), \tag{13}$$

$$F_x = \frac{1}{L^2} \sum_{i,j} \int_0^\beta dt\, C_{ij}(t) \cos\left(\frac{2\pi (x_i - x_j)}{L} \right). \tag{14}$$

Problem: Compute χ, F_x and F_t for $L = 10$, $\beta = 10$, $q = 0.5$ and $\mu = 6.41$. Your numerical result should be accurate to approximately 1%.

c. *Imaginary-time energy in the repulsive Hubbard model*

Consider the repulsive Hubbard model on a two-dimensional square lattice. The system consists of equal numbers of spin-up and spin-down electrons that hop between nearest-neighbor lattice sites. Whenever two electrons of opposite spin occupy the same lattice site, they experience an on-site Coulomb repulsion.

The lattice sites are labeled by $i = (x_i, y_i)$, where $x_i, y_i = 0, 1, \ldots, L-1$. Periodic boundary conditions are imposed in both spatial directions. In the Fock-space formulation, the creation and annihilation operators for an electron of spin $\sigma = \uparrow, \downarrow$ at lattice site i are denoted by $c^\dagger_{\sigma,i}$ and $c_{\sigma,i}$, respectively.

The Hamiltonian of the repulsive Hubbard model is

$$H = -\sum_{\langle ij\rangle,\sigma} \left(c^\dagger_{\sigma,i} c_{\sigma,j} + c^\dagger_{\sigma,j} c_{\sigma,i} \right) + U \sum_i c^\dagger_{\uparrow,i} c_{\uparrow,i} c^\dagger_{\downarrow,i} c_{\downarrow,i}, \tag{15}$$

where $\langle ij\rangle$ denotes nearest-neighbor pairs of lattice sites and $U > 0$ is the strength of the on-site repulsive interaction.

Next, define the many-body state $|\psi\rangle$ by placing one spin-up electron and one spin-down electron on every lattice site whose coordinates satisfy $x_i \equiv 0 \pmod 2$, and $y_i \equiv 0 \pmod 2$. Thus, the occupied sites are

$$(0,0),\ (0,2),\ (2,0),\ (2,2),\ \ldots$$

Assuming that L is even there are exactly $L^2/4$ such lattice sites, and hence the state $|\psi\rangle$ contains $L^2/4$ spin-up electrons and $L^2/4$ spin-down electrons. Every occupied lattice site is therefore doubly occupied.

Problem: Compute the observable $\mathcal{E}$ given by the expression

$$\mathcal{E} = \frac{\langle\psi| H e^{-H/2} |\psi\rangle}{\langle\psi| e^{-H/2} |\psi\rangle}, \tag{16}$$

for $L = 16$ and $U = 8.0$. Your numerical result should be accurate to approximately 1%.

5. Quantum phases of matter

a. *Criticality and stability of a class-D fermion-parity pump*

Consider one-dimensional class D fermionic systems, with no microscopic symmetries other than fermion parity. Restrict to the trivial phase and to free-fermion models.

Using the suspension construction, construct a two-parameter Hamiltonian corresponding to a fermion parity pump.

(a) What is the central charge of the critical theory at the diabolical point?

(b) Under free-fermion perturbations, what does the diabolical point destabilize to?

b. *Transitions between partially symmetry-broken phases*

Consider the Hamiltonian

$$H = -\sum_{\langle j,k\rangle} \cos(\theta_j - \theta_k) - \sum_{\ell=1,2,\ldots} \gamma_\ell \sum_j \cos(\ell Q \theta_j),$$

on a three-dimensional lattice, where Q is a positive integer. Assume that

$$\gamma_2, \gamma_3, \gamma_4, \ldots > 0.$$

What is the generic nature of the transition between the partial symmetry-breaking (SSB) phases obtained by tuning through $\gamma_1 = 0$, for each Q?

c. Accidental Dirac nodes in a maple-leaf spinon model

Consider the following six-band single-particle Bloch Hamiltonian for a uniform U(1) spinon ansatz on the maple-leaf lattice:

$$h(\mathbf{k}) = \begin{pmatrix} \lambda_z & t_h & t_t PQ & t_d Q & t_t Q & t_h \\ t_h & \lambda_z & t_h & t_t Q & t_d P^{-1} & t_t P^{-1} \\ t_t P^{-1}Q^{-1} & t_h & \lambda_z & t_h & t_t P^{-1} & t_d P^{-1}Q^{-1} \\ t_d Q^{-1} & t_t Q^{-1} & t_h & \lambda_z & t_h & t_t P^{-1}Q^{-1} \\ t_t Q^{-1} & t_d P & t_t P & t_h & \lambda_z & t_h \\ t_h & t_t P & t_d PQ & t_t PQ & t_h & \lambda_z \end{pmatrix}.$$

This matrix itself, with no additional overall minus sign or Nambu-space factor, defines $h(\mathbf{k})$.

Take

$$\lambda_z = 0, \qquad t_d = 1, \qquad t_h = -0.73, \qquad t_t = 0.19.$$

The reciprocal-lattice vectors are

$$\mathbf{b}_1 = \frac{2\pi}{21}(5\sqrt{3}, 3), \qquad \mathbf{b}_2 = \frac{2\pi}{21}(\sqrt{3}, 9).$$

Parametrize the reciprocal primitive cell by

$$\mathbf{k} = u\mathbf{b}_1 + v\mathbf{b}_2, \qquad 0 \le u, v < 1.$$

The phase factors in the Bloch Hamiltonian are therefore

$$P = e^{2\pi i u}, \qquad Q = e^{2\pi i v}.$$

Points related by

$$(u, v) \sim (u + m, v + n), \qquad m, n \in \mathbb{Z},$$

represent the same crystal momentum.

At each $\mathbf{k}$, order the six eigenvalues of $h(\mathbf{k})$ as

$$\epsilon_1(\mathbf{k}) \le \epsilon_2(\mathbf{k}) \le \cdots \le \epsilon_6(\mathbf{k}).$$

Search the full reciprocal primitive cell, rather than only a conventional high-symmetry path, and determine the following:

1. Every isolated node at which the two middle bands cross,

   $$\epsilon_3(\mathbf{k}) = \epsilon_4(\mathbf{k}).$$

   Report the fractional coordinates (u, v) of every inequivalent node to an absolute accuracy of 5×10^{-6} in each coordinate.

2. The common energy of the middle two bands at the nodes, to an absolute accuracy of 10^{-8}.

3. The total number of inequivalent nodes in the reciprocal primitive cell. Count nodes on periodically identified boundaries only once.

4. Whether the restriction of these nodes to $\overline{\Gamma M}$ lines is enforced by the physical wallpaper group $p6$ or is accidental within this hopping ansatz. The group $p6$ is generated by translations and a sixfold rotation C_6 and contains no mirror reflections. The relevant M points may be represented by

   $$\frac{\mathbf{b}_1}{2}, \qquad \frac{\mathbf{b}_2}{2}, \qquad \frac{\mathbf{b}_1 - \mathbf{b}_2}{2},$$

   together with symmetry- and reciprocal-lattice-equivalent points. Report 1 if yes, else 0.

5. The Berry phase, modulo 2π, of band 3 around a sufficiently small counterclockwise loop enclosing exactly one node and no other band crossing.

End the response with a compact summary containing the ordered list of node coordinates, the common nodal energy, the number of nodes, the answer "symmetry-enforced" or "accidental within the ansatz," and the Berry phase modulo 2π.

d. Chern number and band gaps of a chiral maple-leaf spinon model

Consider the following six-band single-particle Bloch Hamiltonian:

$$h_\phi(\mathbf{k}) = \begin{pmatrix} 0 & t_h e^{i\phi} & t_t PQ & t_d Q & t_t Q & t_h e^{-i\phi} \\ t_h e^{-i\phi} & 0 & t_h e^{i\phi} & t_t Q & t_d P^{-1} & t_t P^{-1} \\ t_t P^{-1}Q^{-1} & t_h e^{-i\phi} & 0 & t_h e^{i\phi} & t_t P^{-1} & t_d P^{-1}Q^{-1} \\ t_d Q^{-1} & t_t Q^{-1} & t_h e^{-i\phi} & 0 & t_h e^{i\phi} & t_t P^{-1}Q^{-1} \\ t_t Q^{-1} & t_d P & t_t P & t_h e^{-i\phi} & 0 & t_h e^{i\phi} \\ t_h e^{i\phi} & t_t P & t_d PQ & t_t PQ & t_h e^{-i\phi} & 0 \end{pmatrix}.$$

This Hamiltonian contains a translation-invariant chiral deformation on the six bonds forming the oriented sublattice cycle

$$1 \longrightarrow 2 \longrightarrow 3 \longrightarrow 4 \longrightarrow 5 \longrightarrow 6 \longrightarrow 1.$$

Equivalently, on every bond oriented as $a \to b$,

$$h_{ab} = t_h e^{i\phi}, \qquad h_{ba} = t_h e^{-i\phi}.$$

All remaining matrix elements are unchanged.

Use the parameters

$$t_d = 1, \qquad t_h = -0.73, \qquad t_t = 0.19, \qquad \phi = 0.15.$$

The reciprocal-lattice vectors are

$$\mathbf{b}_1 = \frac{2\pi}{21}(5\sqrt{3}, 3), \qquad \mathbf{b}_2 = \frac{2\pi}{21}(\sqrt{3}, 9),$$

and the reciprocal primitive cell is parametrized by

$$\mathbf{k} = u\mathbf{b}_1 + v\mathbf{b}_2, \qquad 0 \le u, v < 1.$$

Define

$$P = e^{2\pi i u}, \qquad Q = e^{2\pi i v}.$$

The boundaries of the (u, v) cell are periodically identified.

At each momentum, order the eigenvalues as

$$\epsilon_1(\mathbf{k}) \le \epsilon_2(\mathbf{k}) \le \cdots \le \epsilon_6(\mathbf{k}).$$

Treat this as a single-spin six-band problem at half filling, so that bands 1, 2, and 3 are occupied.

Determine:

1. The total Chern number C_{occ} of the three occupied bands.
2. The minimum direct gap
$$\Delta_{\text{dir}} = \min_{\mathbf{k}} \left[\epsilon_4(\mathbf{k}) - \epsilon_3(\mathbf{k})\right].$$
3. The indirect gap
$$\Delta_{\text{ind}} = \min_{\mathbf{k}} \epsilon_4(\mathbf{k}) - \max_{\mathbf{k}} \epsilon_3(\mathbf{k}).$$

Report both gaps in units of t_d to an absolute accuracy of

$$2 \times 10^{-5}.$$

To fix the sign convention for C_{occ}, orient the reciprocal cell by increasing u followed by increasing v. On a periodic $N_u \times N_v$ mesh, define

$$\delta_u = \left(\frac{1}{N_u}, 0\right), \qquad \delta_v = \left(0, \frac{1}{N_v}\right).$$

Let $V(\mathbf{k})$ be the 6×3 matrix whose columns are normalized eigenvectors of the three occupied bands. Define the gauge-invariant link variables

$$U_\mu(\mathbf{k}) = \frac{\det\left[V^\dagger(\mathbf{k})V(\mathbf{k}+\delta_\mu)\right]}{|\det[V^\dagger(\mathbf{k})V(\mathbf{k}+\delta_\mu)]|}, \qquad \mu = u, v.$$

The occupied-band Chern number is

$$C_{\mathrm{occ}} = \frac{1}{2\pi} \sum_{\mathbf{k}} \mathrm{Arg}\left[\frac{U_u(\mathbf{k})U_v(\mathbf{k}+\delta_u)}{U_u(\mathbf{k}+\delta_v)U_v(\mathbf{k})}\right],$$

where Arg denotes the principal argument and the sum runs over every plaquette of the periodic mesh.

Check convergence with increasing mesh size and verify independently that both the direct and indirect gaps are positive. End the response with a single line of the form

$$\boxed{C_{\mathrm{occ}} = \cdots, \qquad \Delta_{\mathrm{dir}} = \cdots, \qquad \Delta_{\mathrm{ind}} = \cdots}.$$

e. Symmetry-resolved spectrum of an 18-site maple-leaf spin cluster

Consider the spin-$\frac{1}{2}$ Heisenberg Hamiltonian

$$H = \sum_{(i,j)} J_{ij}\, \mathbf{S}_i \cdot \mathbf{S}_j$$

on the following periodic 18-site maple-leaf cluster.
A site is labelled by (c, a), where

$$c = 0, 1, 2$$

is a unit-cell coordinate understood modulo 3, and

$$a = 0, 1, \ldots, 5$$

is a sublattice index. For every c, include each bond generated by the rules below exactly once. A rule

$$(a, b, d)$$

denotes a bond between

$$(c, a) \qquad \text{and} \qquad (c + d \pmod 3, b).$$

The hexagon bonds have coupling

$$J_h = 1$$

and are generated by

$$(0,1,0), \quad (1,2,0), \quad (2,3,0), \quad (3,4,0), \quad (4,5,0), \quad (5,0,0).$$

The triangle bonds have coupling

$$J_t = -0.58$$

and are generated by

$$(0,2,0), \quad (0,4,2), \quad (1,3,2), \quad (1,5,2), \quad (2,4,2), \quad (3,5,0).$$

The dimer bonds have coupling

$$J_d = -0.31$$

and are generated by

$$(0,3,2), \quad (1,4,2), \quad (2,5,0).$$

This construction gives 18 J_h bonds, 18 J_t bonds, and 9 J_d bonds.
Use

$$\mathbf{S}_i \cdot \mathbf{S}_j = S_i^z S_j^z + \frac{1}{2}\left(S_i^+ S_j^- + S_i^- S_j^+\right),$$

with no additional constant or normalization factor.
Let T denote translation by one unit cell,

$$T : (c,a) \longmapsto (c+1 \pmod 3, a).$$

By exact diagonalization in fixed-S^z sectors, determine:

1. The ground-state energy E_0 and the energy per site $\frac{E_0}{18}$.
2. The ground-state total spin S.
3. Its eigenvalue under T, reported either as e^{ik} or as
$$k \in \left\{0, \frac{2\pi}{3}, \frac{4\pi}{3}\right\}.$$
4. The spin gap
$$\Delta_s = E_{\min}(S^z_{\text{tot}} = 1) - E_0.$$

Report all energies to absolute accuracy

$$10^{-8}.$$

Explain how comparison between the $S^z_{\text{tot}} = 0$ and $S^z_{\text{tot}} = 1$ spectra identifies the total spin and provides a check of $SU(2)$ consistency.
As a basic implementation check, state the dimension of the $S^z_{\text{tot}} = 0$ Hilbert space.
End the response with one line of the form

$$\boxed{E_0 = \ldots, \qquad E_0/18 = \ldots, \qquad S = \ldots, \qquad T = \ldots, \qquad \Delta_s = \ldots}$$

6. Electronic structure theory

a. All-electron atomic solver for boron and magnesium

Task. Build from scratch a self-consistent all-electron atomic structure solver. This is the first of three linked problems that together build the atomic and pseudopotential stage of a minimal plane-wave density functional theory code; the all-electron results you produce here are the input to Problem §6b. Use Python with numpy and scipy only.

Papers. Every paper referenced below is also supplied in the accompanying `papers` folder. Use those copies if a publisher website is unreachable; several of them block automated access, so do not treat a failed download as a dead end.

Conventions. Work in Hartree atomic units internally. Use 1 Ha = 27.211386245988 eV and 1 bohr = 0.529177210903 Angstrom. Solve the non-relativistic Kohn-Sham equations, spin-unpolarized, for spherical atoms with spin-restricted, spherically averaged occupations: Kohn and Sham, Phys. Rev. 140, A1133 (1965), `https://doi.org/10.1103/PhysRev.140.A1133`, supplied as `papers/Kohn_sham.pdf`. For exchange and correlation use the local density approximation with Dirac-Slater exchange, and for correlation the VWN5 parametrization given in Vosko, Wilk and Nusair, Can. J. Phys. 58, 1200 (1980), `https://doi.org/10.1139/p80-159`, supplied as `papers/vosko-et-al-2011-accurate-spin-dependent-electron-liquid-correlation-energies-for-local-spin-density-calculations-a.pdf`, paramagnetic branch. Use VWN, not Perdew-Zunger: the reference data specified below is VWN, and the two parametrizations differ by more than the tolerance you are required to meet.

What to compute

Write a self-consistent radial Kohn-Sham solver for a neutral spherical atom, and run it for boron and magnesium in their neutral ground-state configurations.

Report, for each element: **(1)** the total energy, together with its decomposition into kinetic, Hartree, electron-nucleus and exchange-correlation contributions, and every occupied orbital eigenvalue; **(2)** a grid-convergence study, showing how the total energy behaves as the radial grid is refined, the observed order of convergence, and a grid-converged extrapolated value with an error estimate. A single number from a single grid will not be accepted.

Compare your converged results against the LDA column of the NIST Atomic Reference Data for Electronic Structure Calculations, which is converged to microhartree accuracy. Required agreement is 1e-4 hartree on the total energy and on each occupied eigenvalue. The two reference pages are:

Boron – `https://www.nist.gov/pml/atomic-reference-data-electronic-structure-calculations/atomic-reference-data-electronic-7-4`

Magnesium – `https://www.nist.gov/pml/atomic-reference-data-electronic-structure-calculations/atomic-reference-data-electronic-7-10`

The NIST comparison and the grid-convergence study (results 1 and 2) are required in the report but are not graded. The graded result is **(3)**, for each element in its neutral ground state: the electron density at the nucleus; the Hartree potential and the exchange-correlation potential at r = 1.0 bohr exactly; and the expectation values of r and of r squared over the boron 2s and 2p orbitals and over the magnesium 2p and 3s orbitals, with orbitals normalised to unity. The two potentials are graded to 1e-5 hartree, expectation values to 1e-5 bohr (or bohr squared), and the density at the nucleus to a relative 1e-5. The density is the electron number density n(r) in electrons per cubic bohr, not 4 pi r squared n(r).

Before running the self-consistent problem, validate your radial solver against a potential whose spectrum is known analytically (a hydrogen-like ion), and report that test. This is not a formality. Several natural discretizations of the radial equation, in particular reducing the logarithmic-grid generalized eigenvalue problem to standard form, are severely ill-conditioned, and return well-formed but badly wrong eigenvalues that fail to improve, or actively worsen, as the grid is refined.

Deliverables

Working, documented code that regenerates every number above from scratch. A short report containing results 1, 2 and 3 and the hydrogenic validation test. Result 3 must in addition be summarised by filling in the supplied file `agent_answers1.txt`, keeping its line labels, order and units exactly as given and adding, renaming or removing nothing.

Save your converged all-electron radial wavefunctions, eigenvalues and potentials to a documented plain-text format, since Problem §6b builds directly on them.

Report failures as failures. Where a check does not pass, report it and its magnitude. Do not report any quantity you have not actually computed.

```
================================================================
ANSWER SHEET
```

```
================================================================
Fill in the value on every line. Do not add, remove, rename or
reorder any line. Potentials in hartree, at least six decimals,
signed. Lengths in bohr. Density in electrons/bohr^3 (n(r), not
4 pi r^2 n(r)), at least seven significant digits.

--- RESULT 3 : NEUTRAL GROUND STATES --------------------------------
B    n_nucleus
B    vH_r1
B    vxc_r1
B    r_mean_2s
B    r2_mean_2s
B    r_mean_2p
B    r2_mean_2p
Mg   n_nucleus
Mg   vH_r1
Mg   vxc_r1
Mg   r_mean_2p
Mg   r2_mean_2p
Mg   r_mean_3s
Mg   r2_mean_3s
================================================================

Notes.

n_nucleus
    Electron density at the nucleus.

vH_r1, vxc_r1
    Hartree and exchange-correlation potentials at r = 1.0 bohr.

r_mean_nl, r2_mean_nl
    Expectation values of r and r^2 over orbital nl (normalised).
```

b. Norm-conserving pseudopotentials for boron and magnesium

Task. Generate norm-conserving pseudopotentials for boron and magnesium from all-electron atomic calculations. This is the second of three linked problems that together build the atomic and pseudopotential stage of a minimal plane-wave density functional theory code. It builds directly on the all-electron solver of Problem §6a, and its output is the input to Problem §6c.

Papers. Every paper referenced below is also supplied in the accompanying `papers` folder. Use those copies if a publisher website is unreachable; several of them block automated access, so do not treat a failed download as a dead end.

Conventions. All conventions from Problem §6a carry over unchanged: Hartree atomic units, the local density approximation with Dirac-Slater exchange and the VWN5 correlation parametrization of Vosko, Wilk and Nusair, Can. J. Phys. 58, 1200 (1980), `https://doi.org/10.1139/p80-159`, spin-unpolarized, spherically averaged occupations. Use the converged all-electron results from Problem §6a as the starting point, and no other source.

What to compute

Generate norm-conserving pseudopotentials using the scheme of Troullier and Martins, Phys. Rev. B 43, 1993 (1991), `https://doi.org/10.1103/PhysRevB.43.1993`, supplied as `papers/pp_for_PW.pdf`.

Use the following choices exactly, and do not retune them. Boron: valence 2s2 2p1, valence charge 3, s and p channels, core radius 1.50 bohr for both channels. Magnesium: valence 3s2, valence charge 2, s and p channels, core radius 2.50 bohr for both channels. Magnesium has no occupied valence p state. Do not build its p channel on the unoccupied 3p all-electron level (which the neutral LDA atom does bind, weakly); generate that channel instead from a scattering state at a reference energy of exactly zero hartree, and state how you did so. Unscreen each pseudopotential using the pseudo-valence density only. Write the pseudo radial function inside the core radius as r to the power l times the exponential of an even polynomial of degree twelve, with coefficients c0, c2, c4, . . . , c12, where c0 is the constant term.

Report, for the bound reference channels: **(1)** the norm-conservation residual inside the core radius; **(2)** the pseudo bound-state eigenvalue; and **(3)** the difference between that eigenvalue and the corresponding all-electron valence eigenvalue from Problem §6a. Define signed differences as pseudo minus all-electron. Results 1 and 3 are exact identities of the construction; report their signed values and require their absolute values to be below 1e-8. For the magnesium p channel, report instead **(1)** the relative core-norm residual, defined as the pseudo core norm minus the all-electron core norm, divided by the all-electron core norm, with the two scattering reference functions scaled to match at the core radius; **(2)** the prescribed reference energy of zero hartree; and **(3)** boundary-matching checks at

that energy, for which a bound-state eigenvalue difference is not applicable. Require the absolute value of the relative core-norm residual to be below 1e-8. Perform these checks using the screened reference potentials.

Results 1 to 3 are required in the report, with their signs, but are not graded. The graded result is **(4)**:

- for each element and each channel, the coefficients c2, c6, c8, c10 and c12 (c0 and c4 are not graded: c4 follows from c2 through the Troullier-Martins curvature condition, and c0 from norm conservation);
- the unscreened p-channel (local) pseudopotential at r = 0;
- the all-electron charge inside the core radius for the boron s, boron p and magnesium s references: `Q_AE_rc` is $\int_0^{r_c} |P_{\mathrm{AE}}(r)|^2\,dr$, with $P_{\mathrm{AE}} = rR_{\mathrm{AE}}$ normalised so that $\int_0^{\infty} |P_{\mathrm{AE}}(r)|^2\,dr = 1$, without occupation factors;
- for each element, the unscreened pseudopotential at the core radius plus the valence charge divided by the core radius (the s and p values coincide there).

Coefficients and charges are graded to 1e-6, and potentials to 1e-5 hartree (1e-6 hartree for the value at the core radius). Give signed values throughout, with at least eight digits after the decimal point or in scientific notation with at least seven significant digits.

Confirm also, and show in your write-up, that each unscreened pseudopotential approaches the bare valence Coulomb tail outside its core radius, and that each pseudo wavefunction is nodeless and joins the all-electron wavefunction smoothly at the core radius. These are not graded numbers, but a construction that fails either of them is wrong regardless of what the residuals say.

Deliverables

Working, documented code that regenerates every number above from scratch, starting from your Problem §6a output. A short report containing results 1 to 4 and the two confirmations above, with a plot comparing the all-electron and pseudo wavefunctions for each channel. Result 4 must in addition be summarised by filling in the supplied file `agent_answers2.txt`, keeping its line labels, order and units exactly as given and adding, renaming or removing nothing.

Save the semilocal pseudopotentials, the pseudo wavefunctions and the radial grid to a documented plain-text format, since Problem §6c builds directly on them.

Report failures as failures. Where a check does not pass, report it and its magnitude. Do not report any quantity you have not actually computed.

```
======================================================================
ANSWER SHEET
======================================================================
Fill in the value on every line. Do not add, remove, rename or
reorder any line. Potentials in hartree, charges dimensionless,
coefficients in the units implied by r in bohr. Signed values, at
least eight digits after the decimal point (or scientific notation
with at least seven significant digits).

--- RESULT 4a : TM COEFFICIENTS ------------------------------------
B    s    c2
B    s    c6
B    s    c8
B    s    c10
B    s    c12
B    p    c2
B    p    c6
B    p    c8
B    p    c10
B    p    c12
Mg   s    c2
Mg   s    c6
Mg   s    c8
Mg   s    c10
Mg   s    c12
Mg   p    c2
Mg   p    c6
Mg   p    c8
Mg   p    c10
Mg   p    c12

--- RESULT 4b : LOCAL (p) POTENTIAL AT THE ORIGIN ------------------
B    p    Vion_0
Mg   p    Vion_0

--- RESULT 4c : AE CHARGE INSIDE THE CORE RADIUS -------------------
B    s    Q_AE_rc
B    p    Q_AE_rc
Mg   s    Q_AE_rc

--- RESULT 4d : POTENTIAL AT THE CORE RADIUS ------------------------
B         Vion_rc_plus_Zval_over_rc
```

```
Mg        Vion_rc_plus_Zval_over_rc
=================================================================

Notes.

cK
    Troullier-Martins coefficient of r^K in the exponent of the pseudo
    radial function R = r^l exp(c0 + c2 r^2 + ... + c12 r^12) inside
    r_c. c0 and c4 are not asked for.

Vion_0
    Unscreened p-channel (local) pseudopotential at r = 0.

Q_AE_rc
    All-electron reference charge inside the core radius,
    int_0^rc P_AE^2 dr with int_0^inf P_AE^2 dr = 1, no occupation.

Vion_rc_plus_Zval_over_rc
    Unscreened pseudopotential at r_c plus Z_val / r_c.
```

c. Separable pseudopotentials and ghost states

Task. Convert semilocal norm-conserving pseudopotentials to fully separable form, and determine whether the conversion has introduced a ghost state. This is the third of three linked problems that together build the atomic and pseudopotential stage of a minimal plane-wave density functional theory code. It builds directly on the pseudopotentials generated in Problem §6b.

Papers. Every paper referenced below is also supplied in the accompanying `papers` folder. Use those copies if a publisher website is unreachable; several of them block automated access, so do not treat a failed download as a dead end.

Conventions. All conventions from Problems §6a and §6b carry over unchanged: Hartree atomic units, the local density approximation with Dirac-Slater exchange and VWN5 correlation, spin-unpolarized. Use the semilocal pseudopotentials and pseudo wavefunctions you generated in Problem §6b, with boron valence charge 3 and magnesium valence charge 2, and no other source. All analysis in this problem is carried out on the screened pseudo-atom: each potential (semilocal, local, separable) is the corresponding unscreened potential plus the Hartree and exchange-correlation potentials of the Problem §6b pseudo-valence density, held fixed; the all-electron comparison uses the self-consistent all-electron potential of Problem §6a. Logarithmic derivatives are those of R (not of P = rR), at the core radius, in inverse bohr.

What to compute

Convert the semilocal pseudopotentials of each element to the fully separable form of Kleinman and Bylander, Phys. Rev. Lett. 48, 1425 (1982), `https://doi.org/10.1103/PhysRevLett.48.1425`, supplied as `papers/kleinman_bylander.pdf`. Take the p channel as the local part for both elements.

Then determine, for each element, whether the separable operator carries a ghost state: a spurious bound state of the separable form that has no counterpart in the original semilocal potential, and which would corrupt any subsequent solid-state calculation while leaving the atomic construction looking perfectly healthy. Use the criteria of Gonze, Käckell and Scheffler, Phys. Rev. B 41, 12264 (1990), `https://doi.org/10.1103/PhysRevB.41.12264`, supplied as `papers/Ghost_states_from_pp.pdf`.

Use logarithmic derivatives as supporting diagnostics. Evaluate the logarithmic derivative at the core radius, on an energy grid running from -1.0 to +1.0 hartree in steps of 0.1 hartree, for three cases: the all-electron atom, the semilocal pseudopotential, and the separable Kleinman-Bylander operator. Determine the graded verdict using the cited spectral criterion or an equivalent infinite-space bound-state analysis: report YES if the separable operator introduces a spurious bound state below its channel's reference energy with no counterpart in the semilocal potential, and NO otherwise. A shift in pole position alone does not establish a ghost; absence of an extra pole on the plotted interval does not exclude a ghost outside it. Carry out the analysis, show the three curves for each channel in your write-up, and state your conclusion.

Report, for each element, with the p channel local: **(1)** D_s, the expectation value of the nonlocal s part (semilocal s minus local potential) in the normalised reference s pseudo wavefunction, and the Kleinman-Bylander energy, the expectation value of the square of that nonlocal part divided by D_s; **(2)** the two lowest l = 0 bound-state energies of the screened local potential alone, in infinite space (NONE for a state that does not exist); for magnesium only the lowest of the two is graded; **(3)** the s-channel logarithmic derivative at all 21 energies of the grid, for the all-electron, semilocal and separable cases; all 21 go in the report, and the values at -1.0, 0.0 and +1.0 hartree are graded; **(4)** every pole of each of these three curves on [-1, +1] hartree, located to within 1e-3 hartree, which the 0.1 hartree grid alone will not do (NONE if there is none); **(5)** whether a below-reference ghost state, as defined above, is present,

as exactly `YES` or exactly `NO`. Energies are graded to 1e-5 hartree, logarithmic derivatives to a relative 1e-4, and pole energies to 2e-3 hartree.

If you find a ghost state, say so plainly and explain which channel carries it and what in the construction is responsible. Do not adjust the local channel, the core radii, or anything else in order to make the ghost disappear, and do not report a clean result you did not obtain.

Deliverables

Working, documented code that regenerates the analysis from scratch, starting from your Problem §6b output. A short report containing the logarithmic derivative curves for all three cases in each channel, the reasoning by which you reached each verdict, and the verdicts themselves, together with results 1 to 5. Results 1 to 5 must in addition be given by filling in the supplied answer format below, keeping its line labels exactly as given and adding, renaming or removing nothing.

Report failures as failures. Where a check does not pass, report it and its magnitude. Do not report any quantity you have not actually computed.

```
======================================================================
ANSWER SHEET
======================================================================
Fill in the value on every line. Do not add, remove, rename or
reorder any line. Energies in hartree, at least six decimals,
signed. Logarithmic derivatives (of R, at r_c) in 1/bohr, at least
six decimals, signed. Write exactly NONE where a quantity does not
exist. ghost_state is exactly YES or exactly NO.

--- B ------------------------------------------------------------
B    D_s
B    E_KB
B    E0_loc
B    E1_loc
B    logder_AE_E-1.0
B    logder_AE_E+0.0
B    logder_AE_E+1.0
B    logder_SL_E-1.0
B    logder_SL_E+0.0
B    logder_SL_E+1.0
B    logder_SEP_E-1.0
B    logder_SEP_E+0.0
B    logder_SEP_E+1.0
B    poles_AE
B    poles_SL
B    poles_SEP
B    ghost_state

--- Mg -----------------------------------------------------------
Mg   D_s
Mg   E_KB
Mg   E0_loc
Mg   logder_AE_E-1.0
Mg   logder_AE_E+0.0
Mg   logder_AE_E+1.0
Mg   logder_SL_E-1.0
Mg   logder_SL_E+0.0
Mg   logder_SL_E+1.0
Mg   logder_SEP_E-1.0
Mg   logder_SEP_E+0.0
Mg   logder_SEP_E+1.0
Mg   poles_AE
Mg   poles_SL
Mg   poles_SEP
Mg   ghost_state
======================================================================

Notes.

D_s, E_KB
    D_s = <phi_s| V_s - V_loc |phi_s>, and the Kleinman-Bylander energy
    E_KB = <phi_s| (V_s - V_loc)^2 |phi_s> / D_s, phi_s normalised.

E0_loc, E1_loc
    Lowest and second-lowest l = 0 bound states of the screened local
    potential in infinite space (only the lowest for Mg).

logder_X_E
    s-channel d ln R / dr at r_c at energy E (hartree), for the
    all-electron (AE), semilocal (SL) and separable (SEP) cases.

poles_X
    All poles on [-1, +1] hartree, ascending, comma-separated, or NONE.
```

d. *Self-consistent field solver for metastable magnesium diboride*

Task. Extend the code you wrote for previous problems into a working plane-wave pseudopotential density functional theory code, and run it self-consistently on the crystal supplied as `structure.cif`. The structure is an unpublished polymorph from a structure-prediction search and is not indexed in any public database, so there is no value to retrieve. Use the pseudopotentials you generated previously. The overall method is that of Payne, Teter, Allan, Arias and Joannopoulos, Rev. Mod. Phys. 64, 1045 (1992), `https://doi.org/10.1103/RevModPhys.64.1045`. You are allowed to look for papers or fetch the concept from your understanding if you do not find any of the papers in the papers folder.

Fixed parameters

The graded results are compared against an independent calculation, so every setting below is prescribed. Do not vary any of them in the graded production calculation, and do not substitute a value you consider better. Additional runs with varied cutoffs or k-point meshes are permitted and required solely for the convergence checks; their results must not replace the graded production results.

- **Geometry.** Use the cell vectors and atomic positions exactly as given in the CIF, with exactly the same number of atoms in the cell. Do not convert to a primitive or a conventional setting, do not symmetrise or re-standardise the cell, and do not relax the geometry. The result depends on the cell contents, so a different but crystallographically equivalent cell gives a different answer.
- **Functional.** Local density approximation, Dirac-Slater exchange with VWN5 correlation as fixed in previous problems, spin-unpolarized.
- **Pseudopotentials.** Your own from previous problem: Troullier-Martins norm-conserving, Kleinman-Bylander separable, p channel local, boron valence charge 3, magnesium valence charge 2.
- **Cutoffs.** 40 hartree for the wavefunctions (a plane wave k+G is included when half its squared length is at most 40 hartree), 160 hartree for the density and potential.
- **Self-consistent k-point mesh.** A zone-centred uniform 8 by 8 by 8 mesh with no offset, in the sense of Monkhorst and Pack, Phys. Rev. B 13, 5188 (1976), `https://doi.org/10.1103/PhysRevB.13.5188`, in the reciprocal lattice of the cell as given.
- **Occupations.** Fermi-Dirac smearing of width 0.01 hartree, held fixed; the Fermi level is the chemical potential at which the smeared occupations sum to the valence electron count.
- **Number of bands.** The total number of valence electrons in the cell, divided by two, plus eight.
- **Self-consistency.** Converged until the total energy changes by less than 1e-8 hartree between iterations. State the density residual you reached as well.

Part A – Building the calculation

Parse the CIF, build the direct and reciprocal lattices and the plane-wave basis, and compute the ion-ion electrostatic energy by Ewald summation, following Ewald, Ann. Phys. 369, 253 (1921), treating each nucleus as a point charge equal to its valence charge. Then build the Kohn-Sham Hamiltonian in the plane-wave basis, diagonalize it at each k point, accumulate the density by fast Fourier transform using the smeared occupations, solve for the Hartree potential in reciprocal space, evaluate the exchange-correlation potential on the real-space grid, and iterate to self-consistency. Treat the zero-wavevector electrostatic terms explicitly: the Hartree, local pseudopotential and Ewald contributions each diverge there and are finite only in combination. State the convention you use, consistent with the one you fixed in previous problems, and show that the divergences cancel.

Part B – Results to report

Count a band as crossing if its lowest energy lies below the Fermi level and its highest energy lies above it. Search the full mesh and report the resulting count.

Report:

- the number of plane waves in the wavefunction basis at Gamma;
- the Ewald energy of the cell: the electrostatic energy of the point valence charges in a uniform neutralising background of equal and opposite total charge, which is independent of the splitting parameter;
- the zero-wavevector pseudopotential term: the total valence electron count divided by the cell volume, times the sum over all atoms in the cell of the integral over all space of the local unscreened pseudopotential plus the valence charge over r;
- the total energy of the cell at the prescribed smearing, and the free energy, the total energy minus the smearing width times the Fermi-Dirac electronic entropy;

- the eigenvalues of bands 1 to 8, minus the Fermi level, at Gamma and at the mesh point with fractional reciprocal coordinates (1/2, 1/2, 1/2);

- the number of distinct bands that cross the Fermi level, as defined above, the index of the lowest crossing band, and the full-mesh minimum and maximum, relative to the Fermi level, of the lowest and of the highest crossing band (NONE if no band crosses).

Bands are labelled by energy order at each k point, band 1 being the lowest, with no attempt to follow band character between k points. Search all 512 mesh points; if you use symmetry to reduce the diagonalizations, unfold the eigenvalues to the full mesh first. Counts and indices must match exactly; the Ewald energy is graded to 1e-6 hartree, the zero-wavevector term to 1e-5 hartree, and all other energies to 5e-4 hartree.

Deliverables

Working, documented code that regenerates the results from the CIF and your pseudopotential files from the previous calculations. A short report containing the Part A validation evidence, the cutoff and mesh convergence checks, the zero-wavevector cancellation argument, the band minimum and maximum table. Report failures as failures. Where a check does not pass, report it and its magnitude. Do not report any quantity you have not actually computed.

```
======================================================================
ANSWER SHEET
======================================================================
Fill in the value on every line. Do not add, remove, rename or
reorder any line. Energies and potentials in hartree, at least
six decimals, signed.
Counts and band indices are whole numbers; write NONE where a
quantity does not exist.

--- CONSTRUCTION ---------------------------------------------------
n_planewaves_Gamma
E_ewald
E_alphaZ

--- ENERGETICS -----------------------------------------------------
E_total
F_free

--- BANDS ----------------------------------------------------------
Gamma_band1_minus_Ef
Gamma_band2_minus_Ef
Gamma_band3_minus_Ef
Gamma_band4_minus_Ef
Gamma_band5_minus_Ef
Gamma_band6_minus_Ef
Gamma_band7_minus_Ef
Gamma_band8_minus_Ef
K111half_band1_minus_Ef
K111half_band2_minus_Ef
K111half_band3_minus_Ef
K111half_band4_minus_Ef
K111half_band5_minus_Ef
K111half_band6_minus_Ef
K111half_band7_minus_Ef
K111half_band8_minus_Ef
n_bands_crossing_Ef
lowest_crossing_band_index
lowest_crossing_band_min_minus_Ef
lowest_crossing_band_max_minus_Ef
highest_crossing_band_min_minus_Ef
highest_crossing_band_max_minus_Ef
======================================================================

Notes.

E_alphaZ
    Zero-wavevector pseudopotential term, as defined in Part B.

K111half
    Mesh point with fractional reciprocal coordinates (1/2,1/2,1/2).

*_minus_Ef
    Energies relative to the Fermi level; bands in energy order.
```

7. Quantum field theory

a. Gauge contribution to a Chern–Simons matter beta function

Consider a three-dimensional Chern–Simons matter theory with gauge group

$$G = \mathrm{USp}(2N)_{k_1} \times \mathrm{USp}(2M)_{k_2}, \qquad N, M \geq 2. \tag{A35}$$

The matter content is

$$\psi_1^i \in (A_N, \mathbf{1}), \qquad \psi_2^i \in (\mathbf{1}, A_M), \qquad i = 1, 2, 3, \tag{A36}$$

$$\varphi_1 \in (A_N, \mathbf{1}), \qquad \varphi_2 \in (\mathbf{1}, A_M), \tag{A37}$$

$$\chi \in (F_N, F_M), \qquad X \in (F_N, F_M). \tag{A38}$$

where $\psi_{1,2}^i$ and χ are Dirac fermions, $\varphi_{1,2}$ are real scalars, X is a complex scalar, and

$$A_N = \wedge_0^2 F_N, \qquad A_M = \wedge_0^2 F_M \tag{A39}$$

are the symplectic-traceless antisymmetric tensor representations.

Let $\Omega^{(N)}_{ab}$ and $\Omega^{(M)}_{\dot{a}\dot{b}}$ be the symplectic forms, normalized by

$$\Omega^{ac}\Omega_{cb} = \delta^a{}_b, \qquad \Omega^{ab}\Omega_{ab} = -2N, \tag{A40}$$

with the analogous convention at the second node. The projector onto A_N is

$$\big(P_A^{(N)}\big)_{ab}{}^{cd} = \frac{1}{2}\left(\delta_a^c\delta_b^d - \delta_a^d\delta_b^c\right) + \frac{1}{2N}\Omega^{(N)}_{ab}\Omega^{cd}_{(N)}, \tag{A41}$$

with $N \to M$ for $P_A^{(M)}$.

The classically marginal interaction is

$$\delta\mathcal{L} = \frac{\lambda}{2}\mathcal{O}_\lambda + \mathrm{h.c.}, \tag{A42}$$

where

$$\mathcal{O}_\lambda = (\bar{\psi}_1^i)^{ab}\big(P_A^{(N)}\big)_{ab}{}^{cd} X_{c\dot{c}} X_{d\dot{d}} \big(P_A^{(M)}\big)^{\dot{c}\dot{d}}{}_{\dot{a}\dot{b}} (\psi_{2,i})^{\dot{a}\dot{b}}. \tag{A43}$$

All kinetic terms are canonical. Masses and scalar self-couplings are tuned to the critical surface.

Conventions Use Hermitian generators normalized by

$$\mathrm{tr}_F(t^A t^B) = 2\delta^{AB}, \qquad [t^A, t^B] = i f^{ABC} t^C. \tag{A44}$$

Define

$$\xi_1 \equiv \frac{2N}{k_1}, \qquad \xi_2 \equiv \frac{2M}{k_2}. \tag{A45}$$

Use

$$\eta_{\mu\nu} = \mathrm{diag}(-,+,+), \qquad \epsilon^{012} = +1, \tag{A46}$$

and work in Landau gauge. The covariant derivatives are

$$D_\mu\psi_1 = \partial_\mu\psi_1 - iA^A_{1\mu}T^A_{A_N}\psi_1, \qquad D_\mu\psi_2 = \partial_\mu\psi_2 - iA^B_{2\mu}T^B_{A_M}\psi_2, \tag{A47}$$

$$D_\mu X = \partial_\mu X - iA^A_{1\mu}t^A_N X - iA^B_{2\mu}X(t^B_M)^T. \tag{A48}$$

All external momenta are incoming and every loop momentum is integrated with

$$\int_q \equiv \int \frac{\mathrm{d}^d q}{(2\pi)^d}. \tag{A49}$$

For node $a = 1, 2$, the gauge propagator and cubic gauge vertex are

$$\langle A^A_{a,\mu}(q) A^B_{a,\nu}(-q)\rangle = \frac{i}{k_a}\delta^{AB}\frac{\epsilon_{\mu\nu\rho}q^\rho}{q^2 - i0}, \tag{A50}$$

$$V^{ABC}_{a,\mu\nu\rho} = ik_a f^{ABC}\epsilon_{\mu\nu\rho}. \tag{A51}$$

The ghost action is the standard Faddeev–Popov action obtained from $\partial^\mu A^A_{a,\mu} = 0$ with the same structure constants and gauge-field normalization.

The phase-stripped quartic scalar-gauge vertices obtained from $|D_\mu X|^2$ are fixed to be

$$V^{(11)AB}_{\mu\nu} = -\eta_{\mu\nu}\{t^A_N, t^B_N\} \otimes \mathbf{1}, \tag{A52}$$

$$V^{(22)AB}_{\mu\nu} = -\eta_{\mu\nu}\mathbf{1} \otimes \{(t^A_M)^T, (t^B_M)^T\}, \tag{A53}$$

$$V^{(12)AB}_{\mu\nu} = -2\eta_{\mu\nu} t^A_N \otimes (t^B_M)^T. \tag{A54}$$

Thus the same-node vertex contains the anticommutator as written, while the mixed-node vertex carries an additional numerical factor of two. No further seagull factor is to be appended to these rules.

Use dimensional reduction with

$$d = 3 - 2\epsilon, \tag{A55}$$

while gamma matrices and epsilon tensors remain strictly three-dimensional:

$$\gamma^\mu\gamma^\nu = \eta^{\mu\nu}\mathbf{1} + \epsilon^{\mu\nu\rho}\gamma_\rho, \qquad \frac{1}{2}\operatorname{tr}(\gamma^\mu\gamma^\nu) = \eta^{\mu\nu}. \tag{A56}$$

Define minimal-subtraction residues by

$$Z_Y = 1 + \frac{K_Y}{\epsilon} + \cdots. \tag{A57}$$

At fixed bare Chern–Simons levels, use

$$\xi_{1,0} = \mu^{2\epsilon}\xi_1, \qquad \xi_{2,0} = \mu^{2\epsilon}\xi_2. \tag{A58}$$

Define the bare deformation coupling by

$$\lambda_0 = \mu^{2\epsilon} Z_\Gamma Z_{\psi_1}^{-1/2} Z_{\psi_2}^{-1/2} Z_X^{-1}\lambda. \tag{A59}$$

Finite Chern–Simons level shifts are not part of the requested minimal-subtraction beta function.

Main question Retaining only the gauge-induced contribution that is linear in λ and quadratic in the Chern–Simons couplings, determine the exact closed-form functions

$$B_{11}(N, M), \qquad B_{22}(N, M), \qquad B_{12}(N, M) \tag{A60}$$

for generic integers $N, M \geq 2$, defined by

$$\beta_\lambda = \lambda\Big[B_{11}(N, M)\xi_1^2 + B_{22}(N, M)\xi_2^2 + B_{12}(N, M)\xi_1\xi_2\Big] + \mathcal{O}\big(|\lambda|^2\lambda, \lambda\xi^4, \lambda g_4^2, \lambda s_6^2, \ldots\big) \tag{A61}$$

in the $\mu\,\mathrm{d}/\mathrm{d}\mu$ convention.

b. *Dynamical soft vacuum*

Consider massless scalar QED, mostly-plus signature, $D_\mu = \nabla_\mu - ieA_\mu$, with $A \to A + \mathrm{d}\Lambda$, $\Phi \to e^{ie\Lambda}\Phi$. Retarded coordinates: $\mathrm{d}s^2 = -\mathrm{d}u^2 - 2\,\mathrm{d}u\,\mathrm{d}r + r^2\gamma_{AB}\mathrm{d}x^A\mathrm{d}x^B$, $t = u + r$; (x, y, z) are the components of $\hat{\mathbf{x}}$; Δ is the Laplacian of the unit sphere. Lorenz gauge throughout.

Gauge sector. The gauge field is restricted to the pure-gauge family $A = \mathrm{d}\Lambda[C, \mu]$, $\Lambda[C, \mu] = \Lambda_C + \Lambda_\mu$, with $\Box\Lambda_C = \Box\Lambda_\mu = 0$ and, as $r \to \infty$ at fixed $(u, \hat{\mathbf{x}})$,

$$\Lambda_C \to C(\hat{\mathbf{x}}), \qquad \Lambda_\mu = r\,\mu(\hat{\mathbf{x}}) + \ldots$$

In the large-r expansion of Λ_C and of Λ_μ at fixed $(u,\hat{\mathbf{x}})$, in powers of r and $\ln r$, every u-independent coefficient other than the leading one is zero. There is no back-reaction: A is exactly $\mathrm{d}\Lambda[C,\mu]$.

Scalar sector. Φ solves $D^\mu D_\mu \Phi = 0$ in this background. Its data φ are defined by

$$\Phi = e^{ier\mu}\Big[\frac{\varphi(u,\hat{\mathbf{x}})}{r} + o(r^{-1})\Big],$$

and every coefficient in the large-r expansion of $e^{-ier\mu}\Phi$ at fixed $(u,\hat{\mathbf{x}})$ vanishes as $u \to -\infty$.

Phase space. The coordinates are (C,μ,φ); the soft-vacuum labels C and μ *are varied*. With $\theta^\mu(\delta) = \sqrt{-g}\,\big[(D^\mu\Phi)^*\delta\Phi + D^\mu\Phi\,\delta\Phi^*\big]$ (the scalar term of the symplectic potential of section 2 of arXiv:1605.09677; variations act on A through C,μ),

$$\Omega_t(\delta_1,\delta_2) = \int_{\Sigma_t} \mathrm{d}^3x\,\big[\delta_1\theta^t(\delta_2) - \delta_2\theta^t(\delta_1)\big], \qquad \Omega_t = t\,\Omega^{(1)} + \Omega^{(0)} + \frac{\ln t}{t}\,\Omega^{(L)} + O(t^{-1}) \quad (t\to\infty),$$

on slices Σ_t of constant t.

Data. With

$$\psi_k(u,\hat{\mathbf{x}}) = -G_k\,\big(u - c_k + i\nu\big)\exp\Big[-\tfrac{1}{2}(u-c_k)^2 - i\nu u\Big], \qquad k = 1,2,$$

$$G_1 = 1 + x + i(y + xz), \quad G_2 = 1 - y + i(x + yz), \quad c_1 = z, \quad c_2 = z+1, \quad \nu = 2 + x, \quad e = 1,$$

the base point is

$$C = xz - y, \qquad \mu = x^2 z + xy, \qquad \varphi = \psi_1,$$

and the two tangent vectors are

$$\delta_1 :\ (\delta C,\delta\mu,\delta\varphi) = (1 + z + xy,\ \ xyz + z^2,\ \ \psi_2), \qquad \delta_2 :\ (\delta C,\delta\mu,\delta\varphi) = (yz - x^2,\ \ xz + y^2,\ \ i\psi_2),$$

with $\delta\varphi^*$ the complex conjugate of $\delta\varphi$.

Let W be the value that $\Omega^{(0)}$ takes for the same $\delta_{1,2}\varphi$ when $C = \mu = 0$ and $\delta_{1,2}C = \delta_{1,2}\mu = 0$.

Answer format: three real numbers $\big(\Omega^{(1)}/\Omega^{(0)},\ \Omega^{(L)}/\Omega^{(0)},\ \Omega^{(0)}/W\big)$.

c. Simultaneous triple-soft photons

The process $\Phi(p_a)\,\bar\Phi(p_b) \to \Phi(p_3)\,\bar\Phi(p_4)$ of massless scalars with charges $\pm e$ has on-shell amplitude

$$\mathcal{M}_4 = \frac{s^2 + 2st - 3}{(s+2)(t-1)}, \qquad s = -(p_a + p_b)^2, \quad t = -(p_a - p_3)^2$$

(mostly-plus signature), generated by neutral short-distance physics. The scalars are minimally coupled to the photon. Let $\mathcal{M}_7$ be the stripped amplitude for the same process with three additional outgoing photons, at lowest order in e, with no photon exchanged between the scalars and no soft singularities other than external-leg poles.

Kinematics, (E,p_x,p_y,p_z):

$$p_a = (1,0,0,1), \qquad p_b = (1,0,0,-1), \qquad \hat{n}_3 = \tfrac{1}{3}(2,-1,2),$$

$$k_1 = \omega_1\big(1,\tfrac{4}{9},\tfrac{8}{9},-\tfrac{1}{9}\big), \qquad k_2 = \omega_2\big(1,\tfrac{2}{3},-\tfrac{1}{3},-\tfrac{2}{3}\big), \qquad k_3 = \omega_3\big(1,-\tfrac{8}{9},\tfrac{4}{9},-\tfrac{1}{9}\big),$$

$$\varepsilon_1 = \tfrac{1}{\sqrt{2}}\big(\tfrac{1}{2} - i,\ 1,\ -i,\ -\tfrac{1}{2} + i\big), \quad \varepsilon_2 = \tfrac{1}{\sqrt{2}}\big(2 - i,\ 1,\ i,\ -2 + i\big), \quad \varepsilon_3 = \tfrac{1}{\sqrt{2}}\big(-1 - \tfrac{i}{2},\ 1,\ -i,\ 1 + \tfrac{i}{2}\big).$$

p_a, p_b and the direction $\hat{n}_3$ of p_3 are fixed; $|\vec{p}_3|$ and p_4 follow from conservation.

Set $\omega_1 = \omega$, $\omega_2 = 2\omega$, $\omega_3 = \frac{3}{2}\omega$. Contract photons 2 and 3 with ε_2, ε_3 and photon 1 with

$$\varepsilon_1(\lambda) = \varepsilon_1 + \lambda\,\varepsilon_1^*, \qquad \lambda \in \mathbb{C},$$

as written (componentwise conjugate, no renormalisation, λ fixed), and write

$$\mathcal{M}_7 = \frac{A(\lambda)}{\omega^3} + \frac{B(\lambda)}{\omega^2} + O(\omega^{-1}).$$

Let λ_* be the value for which $A(\lambda_*) = 0$.

Answer format: the complex number $B(\lambda_*)/A(0)$.

d. Schur indices and accessory parameters of modular differential equations

Consider

$$F_n(\tau;a,g)=[\lambda(1-\lambda)]^{-\kappa(a,g)}\int_0^\lambda\cdots\int_0^\lambda\prod_{i=1}^n dt_i\,\big[t_i(1-t_i)(\lambda-t_i)\big]^a\prod_{1\le i<j\le n}|t_i-t_j|^{2g},$$

where $\lambda=\lambda(\tau)$. The integral is defined initially for $0<\lambda<1$ and extended by analytic continuation. Fix $\kappa(a,g)$ such that F_n satisfies a modular linear differential equation (MLDE) of minimal order r of the form

$$\sum_{j=0}^r\Phi_{2j}(\tau)\,\mathcal{D}^{r-j}\widehat{F}_n=0,\qquad \Phi_{2j}\in M_{2j},$$

Here $\widehat{F}_n$ is normalized to have leading q-coefficient 1. Expand

$$\Phi_{2j}(\tau)=\sum_m c_{j,m}\,E_{2j-12m}(\tau)\,\Delta(\tau)^m,$$

where $E_{2k}=1+O(q)$, are the normalized Eisenstein series of weight $2k$, and Δ is the normalized weight 12 cusp form. The coefficients $c_{j,m}$ for $m\neq 0$ are accessory parameters. Find the 4d $\mathcal{N}=2$ SCFT with the largest c_{4d} whose Schur index is given as $\hat{F}_n$ and has exactly two accessory parameters in its corresponding MLDE.

e. Seiberg duality and mutation distance for 13-node quivers

Consider a pair of 4D $\mathcal{N}=1$ SCFTs, as described by a quiver gauge theory. The task is to determine whether two theories are Seiberg dual, and what is the minimal number of dualities / mutations on nodes which establishes this (if they are dual). For this problem, you are given the adjacency matrix and ranks of the gauge groups, but you can ignore the superpotential data. The two theories are presented as theory **A** and theory **B**.

Ranks A: $R_1=\begin{pmatrix}1&1&1&1&1&1&3&2&72&1292&15&1&1\end{pmatrix}$

Adjacency matrix A:

$$A_1=\begin{pmatrix}
0&2&0&0&0&0&0&0&0&0&0&1&0\\
0&0&2&0&0&0&0&0&0&0&0&0&1\\
1&0&0&2&0&0&0&0&0&0&0&0&0\\
0&1&0&0&2&0&0&0&0&0&0&0&0\\
0&0&1&0&0&2&1&0&0&0&0&0&0\\
0&0&0&1&0&0&0&1&0&0&0&0&0\\
0&0&0&0&0&0&0&2&1&0&0&0&0\\
0&0&0&0&2&0&0&0&18&0&0&1&0\\
0&0&0&0&0&0&0&0&0&18&0&0&0\\
0&0&0&0&0&0&0&1&0&0&86&0&4\\
0&0&0&0&0&0&5&0&1543&0&0&0&1\\
0&0&0&0&0&1&0&0&0&0&0&0&2\\
2&0&0&0&0&0&0&0&72&0&0&0&0
\end{pmatrix}$$

Ranks B: $R_2=\begin{pmatrix}2&3&135&18&1&5&36&1&1&1&1&1&1\end{pmatrix}$

Adjacency Matric B:

$$A_2 = \begin{pmatrix} 0 & 0 & 9 & 6 & 0 & 0 & 0 & 0 & 0 & 0 & 0 & 0 & 0 \\ 0 & 0 & 2 & 1 & 2 & 0 & 0 & 0 & 0 & 0 & 0 & 0 & 3 \\ 0 & 0 & 0 & 0 & 0 & 0 & 4 & 0 & 0 & 0 & 0 & 0 & 0 \\ 0 & 0 & 6 & 0 & 0 & 1 & 0 & 0 & 0 & 0 & 0 & 0 & 0 \\ 0 & 0 & 9 & 4 & 0 & 0 & 0 & 0 & 0 & 0 & 0 & 0 & 0 \\ 4 & 1 & 0 & 0 & 4 & 0 & 0 & 1 & 0 & 0 & 0 & 2 & 0 \\ 36 & 8 & 0 & 22 & 35 & 0 & 0 & 0 & 1 & 0 & 0 & 12 & 0 \\ 2 & 0 & 0 & 0 & 0 & 0 & 0 & 0 & 2 & 0 & 0 & 0 & 0 \\ 0 & 0 & 0 & 2 & 1 & 0 & 0 & 0 & 0 & 2 & 0 & 0 & 0 \\ 0 & 0 & 0 & 0 & 0 & 0 & 0 & 1 & 0 & 0 & 2 & 0 & 0 \\ 0 & 0 & 0 & 0 & 0 & 0 & 0 & 0 & 1 & 0 & 0 & 2 & 0 \\ 1 & 0 & 3 & 2 & 0 & 0 & 0 & 0 & 0 & 1 & 0 & 0 & 0 \\ 4 & 0 & 0 & 0 & 0 & 0 & 0 & 0 & 0 & 0 & 1 & 0 & 0 \end{pmatrix}$$

f. Seiberg duality and mutation distance for 14-node quivers

Consider a pair of 4D $\mathcal{N} = 1$ SCFTs, as described by a quiver gauge theory. The task is to determine whether two theories are Seiberg dual, and what is the minimal number of dualities / mutations on nodes which establishes this (if they are dual). For this problem, you are given the adjacency matrix and ranks of the gauge groups, but you can ignore the superpotential data. The two theories are presented as theory **A** and theory **B**.

Ranks A: $R_1 = \begin{pmatrix} 1 & 1 & 1 & 1 & 1 & 3 & 1 & 1 & 1 & 2 & 1 & 1 & 5 & 3 \end{pmatrix}$

Adjacency matrix A:

$$A_1 = \begin{pmatrix} 0 & 0 & 0 & 0 & 0 & 0 & 0 & 0 & 0 & 0 & 0 & 0 & 0 & 1 \\ 0 & 0 & 0 & 2 & 0 & 0 & 0 & 0 & 0 & 0 & 2 & 0 & 0 & 4 \\ 0 & 1 & 0 & 0 & 0 & 0 & 0 & 2 & 0 & 0 & 0 & 0 & 0 & 0 \\ 1 & 0 & 0 & 0 & 0 & 2 & 0 & 0 & 0 & 0 & 0 & 0 & 0 & 0 \\ 0 & 0 & 0 & 3 & 0 & 0 & 0 & 3 & 0 & 0 & 0 & 0 & 0 & 0 \\ 0 & 0 & 1 & 0 & 2 & 0 & 1 & 0 & 0 & 0 & 0 & 0 & 0 & 0 \\ 0 & 0 & 0 & 2 & 0 & 0 & 0 & 0 & 2 & 0 & 1 & 0 & 0 & 0 \\ 0 & 0 & 0 & 0 & 0 & 2 & 0 & 0 & 0 & 0 & 0 & 0 & 0 & 0 \\ 0 & 0 & 0 & 0 & 0 & 0 & 0 & 1 & 0 & 2 & 0 & 0 & 0 & 0 \\ 0 & 0 & 0 & 0 & 0 & 0 & 1 & 0 & 0 & 0 & 0 & 2 & 0 & 0 \\ 0 & 0 & 0 & 0 & 0 & 0 & 0 & 0 & 0 & 1 & 0 & 0 & 0 & 1 \\ 2 & 0 & 0 & 0 & 0 & 0 & 0 & 0 & 3 & 0 & 2 & 0 & 0 & 4 \\ 0 & 3 & 0 & 0 & 0 & 0 & 0 & 0 & 0 & 0 & 0 & 3 & 0 & 0 \\ 0 & 0 & 0 & 0 & 0 & 0 & 0 & 0 & 0 & 0 & 0 & 0 & 2 & 0 \end{pmatrix}$$

Ranks B: $R_2 = \begin{pmatrix} 1 & 1 & 1 & 1 & 25 & 1 & 1 & 24 & 6 & 4 & 1 & 17 & 1 & 1 \end{pmatrix}$

Adjacency Matric B:

$$A_2 = \begin{pmatrix} 0 & 2 & 0 & 0 & 0 & 0 & 0 & 0 & 0 & 0 & 0 & 0 & 0 & 0 \\ 0 & 0 & 1 & 0 & 0 & 0 & 0 & 0 & 0 & 0 & 0 & 0 & 1 & 0 \\ 0 & 0 & 0 & 2 & 0 & 0 & 0 & 0 & 0 & 0 & 0 & 0 & 0 & 0 \\ 1 & 0 & 0 & 0 & 0 & 2 & 0 & 1 & 0 & 0 & 0 & 0 & 0 & 0 \\ 0 & 0 & 0 & 1 & 0 & 0 & 0 & 0 & 0 & 2 & 0 & 1 & 0 & 0 \\ 0 & 0 & 1 & 0 & 2 & 0 & 1 & 0 & 0 & 0 & 0 & 0 & 0 & 0 \\ 0 & 0 & 0 & 0 & 0 & 0 & 0 & 0 & 4 & 0 & 0 & 0 & 0 & 0 \\ 0 & 0 & 0 & 0 & 1 & 0 & 0 & 0 & 0 & 0 & 0 & 0 & 0 & 0 \\ 0 & 0 & 0 & 0 & 0 & 0 & 0 & 4 & 0 & 0 & 0 & 0 & 0 & 0 \\ 0 & 0 & 0 & 0 & 0 & 4 & 5 & 0 & 18 & 0 & 1 & 0 & 0 & 0 \\ 0 & 0 & 0 & 0 & 0 & 0 & 3 & 0 & 0 & 0 & 0 & 0 & 2 & 0 \\ 0 & 0 & 0 & 0 & 0 & 2 & 0 & 0 & 1 & 4 & 0 & 0 & 1 & 0 \\ 0 & 0 & 0 & 0 & 0 & 0 & 0 & 0 & 3 & 0 & 0 & 0 & 0 & 2 \\ 1 & 0 & 0 & 0 & 0 & 0 & 0 & 0 & 0 & 0 & 1 & 0 & 0 & 0 \end{pmatrix}$$

g. Seiberg duality and mutation distance for 12-node quivers

Consider a pair of 4D $\mathcal{N}=1$ SCFTs, as described by a quiver gauge theory. The task is to determine whether two theories are Seiberg dual, and what is the minimal number of dualities / mutations on nodes which establishes this (if they are dual). For this problem, you are given the adjacency matrix and ranks of the gauge groups, but you can ignore the superpotential data. The two theories are presented as theory **A** and theory **B**.

Ranks A: $R_1 = \begin{pmatrix}1 & 1 & 1 & 1 & 14 & 3 & 1 & 37 & 45 & 1 & 1 & 2\end{pmatrix}$

Adjacency matrix A:

$$A_1 = \begin{pmatrix}0 & 0 & 0 & 1 & 3 & 0 & 0 & 0 & 0 & 2 & 0 & 0\\ 0 & 0 & 1 & 0 & 0 & 0 & 0 & 0 & 0 & 0 & 0 & 2\\ 0 & 0 & 0 & 0 & 6 & 0 & 0 & 0 & 0 & 0 & 0 & 0\\ 0 & 2 & 0 & 0 & 24 & 0 & 2 & 0 & 0 & 0 & 0 & 0\\ 0 & 0 & 0 & 0 & 0 & 0 & 0 & 0 & 3 & 0 & 0 & 0\\ 0 & 0 & 3 & 2 & 32 & 0 & 0 & 0 & 0 & 4 & 0 & 2\\ 0 & 0 & 0 & 0 & 0 & 1 & 0 & 0 & 0 & 0 & 0 & 0\\ 0 & 0 & 2 & 9 & 0 & 10 & 0 & 0 & 0 & 2 & 0 & 1\\ 1 & 0 & 0 & 0 & 0 & 2 & 0 & 1 & 0 & 0 & 2 & 0\\ 0 & 0 & 0 & 0 & 0 & 0 & 1 & 0 & 2 & 0 & 0 & 0\\ 0 & 3 & 0 & 0 & 6 & 0 & 0 & 0 & 0 & 3 & 0 & 0\\ 0 & 0 & 0 & 0 & 0 & 0 & 0 & 0 & 1 & 0 & 0 & 0\end{pmatrix}$$

Ranks B: $R_2 = \begin{pmatrix}1 & 1 & 12 & 1 & 5 & 1 & 1 & 7 & 3 & 5 & 1 & 1\end{pmatrix}$

Adjacency Matric B:

$$A_2 = \begin{pmatrix}0 & 0 & 0 & 0 & 0 & 0 & 0 & 4 & 0 & 0 & 0 & 0\\ 0 & 0 & 0 & 0 & 0 & 3 & 0 & 6 & 0 & 0 & 1 & 0\\ 2 & 3 & 0 & 4 & 0 & 0 & 0 & 0 & 2 & 0 & 0 & 0\\ 3 & 0 & 0 & 0 & 0 & 4 & 0 & 8 & 0 & 0 & 0 & 0\\ 0 & 2 & 0 & 3 & 0 & 0 & 0 & 0 & 0 & 0 & 2 & 0\\ 0 & 0 & 1 & 0 & 0 & 0 & 1 & 0 & 0 & 0 & 0 & 0\\ 0 & 0 & 0 & 0 & 0 & 0 & 0 & 0 & 0 & 3 & 0 & 0\\ 0 & 0 & 2 & 0 & 1 & 0 & 0 & 0 & 0 & 0 & 0 & 0\\ 0 & 0 & 0 & 0 & 0 & 2 & 4 & 3 & 0 & 0 & 6 & 1\\ 0 & 0 & 0 & 0 & 0 & 0 & 0 & 0 & 2 & 0 & 0 & 0\\ 0 & 0 & 0 & 0 & 0 & 0 & 0 & 2 & 0 & 3 & 0 & 0\\ 1 & 0 & 0 & 0 & 0 & 0 & 2 & 0 & 0 & 0 & 0 & 0\end{pmatrix}$$

8. Particle physics

a. Axion-to-photon conversion in a dielectric medium

Compute the rate for axion conversion to photons via scattering off the electrons in a dielectric medium. Assume that there is no external electric field and the medium is a conventional solid state material (non-magnetic, zero temperature), that the axion only interacts via an $aF\tilde{F}$ coupling. Express the result in terms of the dielectric function epsilon of the medium. Consider both relativistic and non-relativistic axions.

Consider the case when the dielectric function of the medium satisfies

$$\mathrm{Im}\left[\frac{-1}{\varepsilon_L(\omega,q)}\right] \;=\; \frac{\pi}{2}\,\omega_p\,\delta(\omega-\omega_p), \tag{A62}$$

Working in natural units ($\hbar = c = 1$), take the axion-photon coupling $g_{a\gamma\gamma} = 10^{-10}\,\mathrm{GeV}^{-1}$, frequency $\omega_p = 16.6\,\mathrm{eV}$, refractive index $n = 1.5$, and axion velocity $v_a = 10^{-3}$. Evaluate the rate Γ_{NR} for (1) $m_a = 25\,\mathrm{eV}$ and (2) $m_a = 15\,\mathrm{eV}$. Express the final numerical answer in scientific form in eV units in the order [(1),(2)]

b. Lorentz structures of an axial-vector tetraquark matrix element

Consider the light-cone matrix element of a four-quark operator containing two quark fields and two antiquark fields, with four open Dirac indices, taken between the vacuum and a spin-1 (axial-vector) tetraquark state characterized by a polarization vector ($\epsilon^\mu(P,\lambda)$). Construct the most general Lorentz-covariant decomposition of this matrix element into independent Lorentz structures, subject to the relevant symmetry constraints. How many independent Lorentz structures appear in this decomposition?

9. Scattering amplitudes

a. Series for pi from higher-subtracted dispersion relations

Starting from the summation-series representation of the Euler beta function, it yields a parametric series representation for π,

$$\pi = 4 + \sum_{n=1}^{\infty} \frac{1}{n!} \left(\frac{1}{n+\lambda} - \frac{4}{2n+1} \right) \left(\frac{(2n+1)^2}{4(n+\lambda)} - n \right)_{n-1}. \tag{A63}$$

On the other hand, higher-subtracted crossing-symmetric dispersion relation was proposed by string theory:[1]

$$\begin{aligned} \mathcal{M}(s,t) = & \sum_{p=0}^{N-1} (s+\lambda)^p (t+\lambda)^p \left[\frac{\partial^p}{\partial s^p} \frac{\partial^p}{\partial t^p} \mathcal{M}(s,t) \right]_{s=-\lambda,\, t=-\lambda} \\ & - \frac{1}{\pi} \int_{\mathcal{C}_1} d\sigma \Bigg\{ \mathcal{H}^{(\lambda)}(\sigma,s,t) \mathcal{A}^{(s)} \left(\sigma, \frac{(s+\lambda)(t+\lambda)}{\sigma+\lambda} - \lambda \right) \\ & - \sum_{p=0}^{N-1} (s+\lambda)^p (t+\lambda)^p \left[\frac{\partial^p}{\partial s^p} \frac{\partial^p}{\partial t^p} \mathcal{H}^{(\lambda)}(\sigma,s,t) \mathcal{A}^{(s)} \left(\sigma, \frac{(s+\lambda)(t+\lambda)}{\lambda+\sigma} - \lambda \right) \right]_{s=-\lambda,\, t=-\lambda} \Bigg\}. \end{aligned} \tag{A64}$$

where

$$\mathcal{H}^{(\lambda)}(\sigma,s,t) = \frac{1}{\sigma-s} + \frac{1}{\sigma-t} - \frac{1}{\sigma+\lambda}, \tag{A65}$$

and

$$\mathcal{A}^{(s)}(s,t) = \lim_{\epsilon \to 0^+} \frac{1}{2i} \left[\mathcal{M}(s+i\epsilon,t) - \mathcal{M}(s-i\epsilon,t) \right]. \tag{A66}$$

Please use this disperse relation to derive a new parameter-dependent series for π. Choose a suitable value of the parameter λ, derive the resulting series explicitly, and verify numerically that it converges to π. Finally, compare its convergence rate with that of the original series and determine whether the higher-subtracted construction provides genuinely faster convergence or merely amounts to a rearrangement obtained by adding a zero-sum subtraction term.

Report the following three numerical outputs, in order:

- Report 1 if the higher-subtracted series converges faster than the original series, and 0 otherwise.
- For $\lambda = \frac{21}{2}$, compute the absolute error between π and the partial sum of the first 10 terms of the original series derived from the Euler beta (shifted open-string) amplitude.
- For $\lambda = \frac{21}{2}$, compute the absolute error between π and the partial sum of the first 10 terms of the series derived from the higher-subtracted crossing-symmetric dispersion relation.

---

[1] This prompt does not specify N explicitly and our reference answers allow $N = 1$ and $N = 2$ corresponding to choices observed in our evaluation. A manual check should be used to account for correct answers based on other choices of N.

b. Hidden-zero constraints on partial waves and effective-field-theory coefficients

Consider a planar massless four-point scalar amplitude in spacetime dimension d. At mass level $s = k$, write the residue in a Gegenbauer partial-wave basis as

$$R_k(z) = \operatorname*{Res}_{s=k} M_4(s,t) = \sum_{j=0}^{k} c_j^{(k)} C_j^{\lambda}(z), \qquad \lambda = \frac{d-3}{2}, \qquad z = 1 + \frac{2t}{k}.$$

Assume this residue descends from a five-point tree-level residue obeying two independent splitting constraints. These imply a hidden zero at backward scattering,

$$R_k(-1) = 0 \qquad \Longleftrightarrow \qquad t = -k.$$

Task. Determine the arbitrary-d, all-level linear relation among the coefficients $c_j^{(k)}$, using

$$C_j^{\lambda}(1) = \frac{(2\lambda)_j}{j!},$$

and show that in $d = 4$ it reproduces

$$c_0^{(1)} = c_1^{(1)}, \qquad c_0^{(2)} - c_1^{(2)} + c_2^{(2)} = 0.$$

Next expand

$$M_4(s,t) = \sum_{n,m\geq 0} \alpha_{n,m} s^n t^m,$$

and let $\alpha_{n,m}^{(k)}$ denote the contribution from the pole $R_k(t)/(k-s)$. Derive the corresponding all-level relation among $\alpha_{n,m}^{(k)}$, valid for every fixed n, and verify that for $k = 1, 2$ it gives

$$\alpha_{n,0}^{(1)} = \alpha_{n,1}^{(1)}, \qquad \alpha_{n,1}^{(2)} - \frac{1}{2}\alpha_{n,0}^{(2)} = 2\alpha_{n,2}^{(2)}.$$

Check both relations explicitly at $k = 1, 2, 3$.

Finally, at $d = 7$ and $k = 3$, use

$$c_0^{(3)} = 7, \qquad c_1^{(3)} = -2, \qquad c_2^{(3)} = 5$$

to determine $c_3^{(3)}$, and use

$$\alpha_{n,0}^{(3)} = 5, \qquad \alpha_{n,1}^{(3)} = -1, \qquad \alpha_{n,2}^{(3)} = 2$$

to determine $\alpha_{n,3}^{(3)}$. Report

$$\boxed{\Xi = 108\, c_3^{(3)} + 67\, \alpha_{n,3}^{(3)}}.$$

Deliverable: A one-page derivation, a short symbolic check for $k = 1, 2, 3$, and a final line containing only the numerical value of Ξ.

c. One-loop double-trace renormalization in cubic matrix scalar theory

Work in $D = 4$ with trace multiplicities

$$n_1 = 6, \qquad n_2 = 7.$$

Use dimensionless variables, with the mass scale set to one. There are five original comb coordinates s_j^1, six original comb coordinates s_j^2, and core coordinates $x > 0$, $y \in \mathbb{R}$.

Define

$$L = \begin{pmatrix} 1 & 0 \\ 1 & 1 \end{pmatrix}, \qquad R = L^{\mathsf{T}}, \qquad D(s) = \operatorname{diag}(1, e^{s}),$$

and, independently for each trace $A \in \{1, 2\}$,

$$W_1^A = LD(s_1^A) \cdots LD(s_{n_A-1}^A),$$

$$W_i^A = RD(s_{i-1}^A)LD(s_i^A) \cdots LD(s_{n_A-1}^A), \qquad 2 \le i \le n_A.$$

An empty product is the identity. Also define

$$B = LD(x)LD(y)L.$$

Tropicalization replaces a positive sum of exponential monomials by the maximum of their exponents; positive coefficients are ignored. For a matrix M with nonzero entries, define

$$\operatorname{Head}(M) = \operatorname{Trop} M_{11} + \operatorname{Trop} M_{22} - \operatorname{Trop} M_{12} - \operatorname{Trop} M_{21}.$$

Set

$$\alpha_{ii}^A = \operatorname{Head}\big(W_i^A B (W_i^A)^{\mathsf{T}}\big),$$

and let $\mathcal{M}_{\mathrm{diag}}$ be the locus on which

$$\alpha_{ii}^A = 0$$

for every i on both traces. These equations specify the grafted-diagonal convention used in this question.

Introduce

$$r = x + |y|, \qquad u = \frac{x}{r}, \qquad h = \min(0, y),$$

and

$$z_k^A = \sum_{j=k}^{n_A-1} s_j^A + h, \qquad 1 \le k \le n_A - 1.$$

For generic points of $\mathcal{M}_{\mathrm{diag}}$, use the **rightmost-negative-suffix indices**

$$k_A = \max\{k : z_k^A < 0\}$$

to label the canonical sectors. Together with the sign of y, these indices specify the sectors to be counted. Ignore lower-dimensional boundaries, and do not count additional arbitrary subdivisions.

Let N_+ and N_- denote the numbers of nonempty full-dimensional canonical sectors with $y > 0$ and $y < 0$, respectively.

For $\sigma \in \{+1, -1\}$, define

$$\mathcal{D}_\sigma(\epsilon) = \mathcal{M}_{\mathrm{diag}} \cap \big\{\sigma y > 0, \quad 0 < r < \epsilon, \quad |s_j^A| \le 1 \text{ for every original comb coordinate}\big\},$$

and the improper integral

$$I_\sigma(\epsilon) = \frac{1}{2^{11}} \int_{\mathcal{D}_\sigma(\epsilon)} \frac{x}{r^3} \exp[-r\,(1 + 3u(1-u))]\, \mathrm{d}x\, \mathrm{d}y\, \mathrm{d}^5 s^1\, \mathrm{d}^6 s^2.$$

The factor π^2 from the loop integration has already been divided out. The prefactor x/r^3 is the $D = 4$ density factor.

The box and exponential above **define a smeared ultraviolet observable**, not the full physical thirteen-point amplitude. In particular, the box is imposed on the original s-coordinates, **not** on the suffix coordinates z.

Let N_{CT} be the number of canonical sectors whose bare radial integral requires any ultraviolet subtraction at $r = 0$. No additional finite counterterm is permitted.

Determine the smallest common integer β for which

$$I_\sigma(\epsilon) = \epsilon^\beta \big(c_{\sigma,0} + c_{\sigma,1}\epsilon + c_{\sigma,2}\epsilon^2 + c_{\sigma,3}\epsilon^3 + c_{\sigma,4}\epsilon^4 + c_{\sigma,5}\epsilon^5\big) + O(\epsilon^{\beta+6}),$$

with both $c_{+,0}$ and $c_{-,0}$ nonzero.

d. Two loop subdivergences

Work in Euclidean $D = 6$. Set every propagator mass, the coupling, the color factor, and the diagram multiplicity to one.

Consider the amputated planar four-point contribution obtained by inserting a two-loop two-point component into the internal channel of a cubic four-point tree. The two propagators connecting the inserted component to the exterior cubic vertices both carry momentum q, with

$$s = q^2.$$

The unrenormalized contribution is defined by

$$\mathcal{A}_{\mathrm{bare}}(s) = \frac{1}{(s+1)^2} \int_{\mathbb{R}^6} \frac{\mathrm{d}^6 k}{\pi^3} \int_{\mathbb{R}^6} \frac{\mathrm{d}^6 \ell}{\pi^3} \frac{1}{D_1 D_2 D_3 D_4 D_5},$$

where

$$\begin{aligned} D_1 &= k^2 + 1, & D_2 &= (k+q)^2 + 1, \\ D_3 &= \ell^2 + 1, & D_4 &= (\ell+q)^2 + 1, \\ D_5 &= (k-\ell)^2 + 1. \end{aligned}$$

Including the two channel propagators, this is a **seven-propagator four-point contribution**. There is no additional symmetry factor and no sum over other four-point diagrams.

Use the following local momentum-subtraction prescription.

a. Three-point components Subtract each logarithmically divergent three-point component at zero values of all momenta external to that component.

b. Two-point components First remove all internal subdivergences. Then impose, on the renormalized two-point component $S_R(t)$,

$$S_R(2) = 0, \qquad \left.\frac{\mathrm{d}S_R(t)}{\mathrm{d}t}\right|_{t=2} = 0,$$

where t is that component's external momentum squared.

c. Compatibility and locality Each subtraction acts on the selected component, not on propagators belonging only to the rest of the diagram. Simultaneous subtraction terms must respect disjointness or nesting; incompatible overlapping components cannot belong to the same forest. No additional finite four-point counterterm is added.

These prescriptions distinguish the two-point and three-point subtraction orders. Internal subdivergences must be removed before forming a proper two-loop subtraction.

Let N_{div} be the number of connected, proper, one-particle-irreducible ultraviolet-divergent components of the complete seven-propagator contribution.

Let N_F be the number of allowed subtraction forests, **including the empty forest**.

Let $\mathcal{A}_R(s)$ be the renormalized four-point contribution, and define the renormalized inserted two-point function by

$$\Sigma_R(s) = (s+1)^2 \mathcal{A}_R(s).$$

Determine b_2, b_3, b_4 from

$$\Sigma_R(2+\delta) = b_2\delta^2 + b_3\delta^3 + b_4\delta^4 + O(\delta^5).$$

Required numerical answer Return **only**

$$\boxed{\left(N_{\mathrm{div}}, N_F, \mathcal{A}_R\left(\tfrac{1}{2}\right), \mathcal{A}_R(3), \mathcal{A}_R(8), b_2, b_3, b_4\right).}$$

The integer entries must be exact. Every real-valued entry must have absolute error at most

$$\boxed{5 \times 10^{-11}}.$$

The loop normalization is fixed by the explicitly displayed measures $\mathrm{d}^6 k/\pi^3$ and $\mathrm{d}^6 \ell/\pi^3$.

e. Nested consecutive amplitude

The process $\Phi(p_a)\,\bar{\Phi}(p_b) \to \Phi(p_3)\,\bar{\Phi}(p_4)$ of massless scalars with charges $\pm e$ has on-shell amplitude

$$\mathcal{M}_4 = \frac{s^2+2st-3}{(s+2)(t-1)}, \qquad s=-(p_a+p_b)^2, \quad t=-(p_a-p_3)^2$$

(mostly-plus signature), generated by neutral short-distance physics. The scalars are minimally coupled to the photon. Let $\mathcal{M}_7$ be the stripped amplitude for the same process with three additional outgoing photons, at lowest order in e, with no photon exchanged between the scalars and no soft singularities other than external-leg poles.

Kinematics, (E, p_x, p_y, p_z):

$$p_a = (1,0,0,1), \qquad p_b = (1,0,0,-1), \qquad \hat{n}_3 = \tfrac{1}{3}(2,-1,2),$$

$$k_1 = \omega_1\big(1, \tfrac{4}{9}, \tfrac{8}{9}, -\tfrac{1}{9}\big), \qquad k_2 = \omega_2\big(1, \tfrac{2}{3}, -\tfrac{1}{3}, -\tfrac{2}{3}\big), \qquad k_3 = \omega_3\big(1, -\tfrac{8}{9}, \tfrac{4}{9}, -\tfrac{1}{9}\big),$$

$$\varepsilon_1 = \tfrac{1}{\sqrt{2}}\big(\tfrac{1}{2}-i,\, 1,\, -i,\, -\tfrac{1}{2}+i\big), \quad \varepsilon_2 = \tfrac{1}{\sqrt{2}}\big(2-i,\, 1,\, i,\, -2+i\big), \quad \varepsilon_3 = \tfrac{1}{\sqrt{2}}\big(-1-\tfrac{i}{2},\, 1,\, -i,\, 1+\tfrac{i}{2}\big).$$

p_a, p_b and the direction $\hat{n}_3$ of p_3 are fixed; $|\vec{p}_3|$ and p_4 follow from conservation. $\mathcal{M}_7$ is contracted with $\varepsilon_1, \varepsilon_2, \varepsilon_3$ as written.

Let $F(\omega_1,\omega_2,\omega_3) = \omega_1\omega_2\omega_3\,\mathcal{M}_7$. For a permutation (a,b,c) of $(1,2,3)$ define the iterated Laurent coefficient

$$C_{a\to b\to c} = [\omega_c^1]\Big([\omega_b^1]\big([\omega_a^1]F\big)\Big) :$$

expand in ω_a at fixed non-zero ω_b, ω_c and take the coefficient of ω_a^1; expand that coefficient in ω_b at fixed non-zero ω_c and take the coefficient of ω_b^1; then expand in ω_c and take the coefficient of ω_c^1. Let

$$A_{\text{lead}} = \lim_{\omega\to 0} F(\omega,\omega,\omega), \qquad J = \sum_{(a,b,c)} \operatorname{sgn}(a,b,c)\, C_{a\to b\to c},$$

the sum running over all six permutations, with $\operatorname{sgn}(1,2,3) = +1$.

Answer format: two complex numbers $\Big(\dfrac{J}{A_{\text{lead}}},\ \dfrac{C_{1\to2\to3} - C_{1\to3\to2}}{A_{\text{lead}}}\Big)$.

10. Holography and entanglement

a. Transmission through warped holographic interfaces

Consider[2] a holographic conformal interface described by three-dimensional Einstein gravity with a common Newton constant G_N on both sides and metric

$$ds^2 = dy^2 + a(y)^2 ds^2_{\mathrm{AdS}_2}, \qquad -\infty < y < \infty,$$

where $ds^2_{\mathrm{AdS}_2}$ is the *unit-radius* AdS_2 metric. All lengths below are expressed in a common reference unit. Take

$$a(y)^2 = \Big(\cosh\frac{y}{2}\Big)^{24/35}, \qquad 16\pi G_N = 1.$$

Derive the energy transmission coefficient in terms of the warp factor for an asymptotically AdS_3 interface geometry. Verify that the specified warp factor has equal asymptotic AdS_3 radii $\ell_L = \ell_R$. With $c_i = 3\ell_i/(2G_N)$, use the convention

$$\mathcal{T}_{L\to R} = \frac{c_{LR}}{c_L}, \qquad \mathcal{T}_{R\to L} = \frac{c_{LR}}{c_R}.$$

Calculate their common value $\mathcal{T}$, the fraction of incident energy transmitted through the interface, to absolute accuracy 10^{-6}.

---

[2] After the evaluations reported in this paper were completed, a solution to this problem appeared publicly in [65] as one element of a broader study.

b. Radion effective actions for higher-dimensional branes

Consider a Randall–Sundrum two-brane setup with d-dimensional UV and IR branes in an AdS_{d+1} bulk governed by Einstein gravity. Work at leading two-derivative order and leading order in small brane-tension detunings. Include the usual gravitational boundary terms and brane tensions, with no brane-localized curvature terms, additional stabilization fields, or quantum corrections.

Derive the low-energy effective action for the radion and the metric in the UV-brane Jordan frame. Fix the dimensionless radion ϕ and the frame by requiring that the Ricci-scalar coupling be exactly $(1-\phi^2)\mathcal{R}[g]$. Choose the positive radion branch $0<\phi<1$; in the leading warped background, the induced IR-brane metric is $g^{\mathrm{IR}}_{\mu\nu}=\Omega^2 g_{\mu\nu}$ with $\phi=\Omega^{(d-2)/2}$.

Write the action in the convention

$$S_{\mathrm{eff}}=\frac{1}{16\pi G_d}\int d^dx\sqrt{-g}\,\left[(1-\phi^2)\mathcal{R}[g]-K_d\,g^{\mu\nu}\partial_\mu\phi\,\partial_\nu\phi-2V(\phi)\right],\qquad V(\phi)=\Lambda_{\mathrm{UV}}+\lambda_{\mathrm{IR}}\phi^{p_d}.$$

Here the metric has mostly-plus signature, K_d is a positive constant with *no factor of* $1/2$ included in its definition, and Λ_{UV} and λ_{IR} are independent signed constants encoding the tension detunings. Take $\lambda_{\mathrm{IR}}\neq 0$ so that the potential power is identifiable. G_d is the constant normalization outside the action, fixed by the $\phi\to 0$ gravitational term.

Determine K_d and the power p_d for general $d>2$.

c. Universal entanglement logarithms in higher-dimensional interface CFTs

Consider the conformal vacuum of an even-dimensional interface CFT with $d>2$ on $\mathbb{R}\times S^{d-1}$, with metric

$$ds^2=-dt^2+R^2\left(d\theta^2+\sin^2\theta\,d\Omega^2_{d-2}\right).$$

Here $d\Omega^2_{d-2}$ is the unit-round-sphere metric. A conformal interface lies at $\theta=\pi/2$, with CFT_1 on $\theta<\pi/2$ and CFT_2 on $\theta>\pi/2$. On a constant-time slice consider

1. $A=\{\theta<\pi/2\}$, a hemisphere whose entangling sphere coincides with the interface;
2. $A=\{\theta_L<\theta<\theta_R\}$, with $0<\theta_L<\pi/2<\theta_R<\pi$, whose two entangling spheres lie away from the interface;
3. $A=\{\pi/2<\theta<\theta_R\}$, with one entangling sphere on the interface and the other in CFT_2.

Anomaly and interface normalization. Define the bulk A-type charges A^d_j by

$$\langle T^{\mu}{}_{\mu}\rangle_j=-2(-1)^{d/2}A^d_jE_d+\sum_\alpha B_{j,\alpha}I_\alpha+\nabla_\mu J^\mu_j,\qquad \int_{S^d}d^dx\sqrt{g}\,E_d=2.$$

Thus E_d is the Euler density normalized to integrate to the Euler characteristic on a closed manifold, I_α are Weyl invariants, and the last term denotes scheme-dependent total derivatives. For example, $E_2=\mathcal{R}/(4\pi)$ and $E_4=(\mathcal{R}^2_{\mu\nu\rho\sigma}-4\mathcal{R}^2_{\mu\nu}+\mathcal{R}^2)/(32\pi^2)$. Use a covariant replica prescription with smooth-cone regularization.

Fix the normalization of the interface charge by the following calibration. Let $\mathcal{C}_I$ be the coefficient of $\log(2R/\epsilon)$ in the hemisphere entropy in configuration 1. For any reference CFT with nonzero A-type charge A^d_{ref} in the convention above, let $\mathcal{C}_{\mathrm{ref}}$ be the corresponding hemisphere logarithmic coefficient without an interface. Define

$$A^d_{\mathrm{eff}}\equiv A^d_{\mathrm{ref}}\,\frac{\mathcal{C}_I}{\mathcal{C}_{\mathrm{ref}}}.$$

The same convention must be used for all three charges; no further rescaling of A^d_{eff} or A^d_j is allowed.

Logarithms and requested coefficients. Use a proper-distance UV cutoff ϵ. Each entangling sphere has radius $\rho=R\sin\theta$, and its logarithm is to be written explicitly as $\log(2\rho/\epsilon)$. Define

$$\mathcal{L}_L=\log\frac{2R\sin\theta_L}{\epsilon},\qquad \mathcal{L}_R=\log\frac{2R\sin\theta_R}{\epsilon},\qquad \mathcal{L}_I=\log\frac{2R}{\epsilon}.$$

Here $S^{\log}_i$ denotes the local UV logarithmic contributions, written with these specified arguments. Finite terms, including finite functions of the latitude angles, are outside the requested quantity.

Give a single replica-partition-function definition of A^d that realizes both A_j^d and A_{eff}^d with the normalization above, and show that the interface definition is independent of the reference CFT. Derive $S_i^{\log}$ for all three configurations. Explain why the round latitude geometry permits the bulk contributions to be expressed using the A-type charges alone, and why the logarithmic divergences are local to the separate entangling components.

For $d = 6$, $R = 10$, $\epsilon = 10^{-10}$, $\theta_L = \pi/10$, and $\theta_R = 7\pi/10$, define the numerical targets by the formal decomposition

$$S_i^{\log} = a_i A_1^6 \mathcal{L}_L + b_i A_2^6 \mathcal{L}_R + c_i A_{\text{eff}}^6 \mathcal{L}_I, \qquad i = 1, 2, 3.$$

Report the three exact numerical triples (a_i, b_i, c_i) in the fixed normalization above, setting the coefficient of any absent contribution to zero. Treat the charges as independent symbolic theory data when extracting these coefficients. *Leave all logarithms factored out: the requested numbers contain neither logarithms nor central charges.*

d. Island surfaces and Page time in a black-string geometry

Consider a black-string background with two branes at equal angles, $\pi/10$, from the vertical in AdS_4. By comparing minimal surfaces that extend from the defect to the brane to minimal surfaces that extend from a defect on one side of the horizon to the other, find the Page time for this configuration in units where the temperature is $1/(2\pi)$.

e. Geometric-entropy Hamiltonian flow in higher-derivative gravity

Work in four spacetime dimensions with $L = z_0 = 1$ and metric signature $(-,+,+,+)$. Use the curvature convention

$$R^{\rho}{}_{\sigma\mu\nu} = \partial_\mu \Gamma^\rho_{\nu\sigma} - \partial_\nu \Gamma^\rho_{\mu\sigma} + \Gamma^\rho_{\mu\lambda}\Gamma^\lambda_{\nu\sigma} - \Gamma^\rho_{\nu\lambda}\Gamma^\lambda_{\mu\sigma}.$$

Define

$$W = C_{\mu\nu\rho\sigma} C^{\mu\nu\rho\sigma},$$

and consider the pure-gravity action

$$\begin{aligned} I[g] = \frac{1}{16\pi G} \int d^4x \, \sqrt{-g} \, (R + 6 + 0.087600\, W + 0.007300\, RW + 0.000843480\, W^2 \\ + 0.000043645\, RW^2 + 0.000079935\, \nabla_\mu W \nabla^\mu W) \end{aligned}$$

All displayed decimals are exact inputs. Work perturbatively on the branch continuously connected to Einstein gravity. Treat the terms linear in W as first perturbative order, treat the remaining three corrections as second order, and discard effects of third and higher perturbative order.

Define geometric entropy using the Lewkowycz–Maldacena smooth-cover conical-response prescription, including the extrinsic-curvature contributions. Apply the prescription to the action in exactly the displayed representative, and fix the defect term by the Dirichlet variational principle. Do not replace geometric entropy by Wald entropy alone.

A solution through the displayed perturbative order is

$$ds^2 = \frac{A(z)}{z^2} \left[-dt^2 + dx^2 + (1 - z^3)\, d\chi^2 + \frac{dz^2}{1 - z^3} \right],$$

where

$$A(z) = 1 - 0.087600\, z^6 - 0.013958640\, z^{12}, \qquad \chi \sim \chi + \frac{4\pi}{3}.$$

On the boundary at $t = 0$, consider the strip

$$-\frac{0.600000}{2} \le x \le \frac{0.600000}{2},$$

wrapping the χ-circle. Let Γ be the connected extremal surface homologous to this strip, and let p be its deepest point. You may assume that, for the stated strip width, this connected surface is the dominant HRT saddle.

At p, let u be the future-directed timelike unit normal to the $t = 0$ slice, and let m be the spacelike unit normal to Γ within the $t = 0$ slice, oriented toward increasing z.

Choose a smooth spacelike Cauchy surface Σ containing Γ. It may be taken to agree with the $t = 0$ surface away from a neighborhood of p. At p, choose the future-directed unit normal n to Σ and the unit vector r that is tangent to Σ and normal to Γ to be

$$n = \sqrt{2}\, u + m, \qquad r = u + \sqrt{2}\, m.$$

Thus

$$n^2 = -1, \qquad r^2 = +1, \qquad n \cdot r = 0.$$

Equivalently, (n, r) is obtained from (u, m) by a boost in the normal plane with

$$\sinh \eta = 1.$$

Let h_{ij} be the induced metric on Σ and define its extrinsic curvature by

$$K_{ij} = h_i{}^{\mu} h_j{}^{\nu} \nabla_{\mu} n_{\nu}.$$

Choose the local extension of Σ so that

$$K_{rr} = 0, \qquad K_{rA} = 0$$

at p, where indices A, B are tangent to Γ. Orient the spatial frame at p by

$$\epsilon_{rx\chi} = +1.$$

Let σ_Γ denote the geometric entropy of Γ, and define its Hamiltonian vector field by

$$X_\sigma O = \{O, \sigma_\Gamma\}.$$

Fix the sign of the bracket by requiring that the Einstein-gravity limit has

$$X_\sigma K_{rr} = +2\pi\, \delta_\Sigma(\Gamma).$$

Let q_{AB} be the induced metric on Γ. Introduce Gaussian normal coordinates (ρ, y^A) on Σ near Γ, with ρ the signed proper distance along r and $y^A = 0$ at p. Normalize the surface delta function invariantly by

$$\int_\Sigma \sqrt{h}\, f\, \delta_\Sigma(\Gamma) = \int_\Gamma \sqrt{q}\, f$$

for every smooth test function f. In these coordinates,

$$\delta_\Sigma(\Gamma) = \delta(\rho), \qquad \int d\rho\, \delta(\rho) = 1.$$

Define the coefficient $Q(y)$ of the delta-function part of the induced-metric flow by

$$q^{AB} X_\sigma h_{AB} = Q(y)\, \delta_\Sigma(\Gamma) + \text{terms less singular than } \delta_\Sigma(\Gamma).$$

The quantity $Q(y)$ is a coefficient in the canonical initial data on the specified Cauchy surface; no invariance under changing Σ is assumed.

Compute $Q(p)$, i.e.

$$Q(y^A = 0),$$

through second perturbative order. Give the answer to four decimal places.

11. Gravitation and cosmology

a. Topological black-hole and Nariai near-horizon geometries

Consider four-dimensional gravity coupled to scalars ϕ^i and Abelian gauge fields, with scalar potential $V(\phi)$ and black-hole potential $V_{\rm BH}(\phi)$. For a Bertotti–Robinson near-horizon geometry $\mathrm{AdS}_2 \times S^2$ with constant scalars $\bar{\phi}^i$ and radii $R_{\rm AdS}$ and R, the conditions are

$$\partial_i V + \frac{1}{R^4}\partial_i V_{\rm BH} = 0, \tag{1}$$

$$V - \frac{2}{R^2} + \frac{V_{\rm BH}}{R^4} = 0, \tag{2}$$

$$-\frac{2}{R_{\rm AdS}^2} = V - \frac{V_{\rm BH}}{R^4}, \tag{3}$$

$$R_{\rm AdS}^2 = \frac{R^2}{1 - R^2 V}, \tag{4}$$

where all potentials are evaluated at $\bar{\phi}$.

Generalize these equations to near-horizon vacua

$$M_2 \times \Sigma_2,$$

allowing topological black holes and Nariai-type solutions. Introduce

$$k, \tilde{k} \in \{-1, 0, +1\},$$

with

$$k = -1, 0, +1 \quad \text{for} \quad M_2 = \mathrm{AdS}_2, \mathbb{R}^{1,1}, \mathrm{dS}_2,$$

and

$$\tilde{k} = +1, 0, -1 \quad \text{for} \quad \Sigma_2 = S^2, T^2, H^2/\Gamma.$$

Let

$$R_{ab}(M_2) = \frac{k}{L^2} g_{ab}, \qquad R_{mn}(\Sigma_2) = \frac{\tilde{k}}{R^2} g_{mn}.$$

Derive the analogues of (1)–(4), explicitly including k and $\tilde{k}$, in a form valid also for $k = 0$. Verify that they reduce to (1)–(4) for $k = -1, \tilde{k} = +1$, and state the conditions for $L^2 > 0$ and $R^2 > 0$.

Finally, for

$$k = 3, \quad \tilde{k} = 2, \qquad \partial_i V = \partial_i V_{\rm BH} = 0, \qquad V = \frac{3}{4}, \qquad V_{\rm BH} = 1,$$

select the $\mathrm{dS}_2 \times S^2$ branch with positive squared radii and report the numerical values of L and R.

b. Late-time scale separation in type IIB flux cosmology

Consider ten-dimensional type IIB supergravity compactified on a six-torus T^6, with a homogeneous internal Ramond–Ramond three-form flux F_3.

Choose a flux ansatz and torus geometry such that the ten-dimensional equations admit a consistent truncation to the following four-dimensional fields:

1. the four-dimensional dilaton,
2. the overall volume modulus of T^6, and
3. an FLRW metric.

Construct the resulting time-dependent cosmological solution and determine its late-time scaling behaviour. In particular, compare the four-dimensional Hubble scale $H(t)$ with the lightest Kaluza–Klein mass scale $m_{\rm KK}(t)$.

Does the solution exhibit parametric scale separation at late times, in the sense that

$$\frac{m_{\rm KK}(t)}{H(t)} \longrightarrow \infty \qquad \text{as} \qquad t \longrightarrow \infty?$$

Finally, determine the late-time exponent γ defined by

$$\frac{m_{\rm KK}(t)}{H(t)} \sim t^{\gamma},$$

and report γ as a single numerical value to three significant figures in the two cases of flat and hyperbolic spatial FLRW metrics. Give this as a ordered tuple $(\gamma_{\rm flat}, \gamma_{\rm hyperbolic})$.

c. Cosmological attractors from products of compact hyperbolic spaces

Consider Einstein Hilbert gravity in 4+ 2n dimensions, where n is an integer. The 2n dimensions are all compact and made up of a direct product of n 2-dimensional compact hyperboloids (Examples of Riemann surfaces). If one keeps the separate volumes of the hyperboloids as degrees of freedom, the lower-dimensional theory has n scalar fields whose kinetic term can be canonically normalised since the Riemann tensor of the scalar manifold in the 4d effective field theory vanishes. In that normalisation the scalar potential is a sum of n different positive exponentials in which multiple of the scalars reside linearly in the potential. It has the form sometimes known as Generalised Assisted Inflation.

1. Find the effective action explicitly
2. Construct the cosmological attractor solution.
3. Lift it back to the higher-dimensional theory. Do you recognize the solution?
4. What would happen if I replace one of the hyperboloids with a sphere? What would the cosmological attractor than look like?

For $n = 3$ report the following numerical values in order:

1. Effective squared exponential slope of the assisted attractor
2. Power of the four-dimensional Einstein-frame scale factor, $a(t) \propto t^p$
3. For a spatially flat 4D Einstein-frame cosmology, output 1 if replacing exactly one H^2 factor by S^2 still admits a smooth, ever-expanding late-time cosmological attractor continuously analogous to the all-hyperbolic scaling solution; otherwise output 0.

d. Euclidean wormholes in compactified type IIB supergravity

Consider Euclidean type IIB supergravity compactified on a six-torus T^6. Perform a dimensional reduction to four dimensions and identify a consistent truncation of the resulting $\mathcal{N} = 8$ supergravity that contains the scalar and axionic fields required to support Euclidean wormhole solutions.

1. Derive the four-dimensional truncated action and determine whether its scalar target-space geometry admits wormholes satisfying the standard regularity criterion to produce a non-singular wormhole.
2. Construct the corresponding four-dimensional Euclidean wormhole solution and lift it explicitly to a ten-dimensional solution of Euclidean type IIB supergravity.
3. Determine whether the wormhole admits an extremal limit. If so, identify and describe the corresponding extremal ten-dimensional solution.
4. Compute the renormalized on-shell action of the wormhole, including all necessary boundary terms.

Also give the following numerical answers in Planck units ($\kappa_4 = 1$):

1. timelike geodesic length in the moduli space relevant for this wormhole
2. the critical value of this length for the solution to be regular
3. the ratio of on-shell action to the axion charge

Report them as a tuple in the above order.[3]

e. Fluctuations in Bondi mass

The vacuum fluctuations of the Bondi mass at null infinity are known to be infinite. However, in real life, we often do measure the mass of distant astrophysical events without any difficulty. This is regularly done by the LIGO observatory for instance.

Now, lets consider a source event that we are observing. For simplicity, we will assume that the source event radiates a massless scalar field. The total energy radiated by the source is E.

Now we have an observer who is at a finite distance R. (In real life, the observer is never at infinity.) This observer notes the total flux of the energy that crosses them over a time interval $[u1, u2]$ with $\delta u = u2 - u1$. Lets make the following model to regulate the fluctuations. We will assume that this observer is only sensitive to angular momentum harmonics with $l < l_{max}$ and set $l_{max} = R/(c\delta u)$. The intuition is that this observer is sensitive to frequencies of size $\omega \; 1/(\delta u)$ and modes with higher values of l die off rapidly by the time they reach R. Its an imprecise model of course, but lets just take this l_{max} as given.

Now, compute the fluctuation $< (\delta E)^2 >$ in the flux of the energy that crosses this observer in this time interval.

The time interval cannot be absolutely precise so we will further smear the endpoints with Gaussians proportional to $e^{-(u-u_1)^2/(2\sigma^2)}$ and $e^{-(u-u2)^2/(2\sigma^2)}$. (Remember to normalize the Gaussians to have unit integral. I haven't done that.) Is the answer finite? Presumably, it depends only on $\delta u = (u1 - u2)$.

What is the value of $(\delta E)^2$. Can you evaluate it numerically for the case where $\delta u = 10s$. $\sigma = 1s$. $R = 1$ light year.

f. Microstate scalar spectrum

Consider the microstate solution of Bena et al. found in arXiv:1607.03908. We will set $R_y = 1$ and also $k = 1, m = 0, n = 3$ and $b^2 = \kappa^2 a^2$ and consider $\kappa = 2.9$. The geometry is asymptotically $AdS_3 \times S_3$. Consider a solution to the equations of motion of a bulk scalar field dual to a marginal operator on the boundary. Fix the dependence of the scalar on the y coordinate to be e^{10iy}. If the dependence on time is $e^{i\omega t}$, find the two smallest allowed values of ω.

Appendix B: Solutions

The solutions to the numerically modified problems in our collection can be found on Hugging Face, where they are given as part of the Harbor task bundle.

If a detailed solution is required, it is simplest to obtain this using an LLM that can solve the problem. Such an LLM can be identified using Table IV. In our experience, Astra often gets not just the final answer but also the intermediate physics correct.

We now describe the solution to the inverse problem (§1b), which no model solved. The following fractional delay equation closely reproduces the displayed curve on $0 \le t \le 5$:

$$f'(t) = {}_0D_t^{1/5} f(t) - 5\,{}_0D_t^{1/3} f(t) + 500 f(t-1) + 550, \qquad t > 0,$$

with the initial data

$$f(t) = -\frac{11}{10} \quad (-1 \le t < 0), \qquad f(0) = 1.0073 \times 10^{-5}.$$

---

[3] The prompt leaves the precise normalization of the metric on moduli space and the axion charge, and the asymptotic value of the moduli, unspecified. Our grading accounts for convention choices observed during our evaluation.

Here the fractional derivatives are Riemann–Liouville derivatives,

$$ {}_0D_t^{\alpha} f(t) = \frac{1}{\Gamma(1-\alpha)} \frac{d}{dt} \int_0^t (t-s)^{-\alpha} f(s)\, ds, \qquad 0 < \alpha < 1. $$

The solution of this equation is plotted in Figure 6 with dots overlaying the original curve.

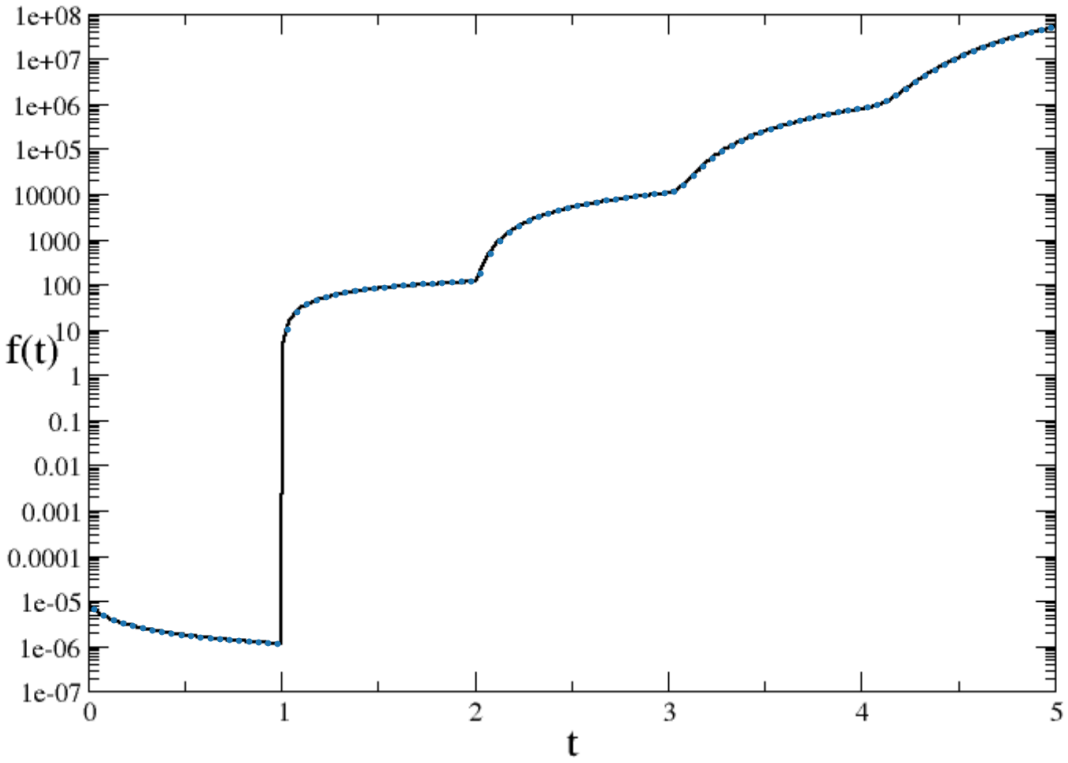

FIG. 6. Numerical solution of the differential equation.

This solution plays upon the phrase "differential equation" since this equation involves both fractional and delay terms. From a strict perspective, this problem might appear "unfair." But, in real life, physicists are often faced with noisy data that they must use to infer the underlying physical process, and sometimes even relax the starting assumptions. So, this question is representative of real research.

The solution above is not claimed to be unique and the reader may check that other equations with similar coefficients can also fit the curve. For this reason, this problem is resistant to a conversion along the lines of Box 2. The prompt asked the agents to output 0 if no equation existed, and output the equation if they found one. We would have graded the agents positively for any equation that provided a good visual fit to the curve, but no agent was able to find such an equation.

It is worth noting that, in a private chat session, separate from the final API runs, Astra did guess that the equation would require fractional derivatives and delay terms. However, even there, it failed to perform an exhaustive search to determine the correct parameters.

Appendix C: Detailed results

In this Appendix, we report grades, token usage, and costs for each problem on the realistic (R) and isolated (I) tracks. Problem identifiers are hyperlinked to their description in Appendix A.

1. Per-problem grades

Problem	**Astra**		**Opus**		**Gemini**		**DeepSeek**		**GLM**	
	R	I	R	I	R	I	R	I	R	I
Boundary-layer perturbations (§1a)	1	0	1	1	1	0	1	0	0	0
Autonomous equation (§1b)	0	0	0	0	0	0	0	0	0	0
Inertial-particle attractors (§1c)	1	1	0	1	0	0	0	0	0	0
Radiation damping (§1d)	1	0	1	1	0	0	1	1	1	0
Two-body electrodynamics (§1e)	1	1	1	1	1	1	0	0	0	0
Theta-logistic growth (§2a)	1	1	1	1	1	1	1	1	1	1
Microbial cross-feeding (§2b)	1	1	1	1	1	1	0	0	0	0
Random-walk bridge minimum (§2c)	1	1	1	1	1	1	0	1	1	1
Three-hole minimax (§2d)	1	1	1	1	1	1	1	1	1	1
Bacteriophage competition (§2e)	1	1	1	1	1	1	1	1	1	1
SLLOD thermostat (§3a)	1	1	1	1	1	1	1	1	1	1
Glass freezing threshold (§3b)	1	1	1	1	0	1	1	1	1	1
Cyclic-shear steady state (§3c)	1	1	1	1	1	1	1	1	1	1
Chiral susceptibilities (§4a)	1	1	1	1	0	0	0	0	0	0
Three-state correlations (§4b)	1	1	1	1	0	0	0	0	0	0
Hubbard imaginary-time energy (§4c)	1	1	1	1	1	0	1	1	0	1
Fermion-parity pump (§5a)	1	1	1	1	1	1	0	0	1	0
Partial symmetry breaking (§5b)	1	1	1	0	1	0	0	1	1	1
Maple-leaf Dirac nodes (§5c)	1	1	1	1	1	1	1	1	1	1
Maple-leaf Chern number (§5d)	1	1	1	1	1	1	1	1	1	1
Maple-leaf cluster spectrum (§5e)	1	1	1	1	1	1	1	0	1	1
All-electron atomic solver (§6a)	1	1	1	1	1	1	1	1	0	1
Norm-conserving potentials (§6b)	1	1	1	1	1	1	1	1	0	1
Pseudopotential ghost states (§6c)	1	1	1	1	1	1	1	1	0	1
Magnesium diboride SCF (§6d)	1	1	1	1	0	0	0	0	0	1
Chern–Simons beta function (§7a)	1	1	0	1	0	0	0	0	0	0
Dynamical soft vacuum (§7b)	1	1	1	1	0	0	0	0	1	0
Simultaneous triple-soft photons (§7c)	1	1	1	1	1	1	0	1	1	0
Schur-index MLDE (§7d)	1	1	1	0	1	0	1	0	0	0
Seiberg duality: 13 nodes (§7e)	1	1	1	1	0	0	1	0	0	1
Seiberg duality: 14 nodes (§7f)	1	1	1	1	1	1	1	1	1	1
Seiberg duality: 12 nodes (§7g)	1	0	1	1	1	1	0	1	0	0
Axion conversion (§8a)	1	1	1	1	1	1	1	0	1	1
Tetraquark Lorentz structures (§8b)	1	1	1	1	1	0	0	0	0	0
Pi dispersion series (§9a)	1	1	0	0	0	0	0	0	0	0
Hidden-zero constraints (§9b)	1	1	1	1	1	1	1	1	1	1
Double-trace renormalization (§9c)	1	1	1	1	1	1	1	1	0	1
Two-loop subdivergences (§9d)	1	1	1	1	0	1	0	0	0	0
Nested triple-soft photons (§9e)	1	1	1	1	1	1	0	0	0	1
Interface transmission (§10a)	1	1	1	1	1	1	1	1	1	0
Radion effective action (§10b)	1	1	1	1	1	1	1	1	0	1
Interface entanglement (§10c)	1	1	1	1	1	1	1	1	1	0
Black-string Page time (§10d)	1	1	1	1	0	0	0	0	0	0
Geometric-entropy flow (§10e)	1	1	1	1	0	0	0	0	0	0
Topological near-horizon geometry (§11a)	1	1	1	1	1	1	1	1	1	1
IIB scale separation (§11b)	1	1	1	1	1	1	0	0	0	0
Hyperbolic compactification (§11c)	1	1	1	1	1	1	1	1	0	1
IIB Euclidean wormholes (§11d)	1	1	1	1	0	0	0	0	0	0
Bondi mass fluctuations (§11e)	1	1	1	1	1	1	0	0	0	1
Microstate scalar spectrum (§11f)	1	1	1	1	0	0	1	0	0	0
Solved	**49**	**46**	**46**	**46**	**34**	**31**	**27**	**25**	**21**	**26**

TABLE IV: Per-problem grades on the R and I tracks. A grade of 1 denotes a pass and 0 denotes a failure.

2. Problem-wise token usage

The tables below report tokens in millions, rounded to three decimal places. Columns titled "uncached" and "cached" refer to input tokens. Sums of the rounded components and rows may not exactly match the displayed totals.

	R				I			
Problem	Uncached	Cached	Output	Total	Uncached	Cached	Output	Total
Boundary-layer perturbations (§1a)	0.092	0.632	0.007	0.730	0.017	0.093	0.007	0.117
Autonomous equation (§1b)	0.019	0.060	0.003	0.082	0.018	0.050	0.005	0.072
Inertial-particle attractors (§1c)	0.128	5.588	0.062	5.778	0.115	3.241	0.074	3.430
Radiation damping (§1d)	0.074	1.052	0.036	1.163	0.029	0.155	0.016	0.199
Two-body electrodynamics (§1e)	0.040	0.214	0.012	0.266	0.027	0.173	0.014	0.215
Theta-logistic growth (§2a)	0.020	0.091	0.007	0.118	0.017	0.077	0.007	0.101
Microbial cross-feeding (§2b)	0.022	0.044	0.008	0.074	0.019	0.067	0.007	0.094
Random-walk bridge minimum (§2c)	0.030	0.111	0.016	0.158	0.030	0.142	0.017	0.190
Three-hole minimax (§2d)	0.023	0.088	0.010	0.121	0.023	0.115	0.011	0.149
Bacteriophage competition (§2e)	0.027	0.167	0.012	0.206	0.035	0.215	0.017	0.266
SLLOD thermostat (§3a)	0.017	0.043	0.003	0.064	0.015	0.049	0.005	0.069
Glass freezing threshold (§3b)	0.022	0.072	0.008	0.102	0.020	0.067	0.009	0.097
Cyclic-shear steady state (§3c)	0.018	0.056	0.004	0.078	0.015	0.073	0.004	0.092
Chiral susceptibilities (§4a)	0.073	0.941	0.033	1.047	0.051	0.855	0.030	0.936
Three-state correlations (§4b)	0.066	1.303	0.029	1.398	0.051	1.011	0.031	1.093
Hubbard imaginary-time energy (§4c)	0.093	1.885	0.041	2.020	0.067	1.298	0.041	1.406
Fermion-parity pump (§5a)	0.050	0.245	0.010	0.305	0.018	0.066	0.008	0.092
Partial symmetry breaking (§5b)	0.044	0.137	0.007	0.188	0.020	0.067	0.010	0.098
Maple-leaf Dirac nodes (§5c)	0.032	0.311	0.014	0.357	0.034	0.281	0.019	0.334
Maple-leaf Chern number (§5d)	0.029	0.185	0.010	0.224	0.034	0.247	0.014	0.294
Maple-leaf cluster spectrum (§5e)	0.021	0.116	0.007	0.144	0.020	0.100	0.007	0.127
All-electron atomic solver (§6a)	0.125	2.075	0.059	2.259	0.106	2.011	0.057	2.173
Norm-conserving potentials (§6b)	0.104	1.525	0.045	1.674	0.092	0.859	0.043	0.994
Pseudopotential ghost states (§6c)	0.101	1.362	0.042	1.504	0.106	1.983	0.054	2.143
Magnesium diboride SCF (§6d)	0.121	2.264	0.057	2.442	0.130	2.697	0.074	2.900
Chern–Simons beta function (§7a)	0.177	2.868	0.036	3.080	0.060	0.520	0.043	0.623
Dynamical soft vacuum (§7b)	0.053	0.296	0.019	0.369	0.030	0.126	0.017	0.173
Simultaneous triple-soft photons (§7c)	0.050	0.285	0.018	0.353	0.030	0.109	0.018	0.156
Schur-index MLDE (§7d)	0.131	1.079	0.016	1.225	0.062	0.739	0.045	0.847
Seiberg duality: 13 nodes (§7e)	0.062	1.193	0.026	1.282	0.056	1.003	0.030	1.089
Seiberg duality: 14 nodes (§7f)	0.073	1.174	0.024	1.272	0.038	0.352	0.018	0.408
Seiberg duality: 12 nodes (§7g)	0.061	0.979	0.027	1.067	0.017	0.066	0.005	0.088
Axion conversion (§8a)	0.054	0.254	0.007	0.316	0.022	0.075	0.012	0.108
Tetraquark Lorentz structures (§8b)	0.037	0.132	0.008	0.177	0.022	0.076	0.011	0.109
Pi dispersion series (§9a)	0.064	0.388	0.014	0.467	0.029	0.162	0.016	0.207
Hidden-zero constraints (§9b)	0.020	0.060	0.007	0.087	0.021	0.085	0.010	0.116
Double-trace renormalization (§9c)	0.032	0.183	0.017	0.231	0.035	0.184	0.019	0.238
Two-loop subdivergences (§9d)	0.038	0.261	0.019	0.318	0.029	0.147	0.016	0.192
Nested triple-soft photons (§9e)	0.055	0.545	0.022	0.622	0.052	1.000	0.036	1.088
Interface transmission (§10a)	0.052	0.157	0.004	0.213	0.015	0.033	0.004	0.053
Radion effective action (§10b)	0.040	0.141	0.007	0.187	0.015	0.048	0.004	0.066
Interface entanglement (§10c)	0.052	0.252	0.009	0.313	0.021	0.059	0.009	0.090
Black-string Page time (§10d)	0.054	0.456	0.013	0.523	0.025	0.114	0.013	0.153
Geometric-entropy flow (§10e)	0.075	0.359	0.015	0.450	0.031	0.138	0.019	0.188
Topological near-horizon geometry (§11a)	0.039	0.139	0.006	0.184	0.015	0.022	0.004	0.041
IIB scale separation (§11b)	0.045	0.183	0.012	0.240	0.025	0.065	0.015	0.104
Hyperbolic compactification (§11c)	0.052	0.250	0.014	0.316	0.025	0.076	0.013	0.114
IIB Euclidean wormholes (§11d)	0.103	0.638	0.020	0.761	0.034	0.134	0.024	0.192
Bondi mass fluctuations (§11e)	0.063	0.278	0.008	0.350	0.019	0.083	0.008	0.111
Microstate scalar spectrum (§11f)	0.057	0.433	0.013	0.503	0.031	0.246	0.016	0.294
Total	2.931	33.552	0.922	37.405	1.869	21.657	1.004	24.529

TABLE V: Token usage by problem for Astra (millions).

	R				I			
Problem	Uncached	Cached	Output	Total	Uncached	Cached	Output	Total
Boundary-layer perturbations (§1a)	0.288	0.902	0.084	1.274	0.423	2.098	0.110	2.631
Autonomous equation (§1b)	1.175	10.628	0.436	12.240	1.301	9.117	0.383	10.801
Inertial-particle attractors (§1c)	0.882	33.643	0.266	34.791	0.973	6.757	0.183	7.913
Radiation damping (§1d)	0.216	5.232	0.185	5.633	0.331	4.575	0.183	5.089
Two-body electrodynamics (§1e)	0.110	1.298	0.095	1.502	0.168	4.230	0.146	4.544
Theta-logistic growth (§2a)	0.038	0.145	0.017	0.200	0.018	0.129	0.013	0.160
Microbial cross-feeding (§2b)	0.123	0.791	0.056	0.970	0.346	4.414	0.095	4.855
Random-walk bridge minimum (§2c)	0.074	0.542	0.061	0.677	0.059	0.742	0.052	0.854
Three-hole minimax (§2d)	0.060	0.311	0.052	0.423	0.057	0.245	0.048	0.350
Bacteriophage competition (§2e)	0.084	0.580	0.031	0.695	0.183	1.943	0.067	2.193
SLLOD thermostat (§3a)	0.018	0.053	0.013	0.085	0.015	0.053	0.011	0.080
Glass freezing threshold (§3b)	0.041	0.132	0.019	0.193	0.033	0.299	0.029	0.361
Cyclic-shear steady state (§3c)	0.058	0.555	0.048	0.661	0.069	0.406	0.038	0.512
Chiral susceptibilities (§4a)	1.372	5.080	0.203	6.654	0.902	8.390	0.212	9.503
Three-state correlations (§4b)	0.481	7.830	0.131	8.442	0.264	8.360	0.124	8.747
Hubbard imaginary-time energy (§4c)	0.154	7.931	0.126	8.211	1.044	2.779	0.115	3.938
Fermion-parity pump (§5a)	0.083	0.996	0.072	1.151	0.079	0.584	0.070	0.733
Partial symmetry breaking (§5b)	0.133	0.185	0.498	0.815	0.016	0.046	0.512	0.574
Maple-leaf Dirac nodes (§5c)	0.110	1.823	0.086	2.018	0.098	1.421	0.079	1.597
Maple-leaf Chern number (§5d)	0.083	0.408	0.036	0.527	0.036	0.384	0.027	0.447
Maple-leaf cluster spectrum (§5e)	0.024	0.128	0.017	0.169	0.022	0.209	0.017	0.248
All-electron atomic solver (§6a)	0.309	10.872	0.203	11.383	0.387	17.845	0.262	18.494
Norm-conserving potentials (§6b)	0.308	13.437	0.165	13.910	0.557	29.553	0.295	30.405
Pseudopotential ghost states (§6c)	0.437	24.729	0.250	25.416	1.351	26.594	0.285	28.231
Magnesium diboride SCF (§6d)	1.467	33.488	0.261	35.216	3.704	36.128	0.272	40.104
Chern–Simons beta function (§7a)	0.042	0.069	0.640	0.751	0.808	7.252	0.382	8.442
Dynamical soft vacuum (§7b)	0.182	2.884	0.166	3.232	0.329	1.222	0.126	1.676
Simultaneous triple-soft photons (§7c)	0.111	0.685	0.098	0.894	0.106	0.950	0.097	1.154
Schur-index MLDE (§7d)	0.189	3.120	0.296	3.605	0.293	2.222	0.239	2.753
Seiberg duality: 13 nodes (§7e)	0.347	1.853	0.092	2.292	0.356	1.655	0.078	2.088
Seiberg duality: 14 nodes (§7f)	0.203	3.115	0.089	3.407	0.104	1.347	0.084	1.535
Seiberg duality: 12 nodes (§7g)	0.159	1.403	0.075	1.637	0.142	1.393	0.066	1.602
Axion conversion (§8a)	0.094	0.212	0.084	0.390	0.090	0.117	0.083	0.290
Tetraquark Lorentz structures (§8b)	0.057	0.254	0.049	0.360	0.089	0.435	0.079	0.603
Pi dispersion series (§9a)	0.111	0.891	0.096	1.098	0.459	1.762	0.229	2.451
Hidden-zero constraints (§9b)	0.023	0.139	0.019	0.181	0.017	0.072	0.013	0.103
Double-trace renormalization (§9c)	0.084	1.155	0.066	1.304	0.091	1.141	0.072	1.304
Two-loop subdivergences (§9d)	0.147	1.697	0.129	1.973	0.154	1.800	0.142	2.097
Nested triple-soft photons (§9e)	0.229	3.267	0.208	3.705	0.359	4.884	0.324	5.567
Interface transmission (§10a)	0.069	0.309	0.309	0.687	0.085	0.182	0.076	0.344
Radion effective action (§10b)	0.097	0.398	0.085	0.580	0.077	0.183	0.070	0.331
Interface entanglement (§10c)	0.063	0.154	0.053	0.270	0.076	0.182	0.066	0.324
Black-string Page time (§10d)	0.125	1.636	0.111	1.872	0.131	1.598	0.117	1.846
Geometric-entropy flow (§10e)	0.371	1.868	0.315	2.554	0.163	0.581	0.393	1.137
Topological near-horizon geometry (§11a)	0.052	0.189	0.047	0.288	0.058	0.269	0.051	0.377
IIB scale separation (§11b)	0.186	0.943	0.095	1.224	0.113	0.750	0.094	0.957
Hyperbolic compactification (§11c)	0.188	1.317	0.091	1.595	0.099	0.793	0.087	0.979
IIB Euclidean wormholes (§11d)	0.124	0.537	0.364	1.025	0.653	3.046	0.305	4.005
Bondi mass fluctuations (§11e)	0.037	0.154	0.032	0.222	0.061	0.140	0.052	0.253
Microstate scalar spectrum (§11f)	0.363	2.281	0.130	2.774	0.779	1.815	0.257	2.852
Total	11.781	192.247	7.150	211.178	18.129	203.095	7.210	228.433

TABLE VI: Token usage by problem for Opus (millions).

	R				I			
Problem	Uncached	Cached	Output	Total	Uncached	Cached	Output	Total
Boundary-layer perturbations (§1a)	1.778	11.668	0.100	13.546	0.436	6.451	0.096	6.983
Autonomous equation (§1b)	1.129	11.698	0.145	12.973	0.358	2.162	0.065	2.585
Inertial-particle attractors (§1c)	1.459	20.230	0.119	21.807	1.981	20.144	0.303	22.428
Radiation damping (§1d)	1.236	11.749	0.248	13.232	3.486	67.675	0.289	71.451
Two-body electrodynamics (§1e)	0.476	5.943	0.127	6.546	0.677	4.590	0.087	5.355
Theta-logistic growth (§2a)	0.169	0.591	0.030	0.789	0.153	0.600	0.027	0.781
Microbial cross-feeding (§2b)	0.700	7.026	0.061	7.788	0.284	2.173	0.059	2.517
Random-walk bridge minimum (§2c)	0.712	6.586	0.107	7.406	0.325	3.763	0.092	4.179
Three-hole minimax (§2d)	0.244	1.562	0.059	1.865	0.308	1.589	0.051	1.948
Bacteriophage competition (§2e)	0.378	3.609	0.056	4.044	0.260	2.148	0.079	2.487
SLLOD thermostat (§3a)	0.217	1.709	0.038	1.965	0.138	0.419	0.024	0.582
Glass freezing threshold (§3b)	0.798	18.988	0.109	19.895	0.547	11.338	0.063	11.948
Cyclic-shear steady state (§3c)	0.310	2.512	0.055	2.877	0.240	1.641	0.048	1.929
Chiral susceptibilities (§4a)	3.343	45.991	0.292	49.625	1.383	27.070	0.306	28.759
Three-state correlations (§4b)	2.596	38.915	0.321	41.831	2.671	61.438	0.311	64.421
Hubbard imaginary-time energy (§4c)	1.167	20.130	0.146	21.443	1.046	5.485	0.121	6.653
Fermion-parity pump (§5a)	0.817	12.298	0.080	13.195	0.300	2.621	0.066	2.987
Partial symmetry breaking (§5b)	0.487	10.460	0.077	11.024	0.274	0.895	0.112	1.282
Maple-leaf Dirac nodes (§5c)	0.494	3.657	0.075	4.226	0.245	2.194	0.057	2.496
Maple-leaf Chern number (§5d)	0.240	1.531	0.052	1.823	0.191	1.652	0.053	1.896
Maple-leaf cluster spectrum (§5e)	0.271	0.653	0.034	0.958	0.306	0.959	0.045	1.310
All-electron atomic solver (§6a)	1.530	37.509	0.150	39.189	0.804	6.519	0.175	7.498
Norm-conserving potentials (§6b)	0.642	8.296	0.135	9.073	0.647	8.300	0.135	9.082
Pseudopotential ghost states (§6c)	0.716	13.306	0.105	14.128	1.362	8.186	0.115	9.663
Magnesium diboride SCF (§6d)	0.776	9.936	0.107	10.819	1.268	13.503	0.146	14.918
Chern–Simons beta function (§7a)	1.595	40.858	0.231	42.684	1.061	20.098	0.214	21.373
Dynamical soft vacuum (§7b)	0.691	8.467	0.151	9.308	0.663	8.652	0.143	9.458
Simultaneous triple-soft photons (§7c)	0.400	3.979	0.079	4.458	0.731	4.637	0.109	5.477
Schur-index MLDE (§7d)	1.046	11.538	0.116	12.700	1.356	37.590	0.147	39.092
Seiberg duality: 13 nodes (§7e)	1.272	16.915	0.172	18.359	0.467	8.061	0.075	8.603
Seiberg duality: 14 nodes (§7f)	0.524	5.053	0.113	5.689	0.439	4.016	0.105	4.560
Seiberg duality: 12 nodes (§7g)	0.705	6.218	0.101	7.024	0.889	13.728	0.317	14.934
Axion conversion (§8a)	0.567	6.262	0.089	6.918	0.362	2.645	0.088	3.095
Tetraquark Lorentz structures (§8b)	0.521	5.122	0.083	5.726	0.341	3.742	0.108	4.190
Pi dispersion series (§9a)	0.660	6.813	0.091	7.564	1.345	36.967	0.191	38.503
Hidden-zero constraints (§9b)	0.124	0.363	0.031	0.518	0.094	0.230	0.021	0.345
Double-trace renormalization (§9c)	0.935	9.712	0.317	10.965	0.995	15.788	0.133	16.917
Two-loop subdivergences (§9d)	0.836	24.216	0.157	25.208	0.402	7.365	0.141	7.908
Nested triple-soft photons (§9e)	0.915	13.822	0.132	14.868	1.321	33.787	0.150	35.258
Interface transmission (§10a)	0.353	2.919	0.051	3.322	0.356	2.214	0.092	2.662
Radion effective action (§10b)	0.612	6.077	0.069	6.757	0.249	1.438	0.062	1.749
Interface entanglement (§10c)	0.506	4.036	0.065	4.607	0.203	1.449	0.084	1.736
Black-string Page time (§10d)	1.788	24.880	0.203	26.871	0.722	16.071	0.175	16.968
Geometric-entropy flow (§10e)	1.204	14.447	0.188	15.839	0.411	5.606	0.168	6.186
Topological near-horizon geometry (§11a)	0.307	2.108	0.062	2.477	0.154	0.775	0.054	0.984
IIB scale separation (§11b)	0.436	3.314	0.061	3.811	0.325	2.958	0.117	3.400
Hyperbolic compactification (§11c)	0.514	4.964	0.076	5.554	0.343	1.752	0.076	2.170
IIB Euclidean wormholes (§11d)	0.774	8.848	0.072	9.694	0.393	1.828	0.096	2.317
Bondi mass fluctuations (§11e)	1.369	5.812	0.100	7.281	0.236	1.777	0.089	2.102
Microstate scalar spectrum (§11f)	0.656	15.667	0.123	16.446	1.692	56.245	0.140	58.077
Total	41.995	558.961	5.759	606.715	35.242	552.935	6.022	594.198

TABLE VII: Token usage by problem for Gemini (millions).

	R				I			
Problem	Uncached	Cached	Output	Total	Uncached	Cached	Output	Total
Boundary-layer perturbations (§1a)	0.124	7.582	0.081	7.787	0.067	10.552	0.156	10.776
Autonomous equation (§1b)	0.101	4.659	0.275	5.036	0.051	6.876	0.275	7.202
Inertial-particle attractors (§1c)	0.589	53.369	0.707	54.665	1.278	94.423	1.928	97.629
Radiation damping (§1d)	0.728	57.747	1.480	59.955	0.703	62.523	1.367	64.593
Two-body electrodynamics (§1e)	0.055	16.744	0.183	16.982	0.016	9.047	0.195	9.258
Theta-logistic growth (§2a)	0.008	0.452	0.026	0.486	0.003	0.165	0.014	0.182
Microbial cross-feeding (§2b)	0.012	1.440	0.090	1.542	0.000	0.073	0.056	0.130
Random-walk bridge minimum (§2c)	0.009	3.314	0.120	3.442	0.012	5.375	0.147	5.534
Three-hole minimax (§2d)	0.024	4.683	0.157	4.864	0.082	3.949	0.360	4.390
Bacteriophage competition (§2e)	0.019	3.627	0.174	3.820	0.029	4.736	0.173	4.938
SLLOD thermostat (§3a)	0.003	0.098	0.011	0.111	0.008	0.057	0.013	0.079
Glass freezing threshold (§3b)	0.004	0.897	0.086	0.986	0.004	0.407	0.046	0.457
Cyclic-shear steady state (§3c)	0.008	1.015	0.041	1.064	0.012	1.734	0.051	1.797
Chiral susceptibilities (§4a)	0.027	15.079	0.198	15.304	0.388	61.153	1.097	62.638
Three-state correlations (§4b)	0.885	97.481	2.128	100.494	1.128	88.608	3.105	92.841
Hubbard imaginary-time energy (§4c)	0.263	53.881	0.618	54.762	0.185	42.488	0.393	43.067
Fermion-parity pump (§5a)	0.001	0.067	0.054	0.121	0.003	0.265	0.040	0.309
Partial symmetry breaking (§5b)	0.055	2.984	0.076	3.115	0.002	0.255	0.074	0.330
Maple-leaf Dirac nodes (§5c)	0.035	7.861	0.173	8.069	0.023	3.690	0.174	3.887
Maple-leaf Chern number (§5d)	0.010	0.531	0.034	0.575	0.021	2.586	0.056	2.663
Maple-leaf cluster spectrum (§5e)	0.005	0.244	0.018	0.267	0.006	0.214	0.017	0.236
All-electron atomic solver (§6a)	0.177	15.464	0.200	15.840	0.378	33.832	0.416	34.626
Norm-conserving potentials (§6b)	0.294	26.060	0.315	26.669	0.226	19.826	0.321	20.373
Pseudopotential ghost states (§6c)	0.438	41.470	0.432	42.340	0.253	33.535	0.372	34.160
Magnesium diboride SCF (§6d)	0.186	23.585	0.285	24.056	0.375	48.101	0.477	48.953
Chern–Simons beta function (§7a)	0.000	0.010	0.037	0.047	0.067	0.900	0.145	1.112
Dynamical soft vacuum (§7b)	0.032	12.310	0.212	12.554	0.198	11.343	0.300	11.841
Simultaneous triple-soft photons (§7c)	0.033	11.924	0.170	12.126	0.059	8.121	0.161	8.342
Schur-index MLDE (§7d)	0.372	16.236	0.274	16.882	0.066	13.523	0.169	13.759
Seiberg duality: 13 nodes (§7e)	0.325	35.218	0.301	35.844	0.165	26.737	0.200	27.102
Seiberg duality: 14 nodes (§7f)	0.371	53.921	0.522	54.813	0.029	6.125	0.102	6.256
Seiberg duality: 12 nodes (§7g)	0.136	9.850	0.361	10.347	0.056	19.112	0.198	19.366
Axion conversion (§8a)	0.344	7.026	0.264	7.634	0.002	0.872	0.120	0.993
Tetraquark Lorentz structures (§8b)	0.135	8.386	0.069	8.590	0.025	0.391	0.078	0.494
Pi dispersion series (§9a)	0.098	5.776	0.321	6.195	0.033	3.304	0.444	3.781
Hidden-zero constraints (§9b)	0.003	0.160	0.031	0.194	0.003	0.174	0.026	0.203
Double-trace renormalization (§9c)	0.131	10.077	0.551	10.759	0.036	10.455	0.215	10.705
Two-loop subdivergences (§9d)	1.765	119.285	3.302	124.351	1.370	59.971	3.191	64.532
Nested triple-soft photons (§9e)	0.031	17.560	0.216	17.807	0.003	0.420	0.065	0.488
Interface transmission (§10a)	0.015	2.067	0.108	2.189	0.002	0.677	0.113	0.793
Radion effective action (§10b)	0.043	0.237	0.128	0.409	0.249	0.463	0.315	1.028
Interface entanglement (§10c)	0.003	0.408	0.124	0.535	0.082	0.206	0.088	0.376
Black-string Page time (§10d)	2.588	145.265	3.943	151.795	0.013	1.994	0.108	2.114
Geometric-entropy flow (§10e)	1.933	65.117	2.853	69.903	2.311	63.811	4.862	70.985
Topological near-horizon geometry (§11a)	0.001	0.246	0.071	0.318	0.009	0.114	0.030	0.153
IIB scale separation (§11b)	0.031	1.818	0.179	2.029	0.019	4.730	0.144	4.893
Hyperbolic compactification (§11c)	0.235	9.455	0.578	10.269	0.356	2.429	0.207	2.992
IIB Euclidean wormholes (§11d)	0.068	8.332	0.195	8.595	0.111	5.477	0.570	6.158
Bondi mass fluctuations (§11e)	0.001	0.336	0.120	0.457	0.000	0.000	0.000	0.000*
Microstate scalar spectrum (§11f)	0.089	8.382	0.128	8.599	0.230	23.902	0.327	24.459
Total	12.842	989.734	23.020	1025.597	10.748	799.721	23.503	833.972

TABLE VIII: Token usage by problem for DeepSeek (millions). *This task was cut off for exceeding the time limit and did not record token usage.

	R				I			
Problem	Uncached	Cached	Output	Total	Uncached	Cached	Output	Total
Boundary-layer perturbations (§1a)	0.082	2.196	0.074	2.352	0.054	0.092	0.052	0.199
Autonomous equation (§1b)	0.252	4.458	0.141	4.851	0.648	8.215	0.231	9.094
Inertial-particle attractors (§1c)	3.837	61.382	0.332	65.551	7.213	87.645	0.350	95.207
Radiation damping (§1d)	0.525	149.820	0.456	150.802	0.383	41.430	0.440	42.253
Two-body electrodynamics (§1e)	0.122	2.330	0.113	2.565	0.159	3.929	0.152	4.240
Theta-logistic growth (§2a)	0.020	0.146	0.017	0.183	0.111	1.014	0.043	1.168
Microbial cross-feeding (§2b)	0.150	2.793	0.140	3.083	0.059	0.141	0.048	0.249
Random-walk bridge minimum (§2c)	0.146	2.199	0.138	2.484	0.109	1.921	0.326	2.356
Three-hole minimax (§2d)	0.114	1.698	0.111	1.923	0.158	3.683	0.143	3.983
Bacteriophage competition (§2e)	0.046	0.789	0.034	0.869	0.063	1.071	0.048	1.182
SLLOD thermostat (§3a)	0.023	0.061	0.019	0.103	0.054	0.146	0.017	0.217
Glass freezing threshold (§3b)	0.045	1.059	0.024	1.128	0.071	1.871	0.057	1.999
Cyclic-shear steady state (§3c)	0.043	0.762	0.034	0.839	0.015	0.167	0.009	0.191
Chiral susceptibilities (§4a)	0.142	14.229	0.072	14.444	0.558	126.312	0.503	127.373
Three-state correlations (§4b)	0.225	46.087	0.261	46.573	0.534	90.765	0.472	91.771
Hubbard imaginary-time energy (§4c)	0.126	11.616	0.089	11.830	0.207	34.773	0.175	35.155
Fermion-parity pump (§5a)	0.117	0.153	0.113	0.382	0.067	0.803	0.178	1.047
Partial symmetry breaking (§5b)	0.177	3.521	0.105	3.802	0.123	0.293	0.121	0.537
Maple-leaf Dirac nodes (§5c)	0.106	4.206	0.084	4.395	0.081	1.791	0.073	1.945
Maple-leaf Chern number (§5d)	0.058	1.032	0.048	1.138	0.024	0.276	0.017	0.317
Maple-leaf cluster spectrum (§5e)	0.051	0.601	0.044	0.696	0.110	2.025	0.048	2.183
All-electron atomic solver (§6a)	0.387	41.514	0.303	42.204	1.751	30.361	0.290	32.402
Norm-conserving potentials (§6b)	1.151	19.292	0.186	20.628	0.508	24.340	0.202	25.050
Pseudopotential ghost states (§6c)	0.672	13.606	0.162	14.440	0.682	13.173	0.171	14.026
Magnesium diboride SCF (§6d)	1.562	246.063	0.322	247.947	0.441	81.718	0.305	82.464
Chern–Simons beta function (§7a)	0.010	0.058	0.512	0.580	0.483	36.427	0.685	37.596
Dynamical soft vacuum (§7b)	0.229	14.052	0.212	14.493	0.564	27.280	0.384	28.228
Simultaneous triple-soft photons (§7c)	0.208	10.999	0.176	11.383	0.272	14.458	0.251	14.981
Schur-index MLDE (§7d)	0.321	36.370	0.227	36.918	2.381	78.341	2.059	82.781
Seiberg duality: 13 nodes (§7e)	0.273	54.723	0.239	55.235	0.267	38.951	0.218	39.436
Seiberg duality: 14 nodes (§7f)	0.119	11.520	0.069	11.708	0.114	4.641	0.058	4.813
Seiberg duality: 12 nodes (§7g)	0.316	22.589	0.085	22.990	0.153	3.261	0.120	3.534
Axion conversion (§8a)	0.056	0.587	0.045	0.688	0.117	0.466	0.101	0.684
Tetraquark Lorentz structures (§8b)	0.123	0.426	0.120	0.670	0.202	0.986	0.240	1.428
Pi dispersion series (§9a)	0.162	3.319	0.153	3.634	0.151	2.760	0.264	3.174
Hidden-zero constraints (§9b)	0.013	0.124	0.010	0.147	0.012	0.090	0.009	0.111
Double-trace renormalization (§9c)	0.058	1.400	0.300	1.758	0.282	11.608	0.395	12.284
Two-loop subdivergences (§9d)	0.015	0.050	0.512	0.577	1.415	163.934	1.498	166.847
Nested triple-soft photons (§9e)	0.248	13.602	0.222	14.073	0.488	124.436	0.411	125.336
Interface transmission (§10a)	0.132	0.855	0.117	1.104	0.045	0.384	0.041	0.471
Radion effective action (§10b)	0.135	5.591	0.084	5.810	0.086	0.219	0.084	0.388
Interface entanglement (§10c)	0.065	0.119	0.188	0.371	0.039	0.115	0.155	0.310
Black-string Page time (§10d)	0.195	15.949	0.215	16.359	0.039	0.179	0.169	0.387
Geometric-entropy flow (§10e)	2.466	65.662	0.856	68.984	0.290	8.064	0.403	8.757
Topological near-horizon geometry (§11a)	0.049	0.086	0.046	0.181	0.037	0.027	0.035	0.099
IIB scale separation (§11b)	0.337	14.457	0.307	15.101	0.117	0.434	0.229	0.781
Hyperbolic compactification (§11c)	0.011	0.051	0.512	0.574	0.113	1.808	0.350	2.270
IIB Euclidean wormholes (§11d)	0.339	7.212	0.497	8.048	0.140	0.796	0.644	1.580
Bondi mass fluctuations (§11e)	0.142	0.905	0.135	1.181	0.070	0.338	0.066	0.473
Microstate scalar spectrum (§11f)	0.355	33.397	0.433	34.185	0.230	1.839	0.185	2.254
Total	16.554	945.717	9.692	971.963	22.293	1079.793	13.524	1115.610

TABLE IX: Token usage by problem for GLM (millions).

3. Problem-wise costs

The costs below are obtained by converting token counts to USD using public API rates. The costs for GLM are notional since a coding plan was used.

	Astra		Opus		Gemini		DeepSeek		GLM	
Problem	R	I	R	I	R	I	R	I	R	I
Boundary-layer perturbations (§1a)	2.11	0.64	3.30	4.73	2.58	1.17	0.18	0.27	1.01	0.33
Autonomous equation (§1b)	0.42	0.50	16.72	15.99	2.27	0.67	0.39	0.39	2.13	4.06
Inertial-particle attractors (§1c)	10.30	8.37	16.46	9.87	3.06	4.13	1.35	3.26	22.79	34.42
Radiation damping (§1d)	3.79	1.29	5.82	6.24	2.74	8.77	2.34	2.23	41.70	13.24
Two-body electrodynamics (§1e)	1.31	1.22	2.70	4.61	1.28	1.18	0.34	0.29	1.27	1.91
Theta-logistic growth (§2a)	0.67	0.63	0.57	0.38	0.28	0.26	0.04	0.02	0.14	0.61
Microbial cross-feeding (§2b)	0.72	0.67	1.90	4.50	1.28	0.60	0.12	0.07	1.55	0.33
Random-walk bridge minimum (§2c)	1.30	1.38	1.71	1.49	1.43	0.87	0.17	0.21	1.39	2.09
Three-hole minimax (§2d)	0.90	0.96	1.40	1.30	0.52	0.54	0.22	0.48	1.09	1.81
Bacteriophage competition (§2e)	1.08	1.48	1.16	2.64	0.76	0.65	0.24	0.24	0.42	0.58
SLLOD thermostat (§3a)	0.43	0.47	0.36	0.31	0.43	0.23	0.01	0.02	0.13	0.19
Glass freezing threshold (§3b)	0.76	0.78	0.62	0.81	2.43	1.50	0.11	0.06	0.44	0.84
Cyclic-shear steady state (§3c)	0.49	0.45	1.36	1.18	0.63	0.48	0.06	0.08	0.41	0.10
Chiral susceptibilities (§4a)	3.51	2.99	11.93	10.42	7.05	4.22	0.34	1.80	4.22	35.83
Three-state correlations (§4b)	3.58	3.20	6.59	5.47	6.07	7.78	3.40	4.60	13.45	26.42
Hubbard imaginary-time energy (§4c)	5.10	4.17	4.87	8.07	2.93	1.65	1.14	0.78	3.59	10.10
Fermion-parity pump (§5a)	1.39	0.67	2.05	1.91	1.84	0.67	0.07	0.05	0.70	1.08
Partial symmetry breaking (§5b)	1.02	0.82	10.65	10.33	1.44	0.69	0.13	0.09	1.62	0.78
Maple-leaf Dirac nodes (§5c)	1.41	1.64	2.63	2.34	0.93	0.56	0.27	0.24	1.61	0.90
Maple-leaf Chern number (§5d)	1.03	1.35	1.21	0.80	0.49	0.47	0.05	0.09	0.56	0.18
Maple-leaf cluster spectrum (§5e)	0.71	0.70	0.49	0.48	0.38	0.47	0.02	0.02	0.42	0.89
All-electron atomic solver (§6a)	6.57	6.18	7.78	10.74	4.52	1.75	0.39	0.82	12.67	11.62
Norm-conserving potentials (§6b)	5.06	4.15	7.53	14.61	1.61	1.61	0.62	0.57	7.45	7.93
Pseudopotential ghost states (§6c)	4.71	6.01	12.12	17.78	1.93	2.07	0.90	0.72	5.19	5.13
Magnesium diboride SCF (§6d)	6.61	8.00	19.25	31.19	1.73	2.51	0.54	0.97	67.58	23.21
Chern–Simons beta function (§7a)	6.86	3.44	13.03	13.13	5.13	3.11	0.04	0.20	2.28	13.16
Dynamical soft vacuum (§7b)	1.93	1.36	4.80	4.41	1.72	1.68	0.34	0.49	4.91	9.57
Simultaneous triple-soft photons (§7c)	1.80	1.36	2.65	2.66	0.90	1.30	0.29	0.26	3.92	5.24
Schur-index MLDE (§7d)	3.49	3.78	7.49	6.68	2.09	4.39	0.54	0.30	10.90	32.76
Seiberg duality: 13 nodes (§7e)	3.28	3.19	3.95	3.66	2.87	1.24	0.67	0.45	15.66	11.46
Seiberg duality: 14 nodes (§7f)	3.30	1.73	3.42	2.48	1.19	1.03	1.06	0.17	3.47	1.62
Seiberg duality: 12 nodes (§7g)	3.09	0.51	2.58	2.32	1.37	2.88	0.53	0.37	6.69	1.59
Axion conversion (§8a)	1.30	0.93	2.19	2.13	1.23	0.80	0.46	0.15	0.43	0.73
Tetraquark Lorentz structures (§8b)	1.00	0.92	1.32	2.10	1.08	0.94	0.17	0.10	0.81	1.59
Pi dispersion series (§9a)	1.91	1.34	2.66	7.23	1.35	4.50	0.45	0.56	1.76	2.09
Hidden-zero constraints (§9b)	0.63	0.86	0.52	0.36	0.23	0.17	0.04	0.03	0.09	0.08
Double-trace renormalization (§9c)	1.42	1.58	1.97	2.12	2.62	2.43	0.76	0.33	1.76	5.15
Two-loop subdivergences (§9d)	1.66	1.31	3.67	3.98	3.03	1.38	5.21	4.60	2.29	51.19
Nested triple-soft photons (§9e)	2.31	3.45	5.97	9.25	2.22	4.09	0.37	0.08	4.86	34.85
Interface transmission (§10a)	1.02	0.44	6.59	1.99	0.67	0.78	0.15	0.14	0.92	0.35
Radion effective action (§10b)	0.97	0.42	2.27	1.82	1.17	0.53	0.17	0.46	2.01	0.55
Interface entanglement (§10c)	1.35	0.77	1.40	1.73	0.93	0.57	0.15	0.13	0.95	0.77
Black-string Page time (§10d)	1.78	1.10	3.16	3.31	3.97	2.40	6.38	0.15	5.37	0.84
Geometric-entropy flow (§10e)	2.07	1.46	8.54	8.79	2.69	1.36	4.39	6.91	24.29	4.27
Topological near-horizon geometry (§11a)	0.92	0.42	1.24	1.36	0.62	0.38	0.09	0.04	0.29	0.21
IIB scale separation (§11b)	1.37	1.12	3.02	2.59	0.81	0.90	0.24	0.21	5.58	1.29
Hyperbolic compactification (§11c)	1.61	1.02	3.02	2.40	1.04	0.67	0.82	0.37	2.28	2.17
IIB Euclidean wormholes (§11d)	2.93	1.74	8.01	9.98	1.51	0.79	0.30	0.75	4.54	3.24
Bondi mass fluctuations (§11e)	1.49	0.74	0.85	1.36	1.84	0.64	0.15	0.00	1.03	0.47
Microstate scalar spectrum (§11f)	1.81	1.46	4.94	9.40	2.13	6.01	0.23	0.61	11.08	1.61
Total	116.28	95.20	240.43	275.46	95.01	90.48	37.42	36.23	311.71	371.46

TABLE X: Evaluation costs by problem (USD).